CHEMICAL FRACTIONATIONS IN SOLAR COMPOSITION MATERIAL

by

MELVIN BRUCE FEGLEY, JR.

S.B., MASSACHUSETTS INSTITUTE OF TECHNOLOGY

(1975)

SUBMITTED IN PARTIAL FULFILLMENT
OF THE REQUIREMENTS OF THE
DEGREE OF

DOCTOR OF PHILOSOPHY IN

EARTH AND PLANETARY SCIENCE

at the

MASSACHUSETTS INSTITUTE OF TECHNOLOGY

June 1980

Signature of Author _____
Department of Earth and Planetary Sciences
May 5, 1980

Certified by _____
John S. Lewis
Thesis Supervisor

Accepted by _____
Theodore Madden
Chairman, Department Committee

CHEMICAL FRACTIONATIONS IN SOLAR COMPOSITION MATERIAL

by

MELVIN BRUCE FEGLEY, JR.

Submitted to the Department of Earth and Planetary Sciences on April 25, 1980 in partial fulfillment of the requirements for the Degree of Doctor of Philosophy in Earth and Planetary Science

ABSTRACT

Chemical thermodynamic techniques are used to study three diverse problems in meteoritics and planetary science. The problems are volatile element fractionations in the solar nebula, barium titanate condensation in the solar nebula, and the thermochemistry of selected trace elements in the atmosphere of Jupiter.

Chemical equilibrium calculations for the alkalis, halogens, and phosphorus are reported for two extreme models of accretion. A comparison of the predicted condensates in the two accretion models with available observations of Na, K, F, Cl, Br and P abundances in the terrestrial planets and with the observed mineralogy of ordinary chondrites indicates that available data are compatible with a close approach to chemical equilibrium in the inner regions of the solar nebula.

The observation of pure $BaTiO_3$ particles in the Allende meteorite has stimulated the development of a simple and consistent model to explain the observations. The suggested model involves nonideality of the $BaTiO_3$-$CaTiO_3$ solid solution. This nonideality permits significant fractionation of Ba from Ca and Sr during condensation, leading to the formation of pure $BaTiO_3$ particles. The quantitative treatment of trace element solid solution formation used in this study provides a firm basis for analogous discussions of trace element fractionations in meteorites or other solar system material.

The thermochemistry of several hundred compounds of twelve selected trace elements (Ge, Se, Ga, As, Te, Pb, Sn, Cd, Sb, Tl, In, and Bi) has been investigated in the Jovian atmosphere. The results indicate that AsF_3, InBr, TlI and SbS, in addition to CO, PH_3, GeH_4, AsH_3, H_2Se, HCl, HF, and H_3BO_3 proposed by Barshay and Lewis (1978) may be potential chemical tracers of atmospheric dynamics. The reported observation of GeH_4 is interpreted on the basis of new calculations as implying rapid vertical transport from levels where $T > 800°K$. Upper limits are also set on the abundances of many gaseous compounds of the elements investigated.

Thesis Supervisor: Professor John S. Lewis

Title: Professor of Geochemistry

"Let this book be dedicated to the chemists of the newer generation, who will not wish to reject all inferences from conjecture or surmise, but who will not care to speculate concerning that which may be surely known. The fascination of a growing science lies in the work of the pioneers at the very borderland of the unknown, but to reach this frontier one must pass over well-traveled roads; of these one of the safest and surest is the broad highway of thermodynamics".

Gilbert Newton Lewis and Merle Randall, Thermodynamics 1923.

TABLE OF CONTENTS

LIST OF TABLES

LIST OF FIGURES

PREFACE

Many workers including Grossman, Larimer, Lewis, Lord, Ringwood, Urey, and Wood among others, have used chemical thermodynamic calculations to explain (more or less successfully) a wide variety of chemical fractionations in cool stellar atmospheres, meteorites, and the primitive solar nebula. This large body of work, which has been most recently reviewed by Barshay and Lewis (1976) and by Grossman and Larimer (1974), has influenced our concepts of the origin of the solar system.

The principles of chemical thermodynamics have also been applied to many diverse problems in planetary science. Urey (1952) suggested the concept of chemical equilibrium between the lithosphere and atmosphere of a hot planet. This suggestion was later developed by Mueller (1963, 1964, 1965) who presented a strong case for a model in which the temperature, pressure and composition at the surface of Venus determines the composition of its atmosphere. Lewis later inverted Mueller's model and has used the concept of chemical equilibrium in an atmosphere-lithosphere system plus data on the composition of the atmosphere of Venus to place limits on the temperature, pressure, composition and oxidation state of the surface (Lewis, 1970; Lewis and

Kreimendahl, 1980).

Thermodynamic techniques developed to study the stability and abundance of cloud-forming condensates in the Cytherean atmosphere have been applied by Lewis (1969a) and by Weidenschilling and Lewis (1973) to a study of cloud-forming condensates in the atmospheres of the outer planets Jupiter, Saturn, Uranus, and Neptune. Furthermore, Lewis (1969b), Barshay and Lewis (1978), and Fegley and Lewis (1979) have used the assumption of chemical equilibrium in the lower Jovian atmosphere and the assumption of an adiabatic solar composition atmosphere to predict observable spectroscopically active species and possible chemical tracers of atmospheric dynamics.

The diversity of problems in meteoritics and in planetary science to which chemical thermodynamics can be applied is illustrated in more detail by the three projects described in this thesis. Part 1 of the thesis, which deals with chemical fractionations in the primitive solar nebula, is composed of two chapters. The first chapter, which is based on results presented by Fegley (1979a,b,c) and Fegley and Lewis (1980), describes an investigation of the equilibrium chemistry of the alkalis, halogens, and phosphorus in a solar composition system. The results of this investigation are then used to discuss volatile element retention by the

terrestrial planets and certain features of chondrite mineralogy. The second chapter, which is based on work by Fegley (1980a,b), describes an investigation of barium titanate ($BaTiO_3$) formation and alkaline earth fractionation in the primitive solar nebula. The results of this work are used to explain the observation of $BaTiO_3$ particulates in the Allende meteorite. Part 2 of the thesis, which deals with chemical equilibria in planetary atmospheres, contains one chapter. This chapter is a study of the thermochemistry of selected trace elements in the Jovian atmosphere and is based on work presented by Fegley (1978) and Fegley and Lewis (1979). The results of this work are used to predict possible chemical tracers of atmospheric dynamics on Jupiter and Saturn.

All three problems, which are currently of great interest in meteoritics and planetary science, can be studied using the well established techniques of chemical thermodynamics. It is the author's intent to illustrate the great versatility of these techniques for research in meteoritics and planetary science by describing three such diverse problems.

PART 1

CHEMICAL FRACTIONATIONS IN THE PRIMITIVE SOLAR NEBULA

CHAPTER I: VOLATILE ELEMENT FRACTIONATIONS IN THE SOLAR NEBULA: THE ALKALIS, HALOGENS, AND PHOSPHORUS.

INTRODUCTION

One of the most intriguing and perplexing problems in planetary science is the method of retention of volatile elements by the terrestrial planets. The retention of volatiles bears upon the origin of the atmospheres of the terrestrial planets, the origin of the Earth's oceans, the oxidation state of the terrestrial planets and the volatile content of the interiors of the terrestrial planets, a factor which influences local melting and volcanism.

Previous work on the thermodynamics of volatile element retention by the terrestrial planets includes that of Lewis (1972) who briefly addressed water retention and that of Lewis *et al.* (1979) who calculated carbon inventories for the terrestrial planets. In the present study the results of an extensive set of equilibrium calculations for the alkalis, halogens, and phosphorus are described.

The objectives of this study are threefold. The first objective is to describe the equilibrium chemistry of the elements Na, K, F, Cl, Br, and P in a solar composition system over a wide range of temperatures and pressures.

The results of the calculations are presented in some detail because the equilibrium chemistry of the elements studied has been either totally neglected or only cursorily examined by previous workers. No results are presented for Li, Rb, Cs, and I because there are insufficient thermodynamic data for many potentially important gases and condensates of these elements. Some limited information on the equilibrium chemistry of lithium in a solar composition system may however be found in Wai and Wasson (1977).

The second objective is to use the results of the equilibrium calculations to discuss volatile element retention by the terrestrial planets. To this end the results of two extreme models of accretion - the strict homogeneous and strict heterogeneous accretion models - are compared with observational data on abundances of the elements studied. The discussion of the two endmember accretion models is based on the concept of a turbulent, chemically homogeneous solar nebula. However, recent work by Cameron (1978) suggests that the nebula may have broken up into a collection of giant gaseous protoplanets, especially at great distances from the Sun. Although the chemical consequences of terrestrial planet formation inside giant gaseous protoplanets may be very different from the consequences of either endmember accretion model being considered,

the complex evolutionary histories proposed for the giant gaseous protoplanets make the chemical consequences of protoplanet formation highly model dependent, and thus difficult to quantify. The present discussion will therefore be restricted to a comparison of the two extreme accretion models for terrestrial planet formation in the solar nebula.

The third and final objective is to provide a firm basis for further discussion of the chemistry of the volatile elements studied. The present results can be used to discuss certain features of chondrite mineralogy (Fegley, 1979a,b,c) and can be integrated into a more quantitative condensation-accretion model in preparation (Barshay and Lewis, 1979).

METHOD OF CALCULATION

Chemical equilibrium calculations were done from 10^{-7} to 10 bars pressure at pressures of 10^{-7}, 10^{-5}, 10^{-4}, 10^{-3}, 10^{-1}, and 10 bars as well as along an adiabatic temperature-pressure profile in the primitive solar nebula (PSN). The temperature range covered was 2100°-300°K.

An adiabatic temperature-pressure profile for the primitive solar nebula was constructed stepwise using the relationship

$$(P/P_o) = (T/T_o)^{C_p/R}, \qquad (1)$$

where P is the total pressure, T the temperature, C_p the bulk heat capacity at temperature T, and R the ideal gas constant. The starting point for the adiabat (P_o, T_o) was chosen as 10^{-4} bar, 600°K, consistent with available compositional data on planets and satellites and Cameron's nebular models (Lewis, 1974, and references therein).

The heat capacity data for hydrogen and helium at various temperatures were obtained from the Handbook of Chemistry and Physics (1961), and a solar abundance ratio (Cameron, 1973) of H_2 to He (0.122 He + 0.878 H_2) was assumed. The heat capacities of the other gases, which account for less than 1 mole %, were ignored.

The calculated nebular adiabat is shown in Figure I-1. The horizontal scales in Figures I-3 and I-4 display numerically the relationships between temperature and pressure and temperature and heliocentric distance along the adiabat. The distance scale was calculated using the relationship

$$(T/T_o) = (R/R_o)^{-1.1}, \qquad (2)$$

where T is the temperature and R is the heliocentric distance in astronomical units (A.U.). The starting point for the distance scale (T_o, R_o) was chosen as 600°K, 1A.U. Both the chosen functional relationship between temperature and

distance in the nebula, and the (T_o, R_o) point are consistent with the arguments of Lewis (1974).

The assumed solar elemental abundances used in the calculations, which are listed in Table I-1, were taken from Cameron (1973). The equilibrium stability fields and abundances of some silicate minerals and iron metal along the nebular adiabat were taken from Barshay and Lewis (1979), with some recalculations to adjust for changes in the thermodynamic data for iron oxides, iron-bearing silicates, and alkali aluminosilicates. Thermodynamic data were taken from the JANAF Tables and subsequent supplements (Stull and Prophet, 1971; Chase et al., 1974; Chase et al., 1975; Chase et al., 1978), the Geological Survey thermodynamic tables (Robie et al., 1978; Robie and Waldbaum, 1968), the National Bureau of Standards compilations (Parker et al., 1971; Wagman et al., 1968; Wagman et al., 1969; Wagman et al., 1976), and a variety of other sources (Duff, 1972a, 1972b; Gottschal, 1958; Jacques, 1963; Komarek, 1963; Letoffe et al., 1974; Letoffe et al., 1976; Mills, 1974; Oetting and McDonald, 1963; Orville, 1972; Richardson and Jeffes, 1949; Saxena, 1973; Seck, 1971; Weibke and Schrag, 1941; and Wellman, 1969). In several cases the tabulated equilibrium constants were incorrect

TABLE I-1

Abundances of the Elements from Cameron (1973)

Element	Normalized Abundance (Si=10^6)
H	31.8×10^9
He	2.21×10^9
O	21.5×10^6
C	11.8×10^6
N	3.74×10^6
Mg	1.06×10^6
Si	1.00×10^6
Fe	0.83×10^6
S	0.50×10^6
Al	85×10^3
Ca	72×10^3
Na	60×10^3
P	9600
Cl	5700
K	4200
F	2450
Br	13.5

and had to be recalculated. For example, the tabulated log K_f data for many phosphorus compounds in Robie and Waldbaum (1968) and Robie et al. (1978) are in error because the $\Delta H^\circ_{f,298}$ values are based upon a white phosphorus reference state while the log K_f values are calculated using the Gibbs energy functions $[(G^\circ-H^\circ_{298})/T]$ for red phosphorus. When the log K_f values are recalculated using a consistent red phosphorus reference state the differences in log K_f are found to be on the order of 3-4 (differences in K_f of a factor of 10^3 to 10^4). (Two separate printings of Robie et al. (1978) USGS Bulletin 1452 are now available. The first printing is the one used in this work. The second printing, which became available only after this work was completed, contains revised tables for phosphorus-bearing compounds as well as for several aluminosilicates. It is important to note that the hydroxyapatite table in the second printing is still incorrect.)

It was also necessary in several cases to calculate from the literature data the equilibrium constant for formation of an element or compound from the constituent elements in their designated reference states. If at all possible this calculation was done by a third law method and double checked using data from a separate source. In some cases a second law method, which is less accurate, was used.

A special discussion of the thermodynamic data used to

calculate log K_f values for chlorapatite and bromapatite is also necessary. Both $\Delta H^\circ_{f,298}$ (Gottschal, 1958) and $\Delta G^\circ_{f,298}$ (Duff, 1972b) values for chlorapatite are available. However, the combination of the data yields a S°_{298} value for chlorapatite which is too low relative to the S°_{298} values for fluor- and hydroxyapatite. Since the $\Delta H^\circ_{f,298}$ values measured by Gottschal (1958) for fluorapatite and hydroxyapatite agree within 1% with other experimental and tabulated values (Jacques, 1963; Parker et al., 1971), his $\Delta H^\circ_{f,298}$ value for chlorapatite has been combined with an estimated S°_{298} value to calculate log K_f values by the second law method. Only a $\Delta G^\circ_{f,298}$ value (Duff, 1972a) for bromapatite is available and it was again necessary to estimate a S°_{298} value in order to calculate log K_f values. In both cases the entropy estimates were made by three separate methods which yielded results that agree within 1%. The subsequent uncertainty in the log K_f values is probably less than that due to the experimental error in the $\Delta H^\circ_{f,298}$ and $\Delta G^\circ_{f,298}$ determinations. Discussion of entropy estimation methods can be found in Stull and Prophet (1967) and Kubaschewski et al. (1967).

The basic computational method used will only be briefly summarized here because similar methods have been described in detail by Barshay and Lewis (1978), Grossman (1972), and Larimer and Bartholomay (1979). The thermodynamic calculations along the nebular adiabat involve the simultaneous determination of the equilibrium abundances of

of all compounds (gases and condensed phases) included in the data set. A mass balance expression, which equates the total abundance (solar abundance) of an element to the sum of the abundances of all compounds containing the element, is written for each element in the data set. All compounds for which reliable thermodynamic data are available are included. The abundance of each compound in the mass balance equation is multiplied by the appropriate stoichiometric coefficient, which is the number of atoms of element in the compound. For example, the mass balance equation for Na is written

$$A_{Na}(\text{Total}) = A_{Na(g)} + A_{NaCl(g)} + 2A_{Na_2SiO_3(ss)} + A_{NaAlSiO_4(c)} + \cdots \quad (3)$$

where the A_i terms are abundances expressed in some consistent units, the label (g) indicates a gas, the label (ss) indicates a solid solution, and the label (c) indicates a pure crystalline phase. The system of mass balance equations is then solved by an iterative technique. A solution is obtained when for each element E

$$(\Sigma E - A_E)/\Sigma E \leq 10^{-5} \quad (4)$$

where ΣE is the assumed solar elemental abundance from

Cameron (1973) and A_E is the total elemental abundance from equation (3).

More than 200 gases and condensates were included in the calculations for this study. Gases were included in Figures I-2 to I-5 if their equilibrium mole fraction along the nebular adiabat was greater than 10^{-15} at any temperature within the range covered by the figure. The abundances and stability fields of condensates stable at equilibrium are also indicated in the figures. Pure condensed phases, e.g., Fe_3P, are stable when their thermodynamic activities equal 1 and are unstable at activities less than 1. Condensed phases which form solid solutions, such as the alkali feldspars, are stable at activities less than 1. Condensates which were found to be either unstable or unimportant within the temperature range of a figure and gases which did not satisfy the above stated criterion are listed in Appendix I.

THE HOMOGENEOUS ACCRETION MODEL

The homogeneous accretion model assumes intimate contact between the condensed and gaseous phases, thereby allowing complete chemical equilibrium between all gases and condensates. The chemical composition of the system is a thermodynamic state function and is path independent.

Assuming that chemical equilibrium is attained and that the system has solar composition, the results presented in Figures I-1 to I-5 and Table I-2 therefore apply to condensation from a hot totally vaporized mixture, volatilization of a homogeneous cold gas and dust mixture, or any intermediate case.

Figure I-1 shows the condensation and formation curves for condensates of the elements Na, K, F, Cl, Br and P, the condensation and reaction curves from Barshay and Lewis (1976) for some compounds of the major elements, the adiabatic pressure-temperature profile for the primitive solar nebula, and a qualitative representation of the formation zones for the terrestrial planets.

Several important points are demonstrated by Figure I-1. First, the sequence of reactions and the composition of condensed phases present at equilibrium are generally pressure independent. Second, the volatile contents (Na, K, F, Cl, Br, and P) of the terrestrial planets and asteroids are in principle predictable by use of this simplified chemical equilibrium model. Third, the correspondence between the phases present at equilibrium and the observed mineralogy of ordinary chondrites reinforces the plausibility of a close approach to chemical equilibrium in the primitive solar nebula.

FIGURE I-1: Stability limits of condensates at chemical equilibrium in a solar composition system from 0 to 2100°K and 10^{-7} to 10 bars total pressure. The $CaTiO_3$ condensation curve, which represents the condensation limits of several refractory oxides, the Fe condensation curve, the $MgSiO_3$ condensation curve, and the tremolite $[Ca_2Mg_5[Si_8O_{22}] (OH)_2]$ condensation curve are from Barshay and Lewis (1976). An adiabatic pressure-temperature profile in the solar nebula and qualitative formation zones for the terrestrial planets are also shown. The astrological symbols from top to bottom along the adiabat represent Mercury, Venus, Earth, and Mars, respectively.

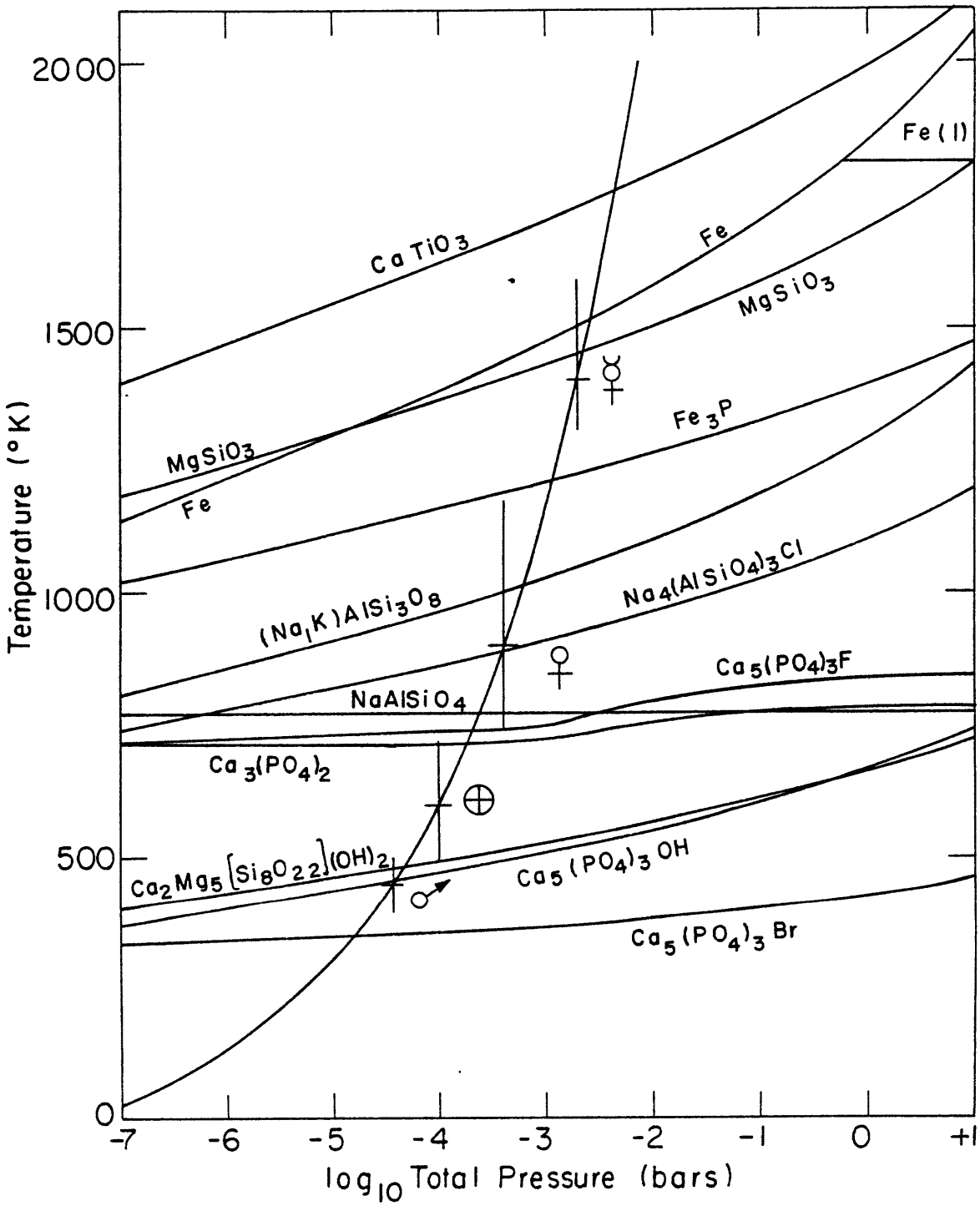
2000
1500
1000
500
0
Temperature (°K)
-7
-6
-5
-4
-3
-2
-1
0
+1
log10 Total Pressure (bars)
Fe (l)
CaTiO3
Fe
MgSiO3
Fe3P
MgSiO3
Fe
(Na,K)AlSi3O8
Na4(AlSiO4)3Cl
Ca5(PO4)3F
NaAlSiO4
Ca3(PO4)2
Ca2Mg5[Si8O22](OH)2
Ca5(PO4)3OH
Ca5(PO4)3Br

Table I-2 and Figures I-2 to I-5 provide information on the equilibrium chemistry of Na, K, F, Cl, Br and P along the nebular adiabat. The results of the calculations are discussed element by element in order of decreasing abundance. Compounds which do not appear in the figures due to extremely low abundances or activities less than 1 are listed in Appendix I.

Sodium

Figure I-2 illustrates the equilibrium abundances and stability fields of sodium-bearing compounds along the nebular adiabat. The abundances at equilibrium of both gaseous and condensed sodium-bearing compounds are shown in the figure. Half of all sodium is condensed in plagioclase feldspar ($NaAlSi_3O_8$ - $CaAl_2Si_2O_8$) by 948°K, and condensation is quantitative at about 858°K. Thermodynamic data for analbite (Robie et al., 1978) and activity coefficient data for plagioclase feldspar (Orville, 1972: Saxena, 1973) were used in the calculations. The 50% condensation curve for $NaAlSi_3O_8$ in plagioclase feldspar is shown in Figure I-1. Sodium silicate (Na_2SiO_3) dissolved in enstatite ($MgSiO_3$) as an ideal solution never exceeds 1% of total sodium. The albite abundance is reduced by the formation of sodalite ($Na_4Al_3Si_3O_{12}Cl$) at about 895°K and later by nepheline ($NaAlSiO_4$) formation at about 775°K. The albite, sodalite,

FIGURE I-2: Equilibrium abundances and stability fields of sodium-bearing gases and condensates along the nebular adiabat. The temperature scale is linear in 1/T. The mole fraction X_i of a species i is defined as its partial pressure P_i divided by the total pressure P. The heavy lines indicate the stability fields of the four condensates whose abundances are also shown graphically. The abbreviations (c) and (ss) following the condensate formulas indicate a pure crystalline solid and a solid solution, respectively. The fraction of total sodium in each compound is also shown.

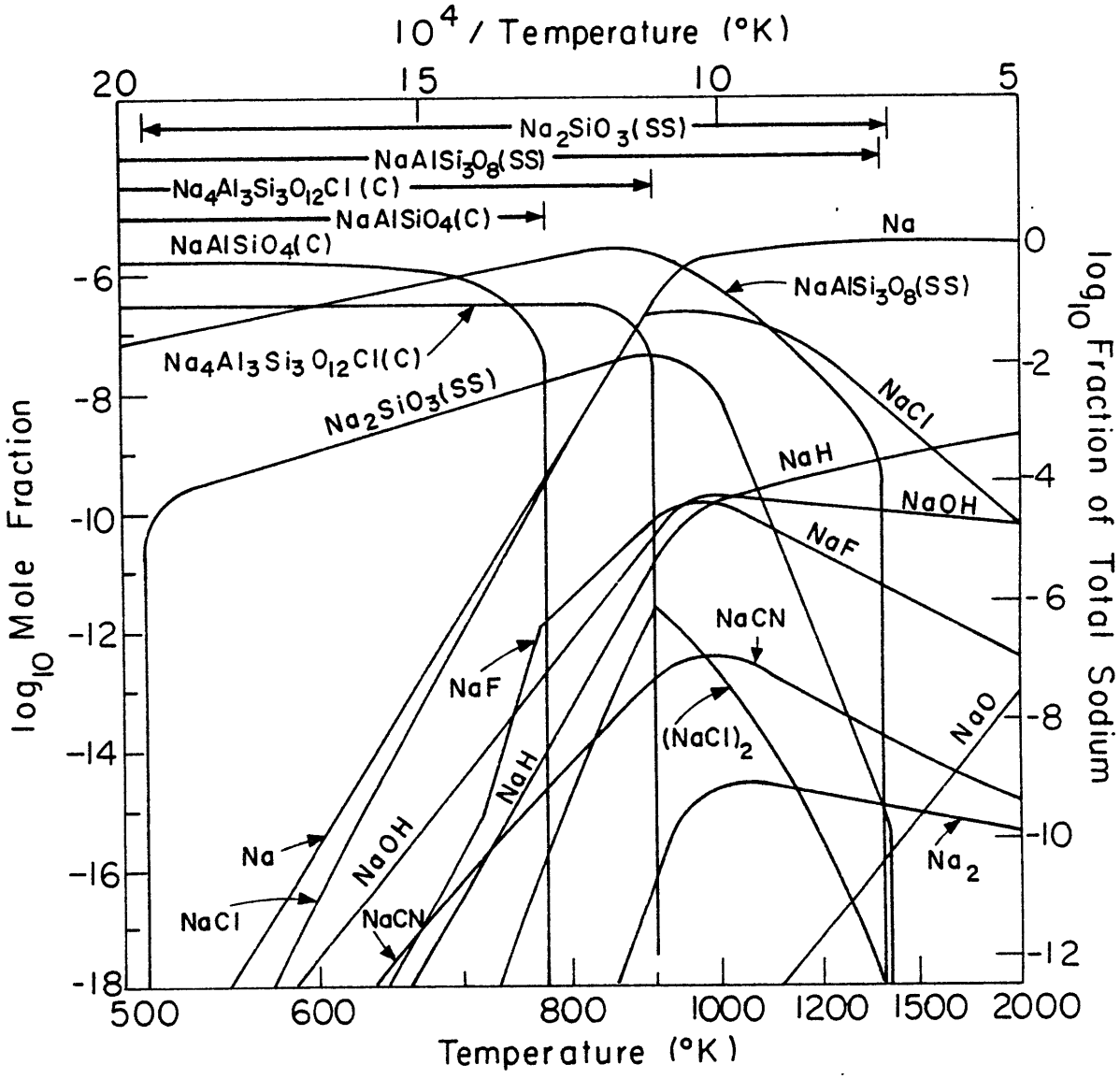
10^4 / Temperature (°K)
20
15
10
5
Na_2SiO_3(SS)
$NaAlSi_3O_8$(SS)
$Na_4Al_3Si_3O_{12}Cl$(C)
$NaAlSiO_4$(C)
$NaAlSiO_4$(C)
Na
$NaAlSi_3O_8$(SS)
$Na_4Al_3Si_3O_{12}Cl$(C)
Na_2SiO_3(SS)
NaCl
NaH
NaOH
NaF
NaCN
NaF
$(NaCl)_2$
NaO
NaH
Na
NaOH
NaCl
NaCN
Na_2
$\log_{10}$ Mole Fraction
$\log_{10}$ Fraction of Total Sodium
-6
-8
-10
-12
-14
-16
-18
0
-2
-4
-6
-8
-10
-12
500
600
800
1000
1200
1500
2000
Temperature (°K)

TABLE I-2

The Homogeneous Accretion Model:

Chemical Reactions Along the Nebular Adiabat

T(°K)	Reaction
1520	Condensation of Fe-Ni alloy (Taenite)
1455	Condensation of $MgSiO_3$ (Enstatite)
1225	Condensation of Fe_3P (Schreibersite)
950-1050	50% condensation of $(Na,K)AlSi_3O_8$ in Plagioclase Feldspar
895	Formation of $Na_4(AlSiO_4)_3Cl$ (Sodalite)
766	Formation of $Ca_5(PO_4)_3F$ (Fluorapatite)
714	Formation of $Ca_3(PO_4)_2$ (Whitlockite)
687	Fe-Ni alloy + H_2S (g) = (Fe,Ni)S (Troilite)
480	Calcium silicates + H_2O (g) = Tremolite
∿460	Whitlockite reacts to form $Ca_5(PO_4)_3OH$ (Hydroxyapatite)
∿350	Formation of $Ca_5(PO_4)_3Br$ (Bromapatite)

and nepheline stability fields all extend below 500°K. The high temperature limits of the sodium silicate and albite stability fields correspond to the appearances of enstatite and anorthite ($CaAl_2Si_2O_8$), respectively. The low temperature limit to the Na_2SiO_3 stability field coincides with the disappearance of enstatite at about 511°K.

The present $NaAlSi_3O_8$ condensation results can be compared with other results from the cosmochemical literature. Grossman (1972) reports that at 10^{-3} atmospheres plagioclase contains 2 mole % $NaAlSi_3O_8$ (high albite) by 1200°K and he estimates that pure alkali feldspars are stable by 1000°K. Later work by Lattimer and Grossman (1978) refines this estimate and indicates that $NaAlSi_3O_8$ (presumably high albite) becomes stable at 1028°K at 10^{-3} atmospheres pressure. In comparison, the present work indicates that analbite becomes stable at 992°K along the primitive solar nebula (PSN) adiabat if analbite solid solution in anorthite is neglected. The small difference between the two sets of results is probably due to the pressure difference (at ~1000°K the PSN adiabat pressure is about 6×10^{-4} bars) and to differences in the $NaAlSi_3O_8$ thermodynamic data used in the two investigations.

A comparison of $NaAlSi_3O_8$ 50% condensation temperatures from Wai and Wasson (1977) and from the present

work also shows only small differences between the results. Wai and Wasson (1977) report $NaAlSi_3O_8$ (presumably high albite) 50% condensation temperatures of 874°K and 982°K at 10^{-6} atmospheres and 10^{-4} atmospheres pressure, respectively. The analbite 50% condensation temperatures from Figure I-1 are 861°K and 970°K at 10^{-6} bars and 10^{-4} bars pressure, respectively. Again the small differences between the two sets of results are probably due to the differences in the $NaAlSi_3O_8$ and $CaAl_2Si_2O_8$ thermodynamic data used in the two investigations. The possible neglect of NaCl(g), which is the second most abundant sodium-bearing gas, by Wai and Wasson (1977) may also be a factor contributing to the observed differences between results. It is therefore concluded that the present $NaAlSi_3O_8$ condensation results are in good agreement with results from previous investigations. No previous nepheline and sodalite condensation results have been reported and thus no comparison is possible.

As previously noted, $NaAlSi_3O_8$ condenses at 992°K along the PSN adiabat if solid solution in anorthite is neglected. Furthermore, $NaAlSiO_4$ condenses at 980°K, neglecting the prior effect of $NaAlSi_3O_8$ condensation. These calculations were done using analbite and nepheline thermodynamic data from Robie et al. (1978). What is the

effect (if any) of the tabulated uncertainties in the analbite and nepheline thermodynamic data upon the condensation temperatures of the two phases?

Using the least positive analbite log K_f values permitted by the uncertainty in the data yields an analbite condensation temperature of 976°K along the PSN adiabat. Using the most positive nepheline log K_f values permitted by the uncertainty in the data yields a nepheline condensation temperature of 987°K along the PSN adiabat. The analbite-nepheline condensation order is now reversed, and once nepheline forms, pure analbite is not stable.

The uncertainties in the alkali aluminosilicate thermodynamic data which are responsible for the changes in the analbite and nepheline condensation temperatures are extremely small on both an absolute and a relative basis. The uncertainties ($\pm$) in the analbite and nepheline ΔG_f° values are ≤ 1 kcal mole^{-1} for ΔG_f° values which are on the order of 10^3 kcal mole^{-1} (approximately a 0.1% uncertainty). On a percentage basis, the uncertainty in the ΔG_f° data for H_2O (liquid), which are some of the most accurate thermodynamic data available, is barely a factor of 5 better (an uncertainty of ~0.02%)!

Factors such as the physical state of the sample and experimental difficulties in the measurement of enthalpy and

heat capacity values, which are responsible for the uncertainty in the analbite and nepheline thermodynamic data, are reviewed in detail elsewhere (Helgeson et al., 1978; Kubaschewski et al., 1967) and will not be discussed here. Suffice it to say that it will be difficult to reduce the small uncertainty in the present data. Thus, on the basis of available thermodynamic data alone it is impossible to unambiguously identify the first sodium-bearing condensate. In fact the nature of this condensate may be critically dependent upon local nebular conditions such as slight departures from strict chemical equilibrium. This point will be discussed further in the section on chondrite mineralogy.

The sodalite condensation temperature, however, is relatively insensitive to large uncertainties in the sodalite thermodynamic data. Sodalite condenses at 953°K along the PSN adiabat (neglecting prior condensation of other alkali-bearing phases). This calculation is based on sodalite thermodynamic data calculated from the vapor pressure measurements of Wellman (1969). The uncertainties in Wellman's NaCl(g) vapor pressure measurements produce an insignificant $\pm$ 2°K change in the sodalite condensation temperature. Furthermore, a thousand-fold increase or decrease in the sodalite equilibrium constants produces only

a $\pm$ 45°K change in the sodalite condensation temperature. Therefore, the present sodalite condensation temperature is regarded as a reasonably certain value that will not be significantly changed when more accurate sodalite thermodynamic data become available.

Phosphorus

The abundances and stability fields of phosphorus-bearing compounds under equilibrium conditions along the nebular adiabat are shown in Figure I-3. The first phosphorus-bearing condensate is schreibersite (Fe_3P) which appears at about 1225°K. Phosphorus is 50% condensed at about 1169°K and is completely condensed by 1053°K. Fluorapatite [$Ca_5(PO_4)_3F$] is formed from Fe_3P at 766°K and the remaining schreibersite reacts to form whitlockite [$Ca_3(PO_4)_2$] at 714°K. The whitlockite and fluorapatite stability fields extend below 500°K. Hydroxyapatite formation as a pure phase and as an ideal solid solution in fluroapatite has also been considered. In the former case hydroxyapatite formation depletes the remaining whitlockite at about 460°K, while in the latter case all whitlockite is converted to hydroxyapatite at about 507°K.

Figures I-1 illustrates the schreibersite, fluorapatite, whitlockite, and hydroxyapatite condensation curves from 10^{-7} to 10 bars pressure. The whitlockite condensation

FIGURE I-3: Abundances and stability fields of phosphorus-bearing compounds along the nebular adiabat under equilibrium conditions. The scale across the top shows the radial distance in astronomical units (AU) from the center of the primitive solar nebula. The heavy lines indicate the stability fields of the four condensates whose abundances are also shown graphically. Phosphorus is 50% condensed at about 1169°K and is completely condensed by about 1053°K. The high temperature limit of the phosphorus-iron solution corresponds to the iron condensation point.

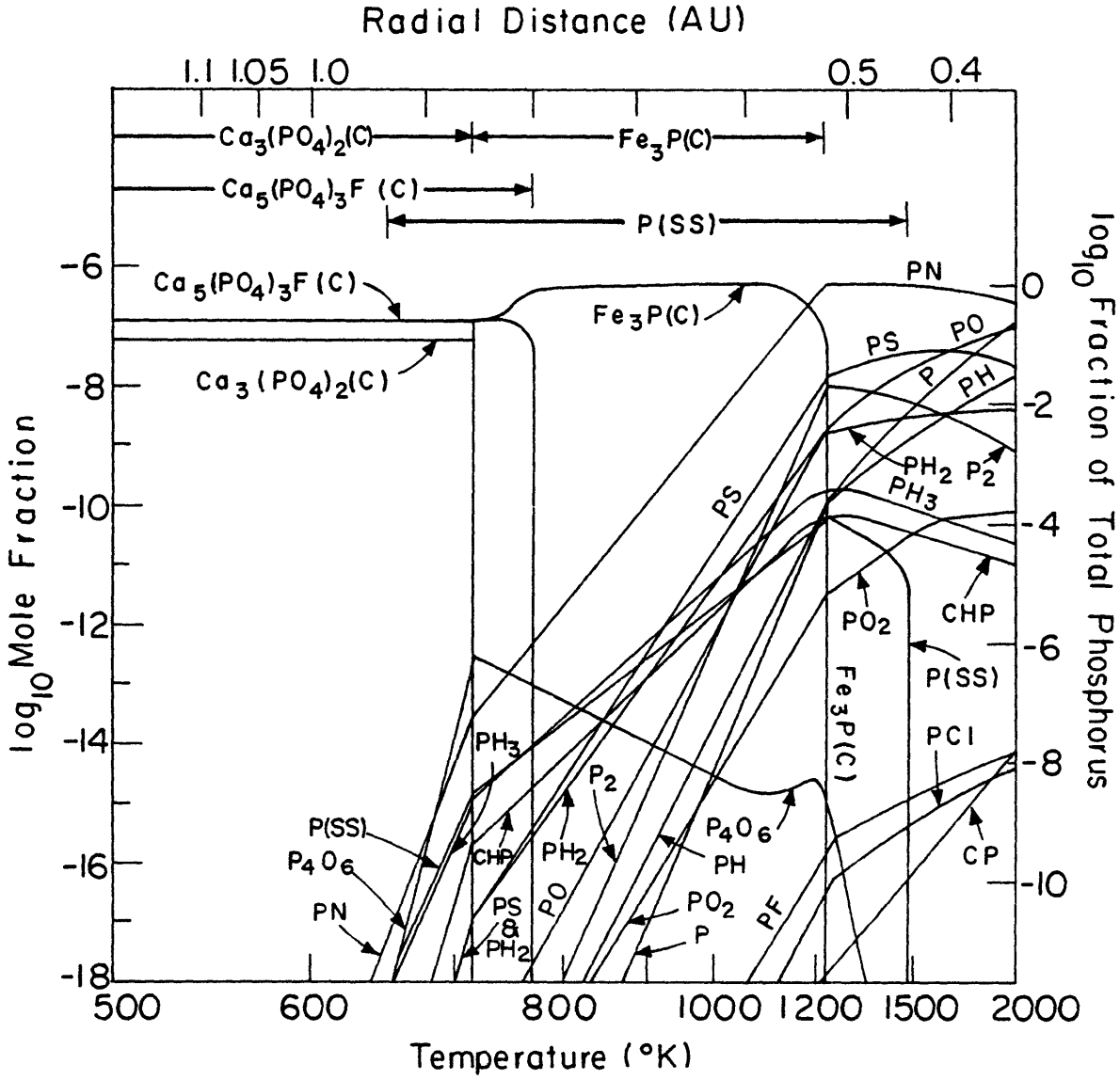
Radial Distance (AU)
1.1 1.05 1.0
0.5 0.4
$Ca_3(PO_4)_2(C)$
$Fe_3P(C)$
$Ca_5(PO_4)_3F$ (C)
P(SS)
$Ca_5(PO_4)_3F$ (C)
$Ca_3(PO_4)_2(C)$
$Fe_3P(C)$
PN
PS
PO
P
PH
PH_2
P_2
PH_3
PO_2
CHP
P(SS)
PCl
CP
P_4O_6
PF
$Fe_3P(C)$
log_{10} Mole Fraction
log_{10} Fraction of Total Phosphorus
-6
-8
-10
-12
-14
-16
-18
0
-2
-4
-6
-8
-10
500
600
800
1000
1200
1500
2000
Temperature (°K)

curve is pressure-independent in the regions of P-T space where CO and CH_4 are the dominant carbon-bearing gases, and has an inflection at the CO/CH_4 watershed where the abundances of these two gases are equal. The hydroxyapatite condensation curve in Figure I-1 is for condensation of pure hydroxyapatite.

Several other authors (Grossman and Olsen, 1974; Wai and Wasson, 1977; and Sears, 1978) have calculated schreibersite condensation temperatures, and the present results can be compared with theirs. The Fe_3P condensation temperatures from Figure I-1 are 100°-300° lower than the literature values, and the largest discrepancies are with the values of Sears (1978). For example, at 10^{-3} bars pressure the Fe_3P condensation temperatures calculated by Sears (1978), Grossman and Olsen (1974), and Wai and Wasson (1977) are 1479°K, 1416°K and 1416°K, respectively, while the value from the present work is 1210°K.

Although Grossman and Olsen (1974), Wai and Wasson (1977), and Sears (1978) cite different sources for their Fe_3P thermodynamic data, all the sources cited ultimately derived the same (estimated) data from an evaluation by Richardson and Jeffes (1949) of the Fe_3P enthalpy determinations of Weibke and Schrag (1941). However, the data used by Richardson and Jeffes to calculate ΔG_f° values for

Fe_3P are out of date and disagree with currently recommended values. For example, for the change in state

$$P_4(g) = 2P_2(g) \qquad 298.15°K$$

Richardson and Jeffes use the enthalpy value of +32,076 cal $mole^{-1}$ while the JANAF value is +54,590 cal $mole^{-1}$. The CODATA enthalpy value for this change in state is +54,756 cal $mole^{-1}$, in good agreement with the JANAF value (CODATA Task Group, 1977).

Therefore, the Fe_3P enthalpy data have been re-evaluated by the same method used by Richardson and Jeffes (1949) but using revised values for the auxiliary thermodynamic data required. This recalculation of Fe_3P log K_f values insures consistency since the same auxiliary data are used to calculate log K_f values for all phosphorus compounds in the data set. It is gratifying to note that an independent estimate of the thermodynamic properties of Fe_3P by Spencer and Kubaschewski (1978) yields log K_f values in excellent agreement with the values calculated in this way.

In addition, Sears (1978) reports that $P_2(g)$ is the dominant phosphorus gas in the temperature range where Fe_3P condensation is occuring and that the alloying effect of Ni_3P raises the Fe_3P condensation temperature significantly. Results from the present work do not verify either

assertion and show instead that the $P_2(g)$ abundance never exceeds 5% of the total phosphorus abundance over the range 300°-2000°K and 10^{-7}-10 bars and that consideration of $(Fe,Ni)_3P$ solid solution only increases the phosphide condensation temperature by ∿2°K. This ΔT is comparable to the 3° - 5°K increase in the Fe condensation temperature due to Ni solid solution (Grossman, 1972; Wai and Wasson, 1977).

It is also important to note that the phosphide condensation temperatures of the previous investigators can be reproduced by using the appropriate log K_f values and phosphorus fugacities. For example, the results of Grossman and Olsen (1974) and Wai and Wasson (1977) can be duplicated by using the Richardson and Jeffes log K_f data for Fe_3P and calculated phosphorus fugacities from the present work. Also the results of Sears (1978) can be reproduced by assuming $P_2(g)$ to be the dominant phosphorus gas and by using the Richardson and Jeffes log K_f values without considering Ni_3P solid solution.

Although ideal solution of phosphorus in iron has been assumed in the results in Figure I-3, the effect of nonideality in the P-Fe alloy upon the Fe_3P condensation temperature has also been considered. Assuming that all

phosphorus is originally dissolved in the iron metal, and taking an activity coefficient of 10^{-5} for the P-Fe alloy, then Fe_3P condensation along the nebular adiabat is lowered by only 70°. It is therefore justifiable to ignore the effects of nonideality in the P-Fe alloy which are probably less than the effects of the uncertainty in the Fe_3P thermodynamic data.

Finally, the present whitlockite condensation temperatures have been compared with some literature values (Wai and Wasson, 1977; Sears, 1978). Wai and Wasson (1977) state that whitlockite is a stable phase below 900°K at 10^{-4} atmospheres pressure and Sears (1978) reports a whitlockite condensation temperature of 770°K. The present value is 714°K. The minor discrepancies appear to be due to differences in the thermodynamic data. Wai and Wasson (1977) and Sears (1978) used the whitlockite thermodynamic data from Robie and Waldbaum (1968) which are incorrect due to inconsistent phosphorus reference states used in compiling the tables. Data for several phosphorus-bearing compounds in the recent compilation of Robie *et al.* (1978) are also incorrect for the same reason. Where necessary the log K_f values for phosphorus-bearing compounds which are included in the present calculations have been recalculated.

Halogens

The equilibrium behavior of chlorine-, fluorine-, and bromine-bearing compounds along the nebular adiabat is shown in Figure I-4 and the stability fields for the pure phases sodalite, fluorapatite, and bromapatite are illustrated in Figure I-1. Sodalite ($Na_4Al_3Si_3O_{12}Cl$) condensation starts at about 895°K and fluorapatite [$Ca_5(PO_4)_3F$] condensation begins at 766°K. Chlorine is 50% condensed at 873° and completely condensed at 823°K. Fluorine condensation is complete by 741°K. No bromine-bearing condensate is stable above 500°K. Bromapatite [$Ca_5(PO_4)_3Br$] condensation as a pure phase occurs around 350°K, and condensation as an ideal solid solution in fluorapatite is complete at about 434°K. However, the bromapatite condensation calculations are based on low-quality thermodynamic data and may involve a considerable uncertainty. Thermodynamic data are lacking for the fluorine and bromine analogs of sodalite and it is conceivable that these phases could condense at higher temperatures than fluorapatite and bromapatite. The thermodynamic activity of chlorapatite [$Ca_5(PO_4)_3Cl$] does not exceed 10^{-6} over the temperature range considered and chlorapatite solid solution in fluorapatite is of negligible importance for chlorine

FIGURE I-4: Abundances and stability fields of chlorine-, fluorine-, and bromine-bearing compounds along the nebular adiabat under equilibrium conditions. The scale across the top shows the approximate total pressure in millibars along the adiabat. The heavy lines indicate the stability fields of the condensates. The abundances of the condensates are also illustrated. Chlorine is 50% condensed at about 873°K and is completely condensed at 823°K. Fluorine is completely condensed at about 741°K. Bromine condensation as $Ca_5(PO_4)_3Br$ does not begin until approximately 350°K.

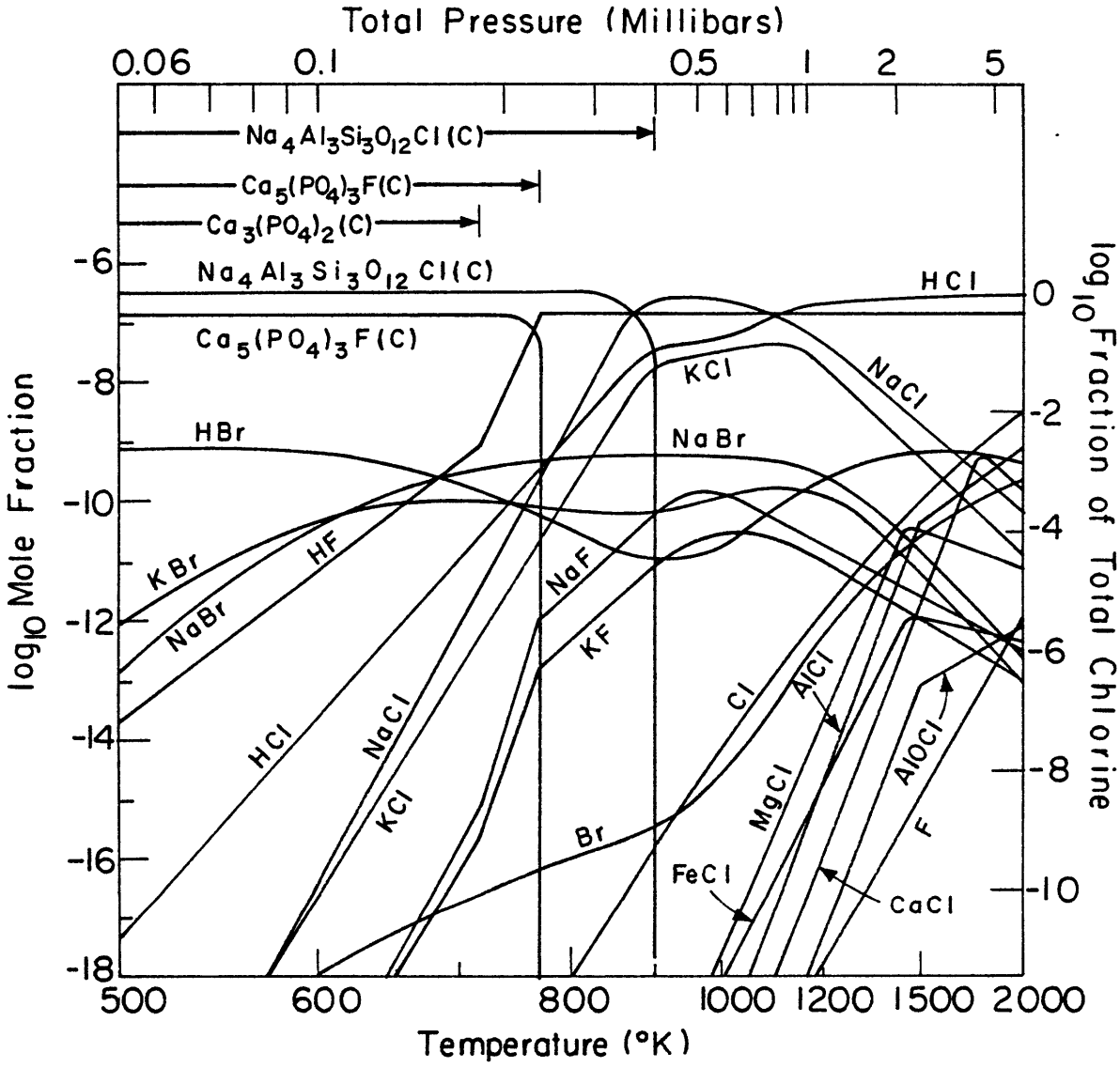
Total Pressure (Millibars)
0.06
0.1
0.5
1
2
5
$Na_4Al_3Si_3O_{12}Cl(C)$
$Ca_5(PO_4)_3F(C)$
$Ca_3(PO_4)_2(C)$
$Na_4Al_3Si_3O_{12}Cl(C)$
$Ca_5(PO_4)_3F(C)$
HBr
KBr
NaBr
HF
HCl
NaCl
KCl
NaF
KF
HCl
KCl
NaCl
NaBr
Cl
AlCl
AlOCl
MgCl
F
Br
FeCl
CaCl
-6
-8
-10
-12
-14
-16
-18
0
-2
-4
-6
-8
-10
500
600
800
1000
1200
1500
2000
Temperature (°K)
$\log_{10}$ Mole Fraction
$\log_{10}$ Fraction of Total Chlorine

retention. For example, at 700°K ideal solid solution of chlorapatite in fluorapatite accounts for only 10^{-5} % of all chlorine.

Wai and Wasson (1977) have calculated 50% condensation temperatures at 10^{-4} bars pressure for fluorapatite and the present results can be compared with theirs. Wai and Wasson report that pure fluorapatite is 50% condensed at 800°K and that fluorapatite with an activity of 0.2 and assumed to be in solution with chlorapatite or other minerals is 50% condensed at 855°K. The present results indicate that along the nebular adiabat fluorapatite condensation starts at 766°K and is complete by 741°K. The differences between the present results and the results of Wai and Wasson (1977) are possibly due to the assumptions made by Wai and Wasson in their calculations and the thermodynamic data they used. For example, Wai and Wasson assumed the presence of whitlockite in their condensation calculations for fluorapatite. However, the present results show that whitlockite does not condense until 714°K, 52° below the onset of fluorapatite condensation. Also, the assumption of fluorapatite solution in chlorapatite is suspect because the present work indicates that chlorapatite condensation does not take place after sodalite condenses. Furthermore, Wai and Wasson used the fluorapatite thermodynamic data

of Robie and Waldbaum (1968), which are incorrect.

Recent determinations of fluorine abundances in chondritic meteorites and in the Sun yield fluorine solar abundances approximately 2-3 times lower than the Cameron (1973) fluorine abundance (Dreibus et al., 1979; Goldberg et al., 1974; Mason, 1979; Pagel, 1979; Suess, 1980). Therefore, the effect of a lower fluorine abundance upon the fluorine condensation results has been briefly investigated. Dreibus et al. (1979) list a fluorine abundance of F=780 on the Si=10^6 scale. Use of their fluorine abundance yields a fluorapatite condensation temperature only 8°K lower than the fluorapatite condensation temperature calculated previously. However, due to the lower fluorine abundance, fluorapatite is now less abundant than whitlockite with the fluorapatite accounting for ∿24% of all phosphorus and the whitlockite accounting for ∿76% of all phosphorus. Recent determinations of the chlorine and bromine solar abundances (Dreibus et al., 1979; Mason, 1979; Suess, 1980) are in good agreement with the Cameron (1973) chlorine and bromine abundances and no calculations based on more recent abundances were done. (A more comprehensive discussion of halogen abundances is given in the section on volatile element retention by the terrestrial planets.)

The present calculations, which indicate that

chlorapatite is never stable once sodalite condenses, are based on chlorapatite log K_f values calculated from an estimated S°_{298} value. Thus, the sensitivity of the results to variations in the chlorapatite log K_f values has been investigated. The uncertainty in the chlorapatite S°_{298} estimate is taken as approximately $\pm$ 1 cal deg^{-1} $mole^{-1}$ on the basis of (1) entropy estimates for fluorapatite, hydroxyapatite, and other compounds for which S°_{298} values are available and (2) 1% agreement between entropy estimates made by three separate methods. This entropy uncertainty translates to an uncertainty of about $\pm$ (0.3-1) kcal $mole^{-1}$ for ΔG°_f values which are on the order of 10^3 kcal $mole^{-1}$. However, this small uncertainty is insufficient to make chlorapatite condense before sodalite condenses or to make chlorapatite stable after sodalite condenses. In fact, the chlorapatite ΔG°_f value at 900°K must be increased by about 50 kcal $mole^{-1}$ (about 5% of the ΔG°_f value) to allow chlorapatite condensation.

Although an uncertainty of several tens of kcal $mole^{-1}$ is clearly not due to uncertainties in the chlorapatite S°_{298} estimate, it could conceivably be due to two factors: (1) experimental errors in the $\Delta H^\circ_{f,298}$ determinations by Gottschal (1958) and (2) uncertainties introduced by the

second law treatment of the data. It is difficult to quantify the effect of these two factors and no attempt to do so will be made. However, it should be noted that the $\Delta H^{\circ}_{f,298}$ values measured by Gottschal (1958) for fluorapatite and hydroxyapatite agree within 1% with other experimental and tabulated values (Jacques, 1963; Parker et al., 1971). Furthermore, experience indicates that log K_f values calculated from second law and third law treatments generally are in good agreement.

Finally, the question of chlorapatite stability in the absence of sodalite condensation has been briefly considered. Assuming that all chlorine is present in the gas phase as HCl(g) and NaCl(g), chlorapatite condensation is predicted to occur in the 656-678°K range along the PSN adiabat. However, halite (NaCl) condensation occurs at 658°K along the PSN adiabat. Thus, even in the absence of sodalite condensation it is not possible to unambiguously decide if chlorapatite is stable. Further discussion of chlorapatite and possible mechanisms for its formation in chondrites will be presented in the section dealing with chondrite mineralogy.

Potassium

Figure I-5 illustrates the chemical equilibrium behavior of potassium-bearing compounds along the nebular

adiabat. The results in Figure I-5 model high sanidine ($KAlSi_3O_8$) condensation as an ideal solution in feldspar. Potassium is 50% condensed at about 1020°K and completely condensed at 952°K. Condensation of high sanidine as a pure phase starts at 943°K and is essentially complete within 100°. Data from Seck (1971) and Saxena (1973) show that $KAlSi_3O_8$ in $NaAlSi_3O_8$-$KAlSi_3O_8$-$CaAl_2Si_2O_8$ exhibits positive deviations from ideality (activity coefficients greater than 1). Thus, the present calculations modeling high sanidine condensation as an ideal solute and as a pure phase bracket the actual $KAlSi_3O_8$ condensation temperature.

Figure I-1 shows the $KAlSi_3O_8$ 50% condensation curve over a wide pressure range. This curve was calculated assuming a high sanidine ideal solution in anorthite ($CaAl_2Si_2O_8$). Actually, at all pressures shown the $KAlSi_3O_8$ 50% condensation curve is 20°-40° higher than the $NaAlSi_3O_8$ condensation curve. The two curves are drawn as one merely to simplify the graphical representation.

Also, potassium may behave similarly to sodium and partition into nepheline and sodalite phases at lower temperatures. Accurate chemical equilibrium calculations cannot be made because thermodynamic data for the potassium analog of sodalite are unavailable and activity data for the

FIGURE I-5: The chemical equilibrium behavior of potassium-bearing compounds along the nebular adiabat. The heavy lines indicate the stability fields of the condensates. The abundances of $KAlSi_3O_8$ and K_2SiO_3 ideal solid solutions in feldspar and enstatite, respectively, are also illustrated. Results are shown for high sanidine ideal solution in feldspar. Potassium is 50% condensed at about 1020°K and is completely condensed by 952°K. Pure $KAlSi_3O_8$ condensation starts at 943°K and is essentially complete within 100°.

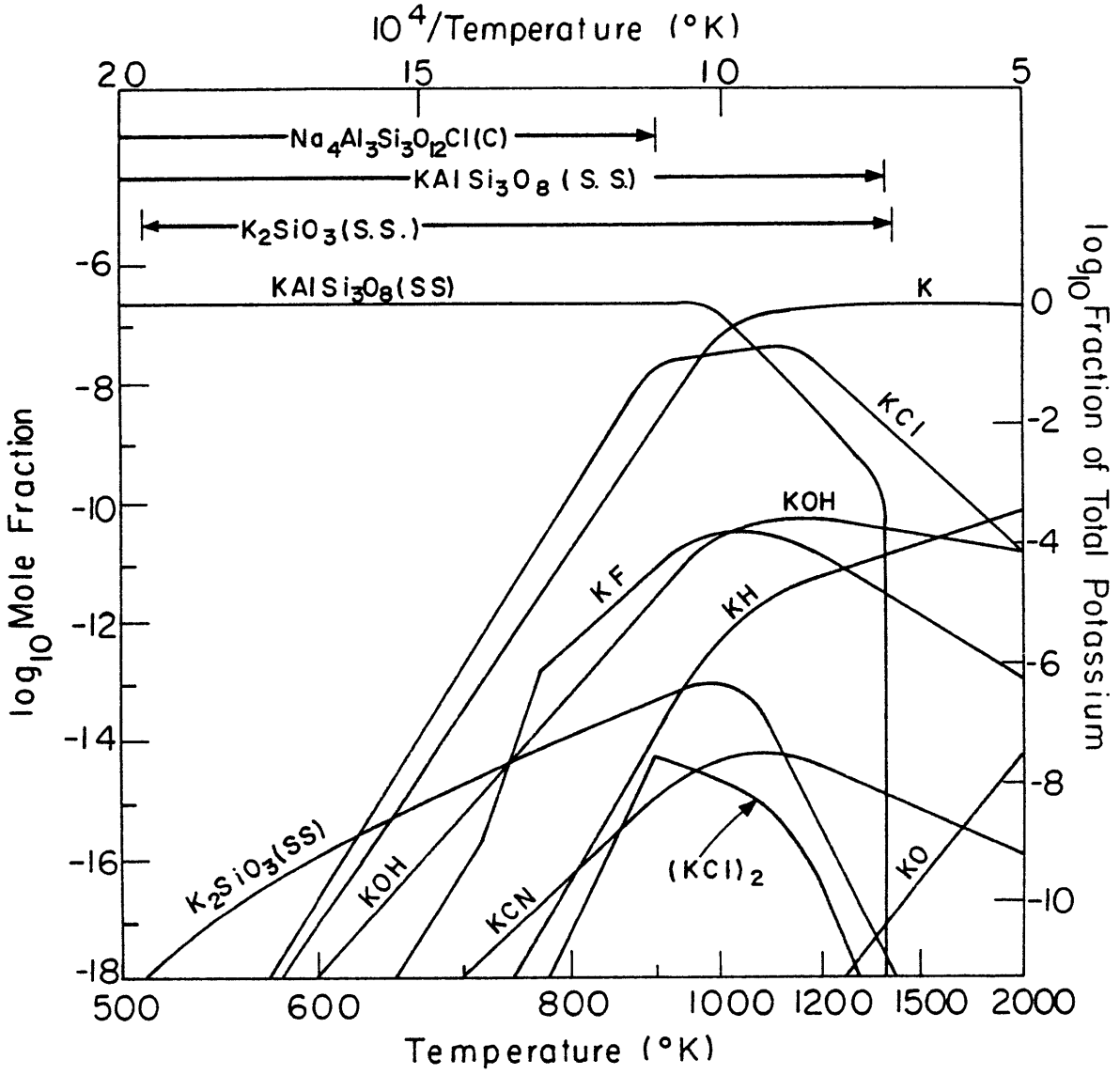
10^4/Temperature (°K)
20
15
10
5
$Na_4Al_3Si_3O_{12}Cl$(C)
$KAlSi_3O_8$ (S. S.)
K_2SiO_3(S.S.)
$KAlSi_3O_8$(SS)
K
KCl
KOH
KF
KH
K_2SiO_3(SS)
KOH
KCN
$(KCl)_2$
KO
$\log_{10}$Mole Fraction
$\log_{10}$Fraction of Total Potassium
-6
-8
-10
-12
-14
-16
-18
0
-2
-4
-6
-8
-10
500
600
800
1000
1200
1500
2000
Temperature (°K)

relevant solid solutions are either unavailable or highly uncertain. However, assuming ideal solution in nepheline and neglecting potassium in sodalite phases, approximately 40% of the potassium will be in kaliophillite ($KAlSiO_4$) at 700°K. Also, pure $KAlSiO_4$ becomes stable at 509°K.

The effect of variations in the $KAlSi_3O_8$ (high sanidine) and $KAlSiO_4$ (kaliophillite) thermodynamic data (Robie et al., 1978) upon the high sanidine-kaliophillite condensation sequence have also been explored. The condensation temperatures along the PSN adiabat for high sanidine and kaliophillite calculated by neglecting (1) solid solution with other phases and (2) the prior condensation of other potassium-bearing phases differ by only 11°K with $KAlSi_3O_8$ condensing at the higher temperature. However, the tabulated uncertainties in the thermodynamic data for high sanidine and kaliophillite are sufficient to reverse the condensation sequence with kaliophillite condensing 8°K above high sanidine (neglecting the prior condensation of kaliophillite). Furthermore, once kaliophillite forms, high sanidine is never stable. Thus, the situation is analogous to that discussed previously for sodium, and on the basis of the available thermodynamic data alone it is impossible to unambiguously identify the initial potassium-bearing condensate. More will be said about this situation in the

section on chondrite mineralogy.

THE HETEROGENEOUS ACCRETION MODEL

The strict heterogeneous accretion model, which is the extreme opposite of the strict homogeneous accretion model, assumes the rapid accretion of small particles into larger bodies, thus preventing the material within these bodies from reacting further with the gas phase. The consequences of this process have been modeled by assuming complete isolation of newly formed condensates from all gases and all previous condensates. Thus, as soon as an element condenses it is removed from further reactions. This chemical disequilibrium model is essentially a generalized and quantifiable, albeit extreme, version of the heterogeneous accretion model for the Earth proposed by Turekian and Clark (1969).

The condensation behavior of the elements Na, K, F, Cl, Br and P in the heterogeneous accretion model has been calculated and the results are presented in Table I-3. The calculations apply to a solar composition gas cooled along the nebular adiabat of Figure I-1 and include newly recalculated condensation temperatures for some compounds considered in Barshay and Lewis (1976). The results in

Table I-3

The Heterogeneous Accretion Model:

Chemical Reactions Along the Nebular Adiabat

T(°K)	Reaction
1520	Condensation of Fe-Ni alloy
1455	Condensation of $MgSiO_3$ (Enstatite)
751	$2Na(g) + H_2S(g) = H_2(g) + Na_2S(s)$
747	$Na(g) + HF(g) = 1/2H_2(g) + NaF(s)$
695	$2K(g) + H_2S(g) = H_2(g) + K_2S(s)$
261	$NH_3(g) + HBr(g) = NH_4Br(s)$
259	$NH_3(g) + HCl(g) = NH_4Cl(s)$
244	$1/4P_4O_6(g) + NH_3(g) + 5/2H_2O(g) = NH_4H_2PO_4(s) + H_2(g)$
134	$NH_3(g) + H_2S(g) = NH_4HS(s)$

Table I-3 plus the results in Barshay and Lewis (1976) describe the major features of the heterogeneous accretion model reaction sequence over the temperature range 2000°-5°K. Finally, it is important to note that the reaction sequence in the heterogeneous accretion model is not path-independent, and that the same results will not be obtained upon the volatilization of a homogeneous cold gas and dust mixture.

The predictions of the homogeneous and heterogeneous accretion models about volatile element chemistry along an adiabat in the primitive solar nebula are summarized in Tables I-2 and I-3. The two extreme models are seen to make very different predictions about the chemistry of the volatile elements Na, K, F, Cl, Br, P and S in the primitive solar nebula. Some features of the heterogeneous accretion model reaction sequence such as the chalcophile behavior of the alkali metals, the failure of S and P to behave as siderophiles, and the failure of P, F, Cl, and Br to behave as lithophiles are especially noteworthy. How do these predictions compare to the limited data on abundances of these volatiles in the terrestrial planets and to the observed mineralogy of the ordinary chondrites?

VOLATILE ELEMENT RETENTION BY THE TERRESTRIAL PLANETS

First, although no observational data about volatile element abundances in the planet Mercury are available, a qualitative comparison of the planet's formation zone and the condensation curves displayed in Figure I-1 suggests that Mercury should be depleted in all the volatile elements considered in this study. The strict heterogeneous accretion model also predicts that Mercury will be depleted in all the volatiles considered. However, the $(Fe,Ni)_3P$ condensation results of Sears (1978) imply that Mercury will retain phosphorus with approximately the solar P/Fe ratio. Second, the measured potassium abundances in very small samples of the surface of Venus (Vinogradov et al., 1973; Surkov et al., 1976) and the observations of HCl and HF in the upper troposphere (Connes et al., 1967) are consistent with the formation of Venus within the stability fields of feldspar, sodalite, and fluorapatite. However, the observations of Cl and K are inconsistent with the predictions of the heterogeneous accretion model that Cl retention at 259°K and K retention at 695°K do not take place in the formation zone at Venus. It is important to note that chemical equilibrium calculations by Lewis et al.

(1979) on the stability of various carbon-bearing species yield abundances of carbon compounds similar to the observed inventories on Venus and Earth. Furthermore Barshay and Lewis (1979) find that a 10^4-fold depletion of H_2O on Venus is entirely compatible with a 10-fold depletion of FeS and a 10- to 100-fold depletion of FeO relative to the Earth. Thus, the need for covering Venus with a veneer of volatile-rich carbonaceous material and then removing all the excess water appears far from obvious.

Third, the (incomplete) data on abundances of Na, K, F, Cl, Br, P, and S in the Earth can be compared with the qualitative predictions of the homogeneous and heterogeneous accretion models. The homogeneous accretion model predicts that the bulk composition of the Earth is similar to that of the H group ordinary chondrites, but is not identical to nor derived from the H chondrites or any other meteorite class (Lewis, 1972). For the volatile elements considered in this study (and sulfur) the homogeneous accretion model predicts (terrestrial/chondritic) abundance ratios $\simeq$ 1.0 for Na, K, F, Cl, P and S and a ratio < 1.0 for Br. Using the three composition models for the Earth presented by Smith (1977) and H chondrite and Cl chondrite analytical data from Mason (1979), abundance ratios for the volatile elements under consideration have been calculated and the results are presented in Table I-4. The abundance ratio

presented is the quantity [$(E/10^6Si)$Earth/$(E/10^6Si)$chondrite], where $(E/10^6Si)$ is shorthand for the elemental abundance relative to 10^6 Si atoms. How accurate are these ratios and what do their values tell us?

First, it is necessary to realize that many assumptions about the radial and lateral distribution of elements within the Earth and about the composition of the core are necessary in the construction of any compositional models for the Earth. Smith (1977) has given a detailed discussion of the assumptions made in the construction of his models and the present discussion will not attempt to repeat all of them or to evaluate their validity. It is possible, however, to illustrate the effect of two sets of assumptions on the abundance ratios calculated above. Thus, if it is assumed that Na, K, Cl, Br, and S occur throughout the entire mantle instead of only in the upper 10%, the terrestrial/H chondrite abundance ratios become Na(0.3), K(1.1), Cl(2.4), Br(3.3), and S(2.7). Similarly, if iron meteorites are not used to model the composition of the core and the crustal and mantle composition alone is used for the composition of the Earth, the P and S terrestrial/H chondrite ratios become P(0.2) and S(0.005).

Second, it is also important to consider the quality of the analytical data for terrestrial samples and

meteorites. Smith (1977) discusses the quality of the analytical data for terrestrial samples and the quality of the chondrite analytical data will be briefly discussed here. The analytical data for Na, K, P, and S in Cl and H chondrites, which are presented in Mason (1979), show maximum variations less than a factor of 2 and are reasonably consistent. However, the F, Cl, and Br analytical results for chondrites show considerably greater variations. Dreibus et al. (1979) compare their halogen analytical results with previous results for carbonaceous, ordinary (L group), and enstatite chondrites. The observed variations for halogen analyses in different meteorites range from 1.1 (Ivuna Cl) - 14.5 (Mocs L6), 1.0 (Bruderheim L6) - 3.7 (Orgueil Cl), and 1.2 (Bruderheim L6) - 9 (Mocs L6) for F, Cl and Br, respectively. Allen and Clark (1977) and Mason (1979) also present comparisons of multiple fluorine analyses by different investigators on a single meteorite. Results tabulated by Mason (1979) for fluorine analyses of the Orgueil Cl and Allegan H5 chondrites display maximum variations of 5.5 and 5.3 times, respectively, and the data presented in Allen and Clark (1977) for the average fluorine content of H-chondrites show a factor of 4 maximum variation. More comprehensive comparisons of halogen analytical data for the chondrites and other types

of meteorites can be found in the papers by Dreibus et al. (1979), Mason (1979), and the articles by Reed in Mason (1971). However, the examples given above are sufficient to illustrate the wide variations between results and the questionable accuracy of many of the data.

Now that we have a rough idea of the accuracy of the abundance ratios presented in Table I-4 we can discuss their implications. As stated earlier, the homogeneous accretion model predicts terrestrial/chondritic abundance ratios $\simeq 1.0$ for Na, K, F, Cl, P, and S and a ratio < 1.0 for Br. The agreement between calculated abundances and predicted inventories is fairly good, especially considering the assumptions made in constructing the terrestrial composition models and the poor quality of the halogen analytical data in meteorites.

For example, the apparent Na, K, and Cl depletions largely disappear if these elements are assumed to occur throughout the entire mantle and not merely the upper 10%. The K abundance in the Earth is, however, highly controversial and Lewis (1971) has proposed that potassium may be enriched in the Earth's core. Somerville and Ahrens (1980) review recent experimental and theoretical work relating to this suggestion and another review will not be presented here. Suffice it to say that the issue of potassium in the

TABLE I-4

Terrestrial/Chondritic Elemental Abundance Ratios

Atomic Number	Element	Abundance Ratios (Earth/Cl Chondrite)	(Earth/H Chondrite)
9	F	2.1	6.5
11	Na*	3.6×10^{-2}	5.3×10^{-2}
15	P	0.56-0.76	0.68-0.91
16	S*	0.54	2.7
17	Cl*	2.1×10^{-2}	0.32
19	K*	0.19	0.20
35	Br*	1.7×10^{-2}-2.1×10^{-2}	0.45-0.57

* An asterik indicates that the element is assumed by Smith (1977) to occur only in the upper 10% of the Earth's mantle. If the elements are assumed to occur throughout the entire mantle the (Cl, H) abundance ratios are Na(0.23, 0.33), S (0.55, 2.7), Cl(0.16, 2.4), K(1.1, 1.1) and Br(0.12, 3.3).

Data Sources

Earth - Smith (1977)

Chondrites - Mason (1979)

Earth's core cannot begin to be resolved until after both potassium and sodium partitioning experiments are done in the relevant pressure-temperature range using diamond anvil cells.

The halogen abundance ratios indicate an apparent enrichment of fluorine and apparently equal abundances of bromine and chlorine. However, the fluorine terrestrial/chondritic abundance ratios depend strongly on which fluorine chondritic abundances are used. For example, the fluorine analytical results of Allen and Clark (1977), Dreibus et al. (1979), and Goldberg et al. (1974), which agree reasonably well with one another, all show fluorine chondritic abundances approximately 2-3 times lower than previously thought. The fluorine terrestrial/Cl chondrite abundance ratios calculated using the fluorine terrestrial abundance from Smith (1977) and fluorine Cl chondrite abundance data from either Smith (1977) or Dreibus et al. (1979) are 0.49 and 2.7, respectively. A high terrestrial/chondritic fluorine abundance ratio may indicate that fluorine condenses in sodalite at higher temperatures than it condenses in fluorapatite. The approximately equal Cl and Br abundance ratios may also indicate that bromine condenses as Br-bearing sodalite at higher temperatures than it condenses

as bromapatite. However, as previously stated, the bromapatite condensation results may involve a considerable uncertainty and no thermodynamic data are available for the fluorine- and bromine-bearing analogs of sodalite.

In contrast to the homogeneous accretion model, the strict heterogeneous accretion model predicts that the Earth will be devoid of any chlorine, bromine, phosphorus, and sulfur. These elements could have been added to the Earth as part of a hypothesized veneer of low temperature volatile-rich material, which presumably would also account for the terrestrial inventories of other volatiles such as carbon, hydrogen, nitrogen, oxygen, and some of the inert gases. However, as Lewis et al. (1979) point out, a comparison of the terrestrial and chondritic C, H, N, and O isotopic compositions fails to identify a particular source for the volatile elements on Earth in terms of carriers with the properties of known meteorite classes.

Fourth, sulfur, chlorine, and possibly bromine have been detected in Martian fines by the Viking x-ray fluorescence experiments (Clark et al., 1976; Clark and Baird, 1979). As Figure I-1 illustrates, the homogeneous accretion model predicts approximately quantitative retention of sulfur and chlorine and less than quantitative bromine retention in the formation zone of Mars along the nebular

adiabat. By contrast, the strict heterogeneous accretion model predicts the absence of any sulfur, chlorine, and bromine in the formation zone of Mars. Retention of sulfur in the strict heterogeneous accretion model can occur only at temperatures so low that H_2O is fully condensed, a condition clearly at odds with our observational data on all the terrestrial planets.

The strict homogeneous accretion model thus predicts that the condensed material in the PSN will become increasingly volatile rich (specifically alkali, halogen, phosphorus, and sulfur rich) with increasing heliocentric distance. This trend is also predicted for the water content of condensed material (Lewis, 1972), but not for the carbon content in the case of complete chemical equilibrium (Lewis et al., 1979). However, a similar trend is also predicted for the carbon content of condensed material if kinetic inhibition of CO(g) reduction prevents the complete attainment of chemical equilibrium (Lewis and Prinn, 1980). These considerations are based on the assumption of a nebular temperature profile similar to the one illustrated in Figure I-1 at the time when nebular chemistry stops and accretion begins.

In contrast, the strict heterogeneous accretion model predicts that the volatile content of condensed material in

the PSN will increase with decreasing temperature and that late formed condensate will be more volatile rich. Note that the heterogeneous accretion model does not predict any explicit relationship between volatile content and heliocentric distance of condensed material in the PSN. Instead, the volatile content of condensed material depends on the extent to which accretion has proceeded when nebular chemistry stops.

VOLATILE ELEMENT MINERALOGY OF CHONDRITES

The chondritic meteorites are thought to be some of the most primitive objects in the solar system. The fact that they contain decay products of extinct radionuclides indicates that the chondrites formed early in the history of the solar system. Furthermore, several lines of evidence including the preservation of isotope anomalies and the physical morphologies of some minerals suggest that the chondrites have not been drastically altered by post-accretional processes. Thus, it is possible that both the chemistry and the mineralogy of the chondrites were established in the primitive solar nebula. It is therefore of great interest to compare the mineralogy of the chondrites with the predicted condensates in the strict homogeneous and strict heterogeneous accretion models.

The following discussion, which is nonexhaustive and which deals with alkali, halogen, and phosphorus-bearing phases, is primarily limited to the mineralogy of the ordinary chondrites. There are several reasons for this choice. First, the ordinary chondrites comprise ∿90% of all known chondrites. Second, the nature of many volatile element-bearing phases in the carbonaceous chondrites is unknown due to problems in laboratory examination of these meteorites. Third, some of the volatile-bearing phases in carbonaceous chondrites are generally thought to be the result of post-accretional alteration processes (McSween, 1979, and references therein). Fourth, the mineralogy of the enstatite chondrites may have been established in a system with carbon to oxygen (C/O) ratios greater than the solar value (Larimer and Bartholomay, 1979, and references therein).

As previously mentioned, there is a close correspondence between phases formed in the homogeneous accretion model and the observed mineralogy of ordinary chondrites. For example, alkali-bearing feldspar and whitlockite are ubiquitous in ordinary chondrites (Fuchs, 1969a; Van Schmus and Ribbe, 1968) and schreibersite, sodalite, nepheline, and fluorapatite have also been observed (Curtis and Schmitt, 1979; Fuchs, 1969a; Kurat, 1967; Noonan et al., 1978; Van Schmus and Ribbe, 1969). The presence of

hydroxyapatite in ordinary chondrites has also been inferred by Van Schmus and Ribbe (1969). Large fluorine and bromine concentrations (800 ppm and 5-10 ppm, respectively) have been observed in apatite in the Modoc chondrite by Mason and Graham (1970). Furthermore, other minerals such as farringtonite [$Mg_3(PO_4)_2$] and lawrencite ($FeCl_2$), which are not equilibrium condensates, are not observed in ordinary chondrites (Farrington, 1915; Fuchs, 1969a). However, Keil (1968) has reported lawrencite in the Indarch enstatite chondrite. Thus, the correspondence between predicted equilibrium condensates in the homogeneous accretion model and phases present in ordinary chondrites suggests a close approach to chemical equilibrium in the primitive solar nebula.

A comparison of the condensates formed in the heterogeneous accretion model and the mineralogy of the ordinary chondrites provides additional information about the attainment of chemical equilibrium in the PSN. The condensates formed in the heterogeneous accretion model (in order of decreasing formation temperature along the nebular adiabat) are Na_2S (751°K), NaF (747°K), K_2S (695°K), NH_4Br (261°K), NH_4Cl (259°K), and $NH_4H_2PO_4$ (244°K). The fact that none of these phases are found in ordinary chondrites also strongly suggests a close approach to chemical equilibrium in the

solar nebula.

Two phases which are found in ordinary chondrites but which are not formed in either accretion model are merrihueite [$(K,Na)_2Fe_5Si_{12}O_{30}$] and chlorapatite. No thermodynamic data are available for merrihueite, which is a rare mineral in the Mezo-Madaras chondrite, so it could not be included in the present calculations. Also chlorapatite, which is common in ordinary chondrites (Fuchs, 1969a), is not an equilibrium condensate. Much of the total chlorine content of chondrites which contain chlorapatite can be accounted for by its presence (Van Schmus and Ribbe, 1969). However, the chlorine in chondrites which do not contain chlorapatite is in unidentified phases (Reed, 1971). It is suggested that the unidentified chlorine-bearing phase is sodalite. Two possible explanations to account for the chlorapatite found in ordinary chondrites are also proposed. First, it is possible that chemical equilibrium was not completely reached in some regions of the solar nebula, causing sodalite formation to be either partially or totally inhibited. As previously mentioned, the chlorine remaining in the gas phase could then form chlorapatite in the 656-678°K temperature range. However, halite forms in the same temperature range and chlorapatite formation may still be inhibited. Second,

it is also possible that the chlorapatite observed in chondrites is the product of reactions in the chondrite parent bodies. Some or all of the sodalite could have reacted with phosphorus-bearing and calcium-bearing minerals to produce chlorapatite.

The suggestion that sodalite minerals are possible candidates for the unidentified halogen-bearing phases in chondrites will now be discussed further. The present calculations show that sodalite is more stable than chlorapatite, and the same situation may prevail for the fluorine and bromine analogs of sodalite and the corresponding apatite minerals. In fact, Grossman et al.(1979) found a high bromine concentration (32.7 ppm) in an Allende amoeboid aggregate containing sodalite and a bromine concentration of 12.1 ppm in another aggregate in which sodalite was possibly present. Lower bromine concentrations (0.65-3.19 ppm) were observed in other amoeboid aggregates which did not contain sodalite.

Sodalite and nepheline, which are equilibrium condensates, have been observed in several types of inclusions in carbonaceous and ordinary chondrites (Grossman et al., 1979; Grossman and Steele, 1976; Noonan et al., 1978; Wark and Lovering, 1977 and references in these papers). Only a few of the many interesting questions associated with the

occurrence of these phases will be mentioned due to space limitations. First, it may be significant that the alkali-bearing phases reported in these various inclusions are usually sodalite and nepheline and are rarely alkali feldspar. As previously mentioned, the nature of the initial alkali-bearing condensate is ambiguous and may be critically dependent upon local nebular conditions, such as slight departures from chemical equilibrium in the PSN. Second, Wark and Lovering (1977) have found sodalite and nepheline in close association with (and sometimes enclosed by) more refractory phases such as spinel ($MgAl_2O_4$), forsterite (Mg_2SiO_4), perovskite ($CaTiO_3$), and diopside ($CaMgSi_2O_6$). The results for the homogeneous and heterogeneous accretion models demonstrate that the observed mineralogy cannot be produced by sequential equilibrium condensation in a solar composition system. Third, Grossman et al. (1979) report that sodalite and nepheline are common in fine-grained inclusions and amoeboid aggregates in Allende. They propose that the amoeboid aggregates originated when coarse-grained Allende inclusion material underwent partial reaction with a low-temperature nebular gas and mixture with FeO-rich olivine. The present calculations (see Figure I-1) indicate that the amoeboid aggregates must have

formed at temperatures lower than 775°K or else nepheline would not have been formed.

SUMMARY AND CONCLUSIONS

The results of chemical equilibrium calculations for several hundred compounds of the elements Na, K, F, Cl, Br and P in a solar composition system are reported. The calculations are carried out over a wide range of temperatures and pressures and along an adiabat in the primitive solar nebula.

Two extreme models of accretion are investigated. In one extreme complete chemical equilibrium between condensates and gases is maintained because the time scale for accretion is long compared to the time scale for cooling or dissipation of the nebula. Condensates formed in this homogeneous accretion model include several phases such as whitlockite, alkali feldspars, and apatite minerals which are found in chondrites. In the other extreme, complete isolation of newly formed condensates from prior condensates and gases occurs due to a time scale for accretion that is short relative to the time required for nebular cooling or dissipation. The condensates produced in this heterogeneous accretion model include alkali sulfides, ammonium halides, and ammonium phosphates. None of these phases are found in chondrites.

Available observations of the Na, K, F, Cl, Br, and P elemental abundances in the terrestrial planets and the mineralogy of the ordinary chondrites are compatible with the predictions of the homogeneous accretion model. These observations in concert with other observable properties such as planetary bulk densities, which are also explainable by the homogeneous accretion model, suggest that chemical equilibrium was closely approached in the inner parts of the solar nebula.

CHAPTER II. BARIUM TITANATE CONDENSATION AND ALKALINE EARTH FRACTIONATIONS IN THE SOLAR NEBULA.

INTRODUCTION

Since the pioneering work of Urey (1952), much progress has been made in understanding the equilibrium chemistry of major elements in solar composition material. These results, which are summarized by Barshay and Lewis (1976) and Grossman and Larimer (1974), have been extremely useful in discussing both the observed major element fractionations in the chondrites and the inferred major element fractionations among the terrestrial planets.

However, it is only recently that much progress has been made in understanding the equilibrium chemistry of trace elements in solar composition material and in applying these results to studies of trace element fractionation mechanisms in the solar nebula. Several factors are responsible for our inadequate understanding of trace element fractionations. First, there is often a complete lack of thermodynamic data for many potentially important gases and condensed phases of trace elements. Second, the existing data are often incomplete, inconsistent, or both and must be critically assessed and evaluated before use. Third, since many (but not all)

trace elements condense in solid solution with more abundant elements, knowledge of the activity coefficients for the relevant solution is required. In many cases this information is either unavailable or highly uncertain.

Despite these daunting limitations it is still possible in some cases to use chemical equilibrium calculations to discuss trace element fractionations in the solar nebula. For example, Boynton (1975) and Davis and Grossman (1979) have examined the condensation behavior of the lanthanides, Boynton (1978) has studied actinide condensation, and Palme and Wotzka (1976) have considered the condensation of refractory siderophiles. The present work deals with the condensation behavior of the alkaline earth elements barium (Ba) and strontium (Sr) which have not been studied previously.

A knowledge of the chemical behavior of barium and strontium in the primitive solar nebula (PSN) is important for at least two reasons:

1. Barium, calcium, and strontium are chemically similar elements which have generally been assumed to fractionate together. However, Tanaka and Okumura (1977) and Masuda and Tanaka (1977) have reported particles of pure barium titanate ($BaTiO_3$) in the matrix and inclusions of the Allende type CV3 carbonaceous chondrite. Furthermore, the neutron activation analytical data of

Grossman et al. (1977) on coarse-grained Allende inclusions provide independent evidence for the existence of a barium-containing phase which is distinct from the calcium- and strontium-containing phases in the inclusions analyzed. The observed $BaTiO_3$ particles, which are not associated with any calcium- or strontium-bearing phases, represent one of the few cases where a trace element is a major constituent of a mineral. How did the $BaTiO_3$ particles form?

2. Fractionation of the alkaline earth elements Ba, Ca, and Sr may provide information about conditions existing in the solar nebula.

An important aspect of the present work is the quantitative treatment of trace element solid solution formation. This treatment, which is based upon experimentally determined phase diagrams of the relevant systems and the thermodynamic properties of solutions, yields a consistent and simple model for the formation of the barium titanate particles found in Allende. Furthermore, the results of the present work provide a firm basis for analogous discussions of trace element fractionations in meteorites or other solar system material by using activity coefficients determined from experimental phase diagrams.

CONDENSATION CALCULATIONS: ASSUMPTIONS AND METHODS

The basic assumptions underlying the present work are (1) the existence of the primitive solar nebula, (2) the local volatilization of all presolar matter, and (3) the complete attainment of thermodynamic equilibrium. Numerous discussions of the validity of these assumptions can be found in the cosmochemical literature (Grossman and Larimer, 1974, and references therein) and they will not be repeated here.

Chemical equilibrium calculations were done from 10^{-7} to 10 bars pressure at pressures of 10^{-7}, 10^{-5}, 10^{-4}, 10^{-3}, 10^{-1}, and 10 bars as well as along an adiabatic temperature-pressure profile in the PSN. The temperature range covered was 2000°-1400°K. Calculations were generally done at 100°K intervals although smaller intervals were used when necessary. For example, the $SrTiO_3$-$CaTiO_3$ and $BaTiO_3$-$CaTiO_3$ solid solution calculations in the 1700°K-1400°K region were done at 20°K intervals.

The assumption of an adiabatic temperature-pressure profile for the PSN is consistent with the arguments advanced by Lewis (1974). The construction of the adiabatic temperature-pressure profile is described in Chapter I. The relationships between temperature and pressure and between temperature and distance along the adiabat are

also presented in Chapter I. For reference, three T-P points along the nebular adiabat are 2000°K-7.2 millibars (mb), 1000°K-0.58 mb, and 600°K-0.1 mb. The results of the present work will not be significantly altered by the choice of a slightly different temperature-pressure profile for the PSN.

The assumed solar elemental abundances used in the calculations, which are taken from Cameron (1973), are illustrated in Table II-1. A recent redetermination of the barium abundance in the Orgueil type C1 carbonaceous chondrite by DeLaeter and Hosie (1978) yields a value of 4.2 on the Si = 10^6 abundance scale. This value is in good agreement with the Cameron (1973) value of 4.8. Also, Shima (1979) has redetermined the abundances of titanium and zirconium in the Orgueil C1 chondrite as 2470 and 11.2, respectively, on the Si = 10^6 abundance scale. The effect of variations in the elemental abundances used upon the results of the chemical equilibrium calculations will be discussed later.

The equilibrium stability fields and abundances of minerals and the thermodynamic activities of some elements along the nebular adiabat are taken from the results of complete chemical equilibrium calculations. The thermodynamic data sources used are listed in Appendix II. The computational method used is described

TABLE II-1

Abundances of the Elements

from Cameron (1973)*

Element	Normalized Abundance ($Si=10^6$)
Ti	2775
Zr	28
Sr	26.9
Ba	4.8

*Only elements not previously listed in Table I-1 are included.

in Chapter I.

CONDENSATION OF TITANIUM AND ZIRCONIUM

Titanium and zirconium are included in the data set so that condensation of alkaline earth titanates and zirconates can be considered. Hafnium was not included in the data set because of its low abundance (Hf = 0.21 on the Si = 10^6 scale in Cameron's 1973 compilation) and because reliable thermodynamic data for the alkaline earth hafnates are unavailable. The calculated perovskite ($CaTiO_3$) condensation temperatures, which are listed in Table II-2 and displayed in Figure II-1, are in good agreement with other values (Grossman and Larimer, 1974; Sears, 1980; Trivedi and Larimer, 1980). The small differences are probably due to the slightly different elemental abundances and thermodynamic data used in the four sets of calculations. Gehlenite ($Ca_2Al_2SiO_7$) and spinel ($MgAl_2O_4$) condensation temperatures are also compared in Table II-2. In both cases the best agreement is with the results of Trivedi and Larimer (1980), who used the same thermodynamic data sources (Larimer, personal communication). Use of the Shima (1979) titanium abundance instead of the Cameron (1973) titanium abundance in the present calculations

TABLE II-2

Mineral Condensation Temperatures

Condensation Temperatures (°K)

	Perovskite				Gehlenite				Spinel		
P(bars)	A	B	C	D	A	B	C	D	A	B	C
10^{-7}	1402	1404	1383	1413	1360	1353	1344	1342	1193	1195	1259
10^{-5}	1528	1530	1503	1534	1486	1481	1471	1470	1306	1313	1375
10^{-3}	1676	1681	1646	1679	1642	1635	1625	1625	1449	1458	1516
10^{-1}	1839	1866	1819	1853	1834	1826	1814	1816	1628	1638	1689

Key

A - This work

B - Trivedi and Larimer (1980

C - Grossman and Larimer (1974)

D - Sears (1980)

lowers the perovskite condensation temperature by approximately 2°K.

Zirconium condenses as baddeleyite (ZrO_2) as previously reported (Grossman and Larimer, 1974). The calculated condensation temperatures, which are shown in Figure II-1, agree well with literature values (Grossman and Larimer, 1974). Use of the Shima (1979) zirconium abundance in place of the Cameron (1973) zirconium abundance in the present calculations lowers the baddeleyite condensation temperature by approximately 22°-34° depending on the pressure. Assuming the baddeleyite is present at unit activity, zircon ($ZrSiO_4$) formation along the PSN adiabat occurs at 1420°K and consumes all baddeleyite. Both zircon and baddeleyite are known meteoritic minerals. Baddeleyite has been observed in some Allende inclusions by El Goresy et al. (1978) and in the Angra dos Reis achondrite by Keil et al. (1976). Zircon was discovered in the Vaca Muerta mesosiderite and in troilite nodules of the Toluca iron by Marvin and Klein (1964), and may be present in small amounts in many chondrites.

Condensation of zirconium as $CaZrO_3$ has also been considered. Pure $CaZrO_3$ is not an equilibrium condensate in a solar composition system. However, calculations along the PSN adiabat assuming ideal solid solution of

FIGURE II-1: Condensation temperatures for ZrO_2 and alkaline earth titanates in a solar composition system. Empty symbols represent the present results, the filled symbols are results from Grossman and Larimer (1974). The small differences are due to the different elemental abundances and different thermodynamic data used in the two investigations. The curves for $SrTiO_3$(s) and $BaTiO_3$(s) are upper limits calculated assuming (1) all titanium is in the gas phase and (2) no solid solution formation among titanates.

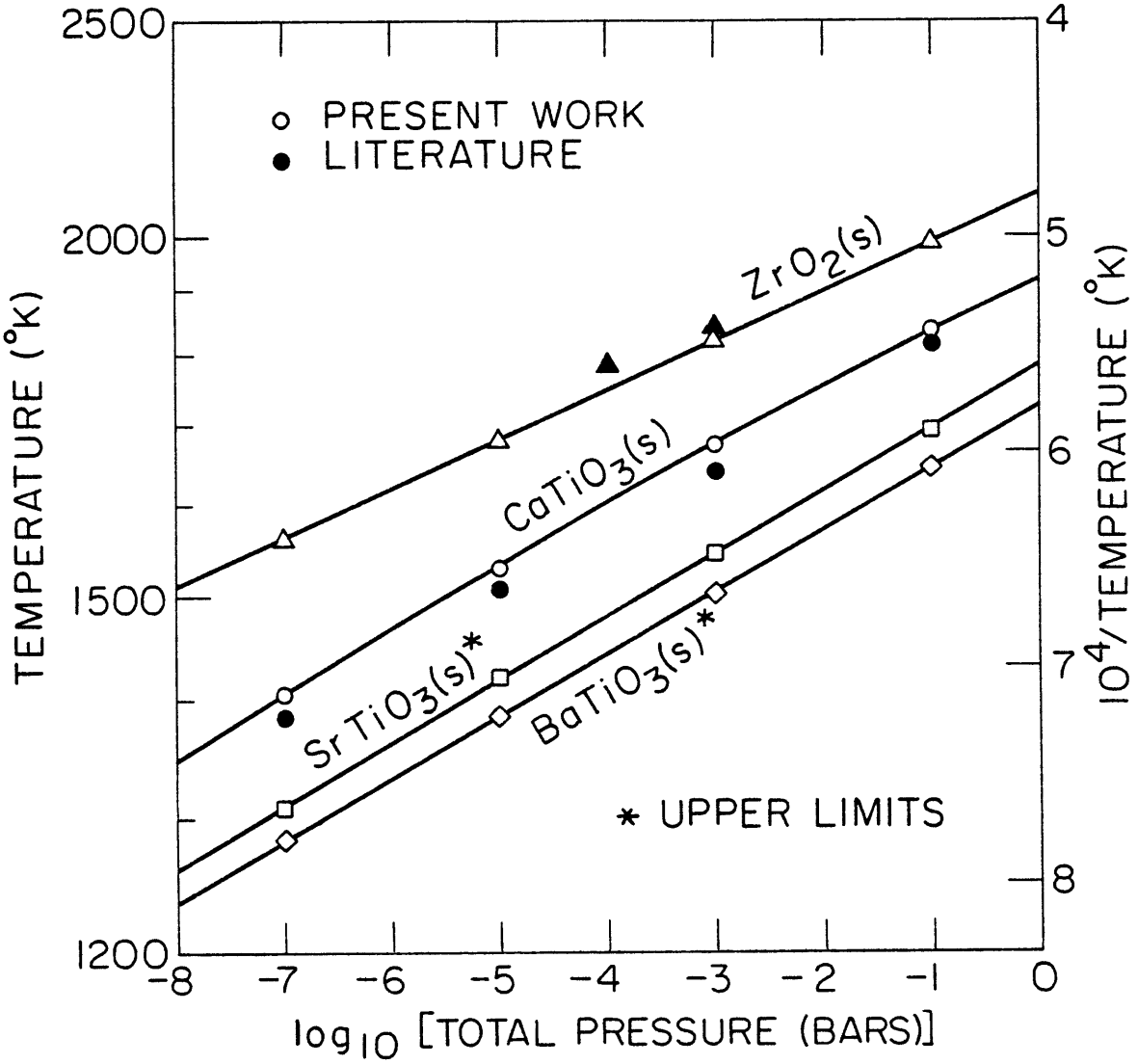
2500
2000
1500
1200
4
5
6
7
8
TEMPERATURE (°K)
10⁴/TEMPERATURE (°K)
PRESENT WORK
LITERATURE
ZrO2(s)
CaTiO3(s)
SrTiO3(s)*
BaTiO3(s)*
* UPPER LIMITS
-8
-7
-6
-5
-4
-3
-2
-1
0
log10 [TOTAL PRESSURE (BARS)]

$CaTiO_3$-$CaZrO_3$ indicate that all zirconium will be dissolved in perovskite within a few degrees of perovskite condensation. A considerable uncertainty may be involved in this result since the $CaZrO_3$ thermodynamic data were calculated by the second law method.

CONDENSATION OF ALKALINE EARTH ELEMENTS

The condensation temperatures for calcium, strontium, and barium titanates are displayed in Figure II-1. The $SrTiO_3$ and $BaTiO_3$ condensation temperatures are calculated assuming that all titanium is in the gas phase and neglecting solid solution formation among titanates. These values, which are upper limits for barium and strontium condensation as pure titanates, demonstrate that $BaTiO_3$ cannot condense prior to either $CaTiO_3$ formation or $SrTiO_3$ formation. None of the other barium- and strontium-bearing phases studied (see Appendix II) are equilibrium condensates, although $SrZrO_3$ may form solid solutions with perovskite.

The assertion that pure $BaTiO_3$ cannot condense prior to perovskite or $SrTiO_3$ condensation is an important constraint upon any model attempting to explain the formation of the $BaTiO_3$ particulates observed in Allende

by Masuda and Tanaka (1977) and Tanaka and Okumura (1977). If pure $BaTiO_3$ condenses prior to perovskite and $SrTiO_3$ condensation, then a model in which the $BaTiO_3$ particles condense, are isolated from further reactions until after perovskite and $SrTiO_3$ condensation is complete, and are then incorporated into some of the inclusions and matrix of Allende can be proposed. However, if $BaTiO_3$ does not condense prior to perovskite condensation more complex models to explain the observed $BaTiO_3$ particulates need to be considered. Thus, the effects of uncertainties in the titanate thermodynamic data, and of uncertainties in the alkaline earth elemental abundances upon the upper limit condensation temperatures for $BaTiO_3$ and $SrTiO_3$ have been carefully investigated.

The calculated uncertainties in the condensation temperatures of $BaTiO_3$, $CaTiO_3$, and $SrTiO_3$ corresponding to the uncertainties in the titanate thermodynamic data are $\pm$ (10-20)°K. The uncertainties in the condensation temperatures due to uncertainties in the barium, calcium, and strontium elemental abundances have been estimated by using elemental abundances from Cameron (1968,1973), DeLaeter and Hosie (1978), and Suess and Urey (1956) in a set of condensation calculations. The results indicate that uncertainties of a factor of two in elemental abun-

dances produce changes in the condensation temperatures of only ± 12°K. More realistic uncertainties in condensation temperatures due to elemental abundance uncertainties are ± 5°K. It should also be emphasized that any uncertainty in the oxygen and titanium elemental abundances will affect the condensation temperatures of $BaTiO_3$, $CaTiO_3$, and $SrTiO_3$ to the same extent, and, while altering the absolute condensation temperatures, will not change the temperature intervals between the titanate condensation points. Thus a reasonable estimate (probably an overestimate) of the uncertainty in the titanate condensation temperatures due to the combined uncertainties in the titanate thermodynamic data and the alkaline earth elemental abundances is ± (15-25)°K. An uncertainty of ± (15-25)°K is insufficient to reverse the $CaTiO_3$-$BaTiO_3$ condensation order (see Figure II-1) although this uncertainty suggests that the calculated $BaTiO_3$ and $SrTiO_3$ condensation temperatures (upper limits) overlap considerably, especially at lower pressures. Therefore, models for the origin of the observed $BaTiO_3$ particles which invoke $BaTiO_3$ condensation prior to perovskite formation do not appear viable and more complex models need to be investigated.

TITANATE SOLID SOLUTIONS

It is therefore appropriate to consider the formation of titanate solid solutions during the condensation of barium and strontium in the PSN. The condensation of Ba and Sr along the PSN adiabat of Chapter I has been considered. However, as previously mentioned, the results of the present work will not be significantly altered by the choice of a different temperature-pressure profile for the PSN.

Employing the rational system for activity coefficients (Castellan, 1971), the pure titanates are selected as both the standard and reference states. Then the concentration of $BaTiO_3$ and $SrTiO_3$ in solid solution is given by

$$\chi_T = (a_T/\gamma_T) \tag{1}$$

where χ_T is the mole fraction, a_T is the thermodynamic activity, and γ_T is the activity coefficient of a titanate in the solid solution. For the case of ideal solid solution $\gamma_T = 1.0$. The amount of each element which is condensed as a titanate is then given by

$$A_T = (a_T/\gamma_T)A_{per} \tag{2}$$

where A_T is the amount of $BaTiO_3$ or $SrTiO_3$ condensed in

perovskite and A_{per} is the amount of perovskite. The fraction of each element condensed is then

$$F_{cond} = (A_T/A_E) \quad (3)$$

where A_E is the assumed solar abundance of the element, and the fraction of each element in the gas is

$$F_{gas} = 1-F_{cond} \quad (4)$$

The formation of $BaTiO_3$ and $SrTiO_3$ ideal solid solutions with perovskite ($CaTiO_3$) was assumed as a first approximation. Results of the ideal solution calculations are shown in Figure II-2 as the $\gamma = 1$ curves for Sr and Ba. (The notation γ_{Sr} and γ_{Ba} is used as an abbreviation for γ_{SrTiO_3} and γ_{BaTiO_3}, respectively.) For the ideal solution case, Sr is 50% condensed in perovskite at 1605°K and completely condensed by 1490°K, while Ba is 50% condensed at 1575°K and completely condensed at about 1464°K. Close inspection of Figure II-2 reveals that no significant fractionation of Ba from either Ca or Sr occurs for the ideal solution case. For example when only 1% of all Sr is left in the gas, 6% of all Ba is still in the gas. The Ba/Sr ratio in a titanate condensed from this gas is only 1.1, while the $BaTiO_3$ particulates are reported to contain no Sr (Masuda and Tanaka, 1977; Tanaka and Okumura, 1977). However, these results assume ideal solid solution of both

FIGURE II-2: The amounts of barium and strontium condensed in perovskite ($CaTiO_3$) along the solar nebula adiabat. Condensation of barium and strontium as $BaTiO_3$ and $SrTiO_3$, respectively, is considered. The curves Sr γ = 1 and Ba γ = 1 are for ideal solid solution of $SrTiO_3$ and $BaTiO_3$, respectively, in perovskite. The curves Ba γ = 5, Ba γ = 20, and Ba γ = 50 are for non-ideal solid solution of $BaTiO_3$ in perovskite. The effect of increasing nonideality (increasing γ values) in the $BaTiO_3$-$CaTiO_3$ solid solution is to decrease the amount of $BaTiO_3$ in perovskite at a given temperature.

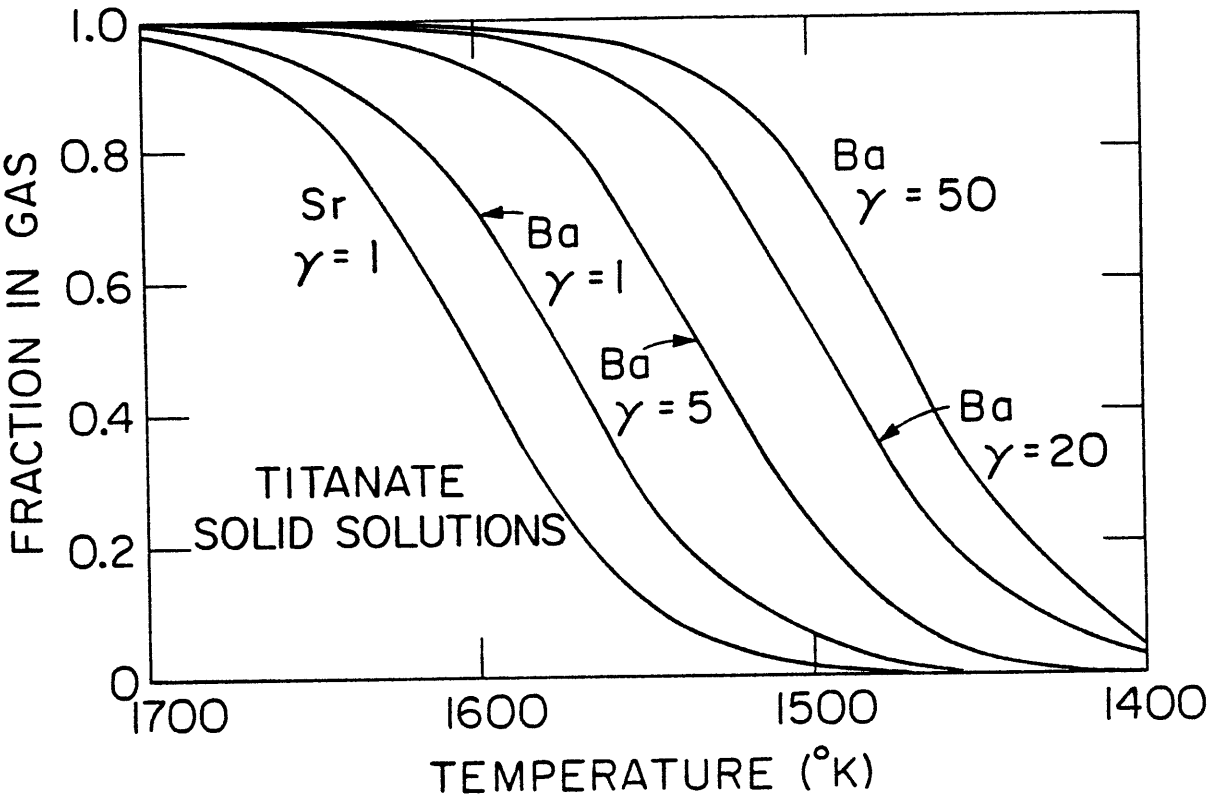
1.0
0.8
0.6
0.4
0.2
0
FRACTION IN GAS
Sr
γ = 1
Ba
γ = 1
Ba
γ = 5
Ba
γ = 20
Ba
γ = 50
TITANATE
SOLID SOLUTIONS
1700
1600
1500
1400
TEMPERATURE (°K)

of both $BaTiO_3$ and $SrTiO_3$ in perovskite. How valid is this assumption?

Detailed studies of the $CaTiO_3$-$SrTiO_3$ system by McQuarrie (1955) and Durst et al. (1950) indicate that there is complete solid solution between $CaTiO_3$ and $SrTiO_3$. The ideal solution approximation is therefore a reasonable assumption for the $CaTiO_3$-$SrTiO_3$ system. However, several detailed studies of the $BaTiO_3$-$CaTiO_3$ system (Durst et al., 1950; DeVries and Roy, 1955; McQuarrie, 1955) show a miscibility gap in the $BaTiO_3$-$CaTiO_3$ system. Thus, the ideal solid solution approximation is invalid for the $BaTiO_3$-$CaTiO_3$ system and nonideal solid solutions must be considered.

Both ionic radii considerations and the phase diagram for the $BaTiO_3$-$CaTiO_3$ system indicate that $BaTiO_3$ dissolved in perovskite will exhibit positive deviations from ideality (γ values greater than unity). The curves for γ_{Ba} = 5,20, and 50 in Figure II-2 illustrate the effect of nonideality on $BaTiO_3$ condensation in perovskite along the PSN adiabat. It is apparent from Figure II-2 that the nonideality of the $BaTiO_3$-$CaTiO_3$ solid solution reduces the amount of $BaTiO_3$ in perovskite at a given temperature. The nonideality of the $BaTiO_3$-$CaTiO_3$ solid solution also provides a mechanism for readily fractionating barium from

calcium and strontium. Furthermore, since barium does not readily enter into perovskite, some fraction of the barium may condense as pure $BaTiO_3$. However, since the fraction of barium remaining in the gas is a function of the activity coefficient γ_{Ba} for the $BaTiO_3$-$CaTiO_3$ system, it is first necessary to calculate γ in order to quantify the proposed model for formation of the pure $BaTiO_3$ particulates.

$BaTiO_3$-$CaTiO_3$ SYSTEM

The phase diagram for the $BaTiO_3$-$CaTiO_3$ system, which is illustrated in Figure II-3, contains all the information necessary to calculate activity coefficients for the two titanates in this system. A discussion of the thermodynamic properties of the $BaTiO_3$-$CaTiO_3$ solid solution, which is outlined below, is based upon the concept of excess thermodynamic functions and the thermodynamic treatment of alkali-metal halide solid solutions by Stephenson (1975). This review is presented in some detail because the general equations which are developed can also be applied to analogous discussions of trace element fractionations using experimental phase diagrams. Additional information on solution thermodynamics may be found in the papers by Thompson (1967) and Thompson and

FIGURE II-3: The phase diagram for the $BaTiO_3$-$CaTiO_3$ system from DeVries and Roy (1955). The miscibility gap (binodal) illustrates that the $BaTiO_3$-$CaTiO_3$ solid solution is nonideal. The abbreviations used in the phase diagram are hex = hexagonal, liq = liquid, and ss = solid solution. Experimental details relevant to the determination of the phase diagram are given by DeVries and Roy (1955).

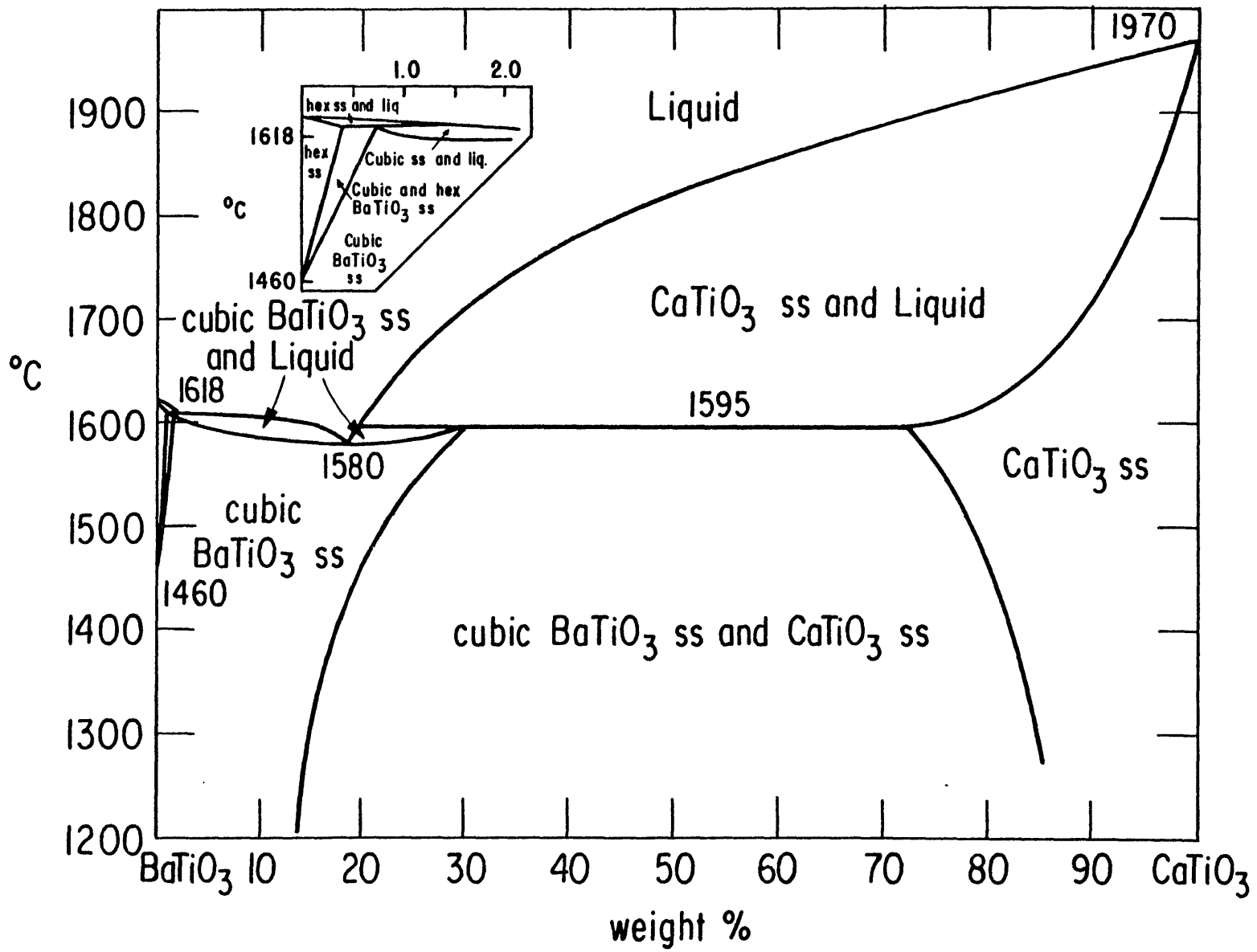
1970
1.0
2.0
hex ss and liq
1618
hex ss
Cubic ss and liq.
Cubic and hex BaTiO3 ss
Cubic BaTiO3 ss
1460
Liquid
1900
1800
°C
1700
cubic BaTiO3 ss and Liquid
CaTiO3 ss and Liquid
°C
1618
1595
1600
1580
CaTiO3 ss
cubic BaTiO3 ss
1500
1460
1400
cubic BaTiO3 ss and CaTiO3 ss
1300
1200
BaTiO3
10
20
30
40
50
60
70
80
90
CaTiO3
weight %

Waldbaum (1969).

The thermodynamic properties of the $BaTiO_3$-$CaTiO_3$ solid solution can be represented by relatively simple analytic functions. The formation of one mole of titanate solid solution is given by the change in state

$$x_1A_1(c) + x_2A_2(c) = x_1A_1 \cdot x_2A_2(c) \quad (P,T \text{ constant}) \tag{5}$$

where component $A_1(c)$ is $BaTiO_3(c)$, component $A_2(c)$ is $CaTiO_3(c)$, and $x_1 + x_2 = 1$. The Gibbs free energy of mixing for the change in state above is

$$\Delta G^M = \Delta G^{ID} + \Delta G^{xs} \tag{6}$$

where the ideal Gibbs free energy of mixing is

$$\Delta G^{ID} = RT(X_1 \ln X_1 + X_2 \ln X_2) \tag{7}$$

and the excess Gibbs free energy of mixing is

$$\Delta G^{xs} = RTX_1X_2[B_g + C_g(X_1-X_2) + \cdots] \tag{8}$$

Stephenson (1975) has pointed out that the function used to represent the excess free energy of mixing is compatible with both Raoult's Law and Henry's Law. The parameters B_g and C_g are functions of the temperature and pressure. However, for condensed phase systems the dependence of these parameters on pressure is negligible

up to moderate pressures and is usually neglected. The temperature dependence of B_g and C_g can be represented (within the limits of accuracy of the experimental data for solid solutions) by the equations

$$B_g = B_h/T + B_s \tag{9}$$

$$C_g = C_h/T + C_s \tag{10}$$

where T is the absolute temperature (°K). Repeated differentiation of equations (7-10) yields all of the thermodynamic properties given in the following equations:

$$\Delta S^{ID} = -R(X_1 \ln X_1 + X_2 \ln X_2) \tag{11}$$

$$\Delta S^{XS} = -RX_1X_2[B_s + C_s(X_1-X_2) + \cdots] \tag{12}$$

$$\Delta H^{ID} = 0 \tag{13}$$

$$\Delta H^{XS} = \Delta H^{M} = RX_1X_2[B_h + C_h(X_1-X_2) + \cdots] \tag{14}$$

$$\Delta C^{M}_{p,x} = 0 \tag{15}$$

$$\Delta \bar{G}_1^{M} = \bar{G}_1 - G_1^{\circ} = RT\ln X_1 + RTX_2^2[B_g + C_g(4X_1-1) + \cdots] \tag{16}$$

$$\Delta \bar{G}_2^{M} - \bar{G}_2 - G_2^{\circ} = RT\ln X_2 + RTX_1^2[B_g + C_g(4X_1-3) + \cdots] \tag{17}$$

$$\Delta \bar{H}_1^{M} = \bar{H}_1 - H_1^{\circ} = RX_2^2[B_h + C_h(4X_1-1) + \cdots] \tag{18}$$

$$\Delta \bar{H}_2^{M} = \bar{H}_2 - H_2^{\circ} = RX_1^2[B_h + C_h(4X_1-3) + \cdots] \tag{19}$$

The symbols $\Delta\overline{G}_i^M$, $\overline{G}_i$, and G_i° used in equations (16-17) are the partial molal Gibbs free energy of mixing of component i, the partial molal Gibbs free energy of component i in solution, and the molar Gibbs free energy of component i in its designated standard state, respectively. Analogous definitions apply to the symbols $\Delta\overline{H}_i^M$, $\overline{H}_i$, and H_i° in equations (18-19). Equation (15), which is not strictly correct, illustrates the approximations introduced by equations (9-10). Although additional terms may be included in equations (9-10), such terms are seldom warranted by the experimental data.

As previously mentioned, the pure components A_1 and A_2 are selected as both the standard and reference states. Then $a_1 = \gamma_1 X_1$ and $a_2 = \gamma_2 X_2$, where the a_i's are thermodynamic activities and the γ_i's are activity coefficients. From equations (16-17) and the relation

$$\Delta\overline{G}_i^M = RT\ln a_i = RT\ln\gamma_i X_i \tag{20}$$

it is apparent that $\ln\gamma_1$ and $\ln\gamma_2$ are given by

$$\ln\gamma_1 = X_2^2[B_g + C_g(4X_1-1) + \cdots] \tag{21}$$

$$\ln\gamma_2 = X_1^2[B_g + C_g(4X_1-3) + \cdots] \tag{22}$$

The activity coefficients γ_1 and γ_2 may be calculated from equations (21-22) as functions of temperature and composition provided that the parameters B_g and C_g are known.

For systems such as the $BaTiO_3$-$CaTiO_3$ system which contain a physically accessible miscibility gap, a method exists for determining B_g and C_g by using the equilibrium between the two phases. Consider the following changes in state

$$A_1(\text{in solid solution } \alpha) = A_1(\text{in solid solution } \beta) \quad (23)$$

$$A_2(\text{in solid solution } \alpha) = A_2(\text{in solid solution } \beta) \quad (24)$$

where solid solution α is the phase rich in component A_1 and solid solution β is the phase rich in component A_2. The equilibrium constants for the changes in state above are given by

$$K_{A_1} = (\gamma_1^\beta X_1^\beta)/(\gamma_1^\alpha X_1^\alpha) \quad (25)$$

$$K_{A_2} = (\gamma_2^\beta X_2^\beta)/(\gamma_2^\alpha X_2^\alpha) \quad (26)$$

where the mole fractions are those of the limiting miscibility at the temperature T. Remembering that $\Delta G° = -RT\ln K$, that $K = 1$ at the limiting miscibility compositions, and taking logarithms of equations (25-26) yields the relations

$$0 = \ln\gamma_1^\beta - \ln\gamma_1^\alpha + \ln(X_1^\beta/X_1^\alpha) \quad (27)$$

$$0 = \ln\gamma_2^\beta - \ln\gamma_2^\alpha + \ln(X_2^\beta/X_2^\alpha) \quad (28)$$

Using equations (21-22) to substitute for $\ln\gamma_1$ and $\ln\gamma_2$ yields the expressions

$$0 = (X_2^{\beta})^2[B_g + C_g(4X_1^{\beta}-1)] - (X_2^{\alpha})^2[B_g + C_g(4X_1^{\alpha}-1)] + \ln(X_1^{\beta}/X_1^{\alpha}) \quad (29)$$

$$0 = (X_1^{\beta})^2[B_g + C_g(4X_1^{\beta}-3)] - (X_1^{\alpha})^2[B_g + C_g(4X_1^{\alpha}-3)] + \ln(X_2^{\beta}/X_2^{\alpha}) \quad (30)$$

which can be used to evaluate the parameters B_g and C_g from a knowledge of the observed two-phase pairs obtained at each temperature. Plots of B_g and C_g versus reciprocal temperature then yield the parameters B_h and B_s and C_h and C_s, respectively.

A second useful approximation to the properties of a real solution, having small positive deviations from ideality, can often be obtained using the single parameter B_h. Such a solution is symmetrical because the Gibbs free energy of mixing is symmetrical about $X_1 = X_2 = 0.5$ and regular because the entropy of mixing is ideal. The following equations list the properties of the symmetrical and regular solution in terms of excess thermodynamic functions

$$\Delta G^{XS} = B_h R X_1 X_2 \quad (31)$$

$$\Delta S^{XS} = 0 \quad (32)$$

$$\Delta H^{XS} = \Delta H^{M} = B_h R X_1 X_2 \quad (33)$$

$$\Delta C_{p,x}^{M} = 0 \quad (34)$$

$$B_g = B_h/T \ , \ B_h = 2T_c \tag{35}$$

$$X_1 = X_2 = 0.5 \text{ at } T_c \tag{36}$$

$$\Delta H^M(X_1 = X_2 = 0.5) \simeq T_c \tag{37}$$

$$\ln\gamma_1 = B_g X_2^2 \tag{38}$$

$$\ln\gamma_2 = B_g X_1^2 \tag{39}$$

The critical mixing temperature T_c is an important characteristic of a solution. The thermodynamic conditions for a critical mixing temperature are

$$(\partial^2 \Delta G^M / \partial X_1^2)_{P,T} = 0 \tag{40}$$

and

$$(\partial^3 \Delta G^M / \partial X_1^3)_{P,T} = 0 \tag{41}$$

Table II-3 summarizes the two-phase data for the $BaTiO_3$-$CaTiO_3$ solid solutions. The same shorthand notation is used as before: component A_1 is $BaTiO_3$, component A_2 is $CaTiO_3$, solid solution α is $BaTiO_3$ rich, and solid solution β is $CaTiO_3$ rich. The two-phase compositions listed in Table II-3 are determined graphically from Figure II-3. (Although the number of significant figures reported for the two-phase compositions and B_g and C_g values are not warranted by the raw data, they are included in order to avoid round-off errors in calculations based on these values.)

TABLE II-3

Two-Phase Data for $BaTiO_3$-$CaTiO_3$ Solid Solutions

T(°K)	$X_{2\alpha}$	$X_{2\beta}$	B_g	C_g	$B_g=B_h/T^*$
1473	0.209	0.915	2.4699	-0.4182	2.6246
1524	0.215	0.912	2.4478	-0.4163	2.5367
1573	0.226	0.906	2.4086	-0.4106	2.4577
1624	0.244	0.898	2.3520	-0.4122	2.3805
1673	0.263	0.889	2.2969	-0.4122	2.3108
1723	0.290	0.877	2.2267	-0.4175	2.2438
1773	0.324	0.862	2.1480	-0.4267	2.1805
1824	0.374	0.843	2.0447	-0.4551	2.1195
1868	0.424	0.817	1.9579	-0.4638	2.0696

*For the symmetrical and regular solution approximation. See text for details.

The B_g and C_g values reported in the fourth and fifth columns of Table II-3 are calculated using equations (29-30), while the B_g values reported in the sixth column of Table II-3 are calculated from equation (35) for the symmetrical and regular solution model. Graphical extrapolation of the two-phase (binodal) compositions after replotting on a mole fraction composition scale yields estimates for the critical mixing temperature T_c and the composition at T_c of $T_c \sim 1933°K$ and $X_1 \sim 0.4$. The fact that the composition at the extrapolated value of T_c is not $X_c = 0.5$ indicates that the $BaTiO_3$-$CaTiO_3$ solid solution is not strictly symmetrical. Linear least squares fits to B_g and C_g versus reciprocal temperature yield the equations

$$B_g = (3557.49341)/T + 0.12205 \ [0.97] \tag{42}$$

$$C_g = (293.52206)/T - 0.60236 \ [0.73] \tag{43}$$

The numbers in brackets are the correlation coefficients (R) for the least squares fits and are given by

$$R = m\sigma_x/\sigma_y \tag{44}$$

where m is the slope of the line, σ_x is the standard deviation of the x-array, and σ_y is the standard deviation of the y-array.

The calculated values of B_g and C_g can now be used

to compute activity coefficients for $BaTiO_3$ and $CaTiO_3$ as a function of temperature and composition by using equations (21-22). The B_g and C_g values can also be used to calculate the corresponding binodal compositions by using equations (29-30) and (42-43). An example of this later type of calculation is given for the NaCl-KCl system by Thompson and Waldbaum (1969).

Table II-4 lists activity coefficients (γ_{Ba}) for $BaTiO_3$ in $BaTiO_3$-$CaTiO_3$ solid solutions. The values listed, which are for perovskite mole fractions of unity and thus correspond to the solar Ti/Ba ratio of $^{X}Ti = 0.998$, are calculated from equations (21) and (38). The agreement between the two sets of values is gratifying and indicates that use of a more complex set of analytic functions to describe the thermodynamic properties of $BaTiO_3$-$CaTiO_3$ solid solutions is unwarranted for the present purposes.

DISCUSSION

On the basis of the results described above, the following model is proposed to describe the formation of the pure $BaTiO_3$ particulates observed in Allende by Tanaka and Okumura (1977) and Masuda and Tanaka (1977). During cooling along the PSN adiabat strontium and barium condense as $SrTiO_3$ and $BaTiO_3$, respectively, in solid

TABLE II-4

$BaTiO_3$ Activity Coefficients

for $X_{CaTiO_3} = 1.0$

T(°K)	Equation 21 γ_{Ba}	Equation 38 γ_{Ba}
1400	21.2	15.8
1500	18.2	13.2
1600	15.9	11.2
1700	14.1	9.7

solution in perovskite. The $SrTiO_3$-$CaTiO_3$ solution is close to ideal and exhibits only small deviations from ideality. By ~1490°K all strontium is condensed in perovskite. However, the $BaTiO_3$-$CaTiO_3$ solution is non-ideal and the amount of $BaTiO_3$ dissolved in perovskite at a given temperature is substantially less than is dissolved in the ideal solution case. The nonideality of the $BaTiO_3$-$CaTiO_3$ solution also provides a mechanism for readily fractionating barium from calcium and strontium. Thus, at ~1490°K when all strontium is condensed in perovskite, ~35% of all barium is still in the gas. At this point, equilibrium between gas phase barium and perovskite stops. This halt may be due to gas-dust separation, conversion of perovskite to a Ti^{3+}-bearing mineral, or to kinetic barriers. The barium remaining in the gas phase then reacts with the remaining gaseous titanium to form $BaTiO_3$. (At ~1490°K the gas phase Ti/Ba ratio is in the range 2.3-1.4). The $BaTiO_3$ particulates then agglomerate due to the unique electrical properties of $BaTiO_3$, an idea suggested by Masuda and Tanaka (1977).

The exact condensation temperature of the $BaTiO_3$ is a function of the amounts of Ba and Ti remaining in the gas phase when all strontium is condensed in perovskite. Figure II-4 illustrates the variation in $BaTiO_3$ condensation

temperatures versus the fraction of barium remaining in the gas phase for F_{gas} values of 0.01 to 1.0. The calculated $BaTiO_3$ condensation temperatures are compatible with the observed mode of occurrence of $BaTiO_3$ in Allende. Tanaka and Okumura (1977) and Masuda and Tanaka (1977) have observed many $BaTiO_3$ particulates in the matrix of Allende. $BaTiO_3$ particulates and skeletal aggregates have also been observed in some inclusions by Tanaka and Okumura (1977). They have estimated the mineralogical compositions of several $BaTiO_3$-bearing inclusions from their electron microprobe analytical maps as a spinel-hercynite assemblage [$(Mg,Fe)Al_2O_4$], diopside ($CaMgSi_2O_6$), nepheline ($NaAlSiO_4$) and augite. The 10^{-3} bar condensation temperatures of these phases are spinel (1449°K), diopside (1413°K), enstatite (1351°K), and nepheline (775°K) (enstatite-Lattimer and Grossman, 1978; diopside-Trivedi and Larimer, 1980; spinel and nepheline-this work). The condensation temperatures for hercynite and augite, which are not listed, are unknown. The spinel, diopside, enstatite, and nepheline condensation temperatures are compatible with the calculated $BaTiO_3$ condensation temperatures and are also compatible with the suggestion that $BaTiO_3$ particles may have been condensation nuclei for some of the major phases.

Furthermore, Grossman et al. (1977) have presented neutron activation data suggesting the presence of a separate Ba-bearing phase in several coarse grained Allende inclusions. They suggest that the material in these inclusions condensed from the solar nebula by ~1437°K (at 10^{-3} bars pressure). Again the estimated condensation temperatures for the major phases are compatible with the range of $BaTiO_3$ condensation temperatures in Figure II-4.

The effect of several other factors which cannot be quantitatively considered at present due to a lack of the relevant data may also be briefly mentioned. First, the formation of strontium zirconate ($SrZrO_3$) solid solutions with perovskite will increase the temperature at which all strontium is condensed in perovskite. The $SrZrO_3$-$CaTiO_3$ solid solution is expected to be close to ideal because the $CaZrO_3$-$CaTiO_3$ and $SrTiO_3$-$CaTiO_3$ systems exhibit near ideal behavior (Durst et al., 1950; McQuarrie, 1955; McQuarrie and Behnke, 1954). However, McQuarrie and Behnke (1954) have shown that the $BaZrO_3$-$CaTiO_3$ system possesses a miscibility gap and exhibits considerable non-ideality. Thus, solid solution of $BaZrO_3$ in perovskite is expected to be negligible, while solid solution of $SrZrO_3$ in perovskite will increase the strontium 100% condensation temperature.

FIGURE II-4: $BaTiO_3$ condensation temperatures along the solar nebula adiabat. The $BaTiO_3$ condensation temperature is a function of the amount of barium in the gas phase (for constant titanium activities). When all barium is in the gas phase, $BaTiO_3$ condenses at ~1424°K. The calculated $BaTiO_3$ condensation temperatures are compatible with the observed mode of occurrence of $BaTiO_3$ in Allende (Tanaka and Okumura, 1977; Masuda and Tanaka, (1977).

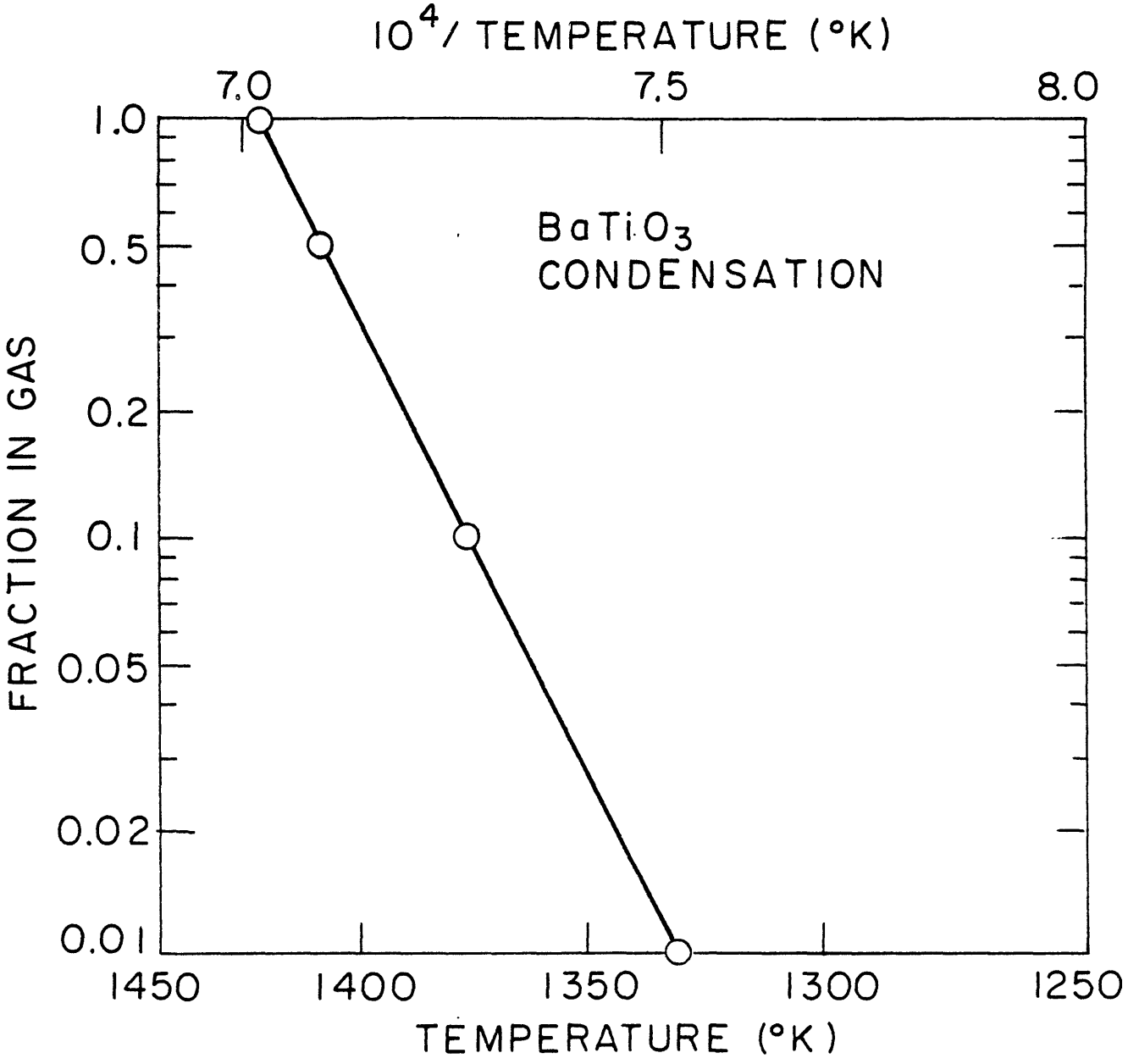
10^4/ TEMPERATURE (°K)
7.0
7.5
8.0
1.0
0.5
0.2
0.1
0.05
0.02
0.01
FRACTION IN GAS
$BaTiO_3$
CONDENSATION
1450
1400
1350
1300
1250
TEMPERATURE (°K)

Second, the effect of possible strontium and barium solution in other calcium-bearing phases such as hibonite ($CaAl_{12}O_{19}$) and melilite ($Ca_2Al_2SiO_7$-$Ca_2MgSi_2O_7$) cannot be calculated due to a lack of thermodynamic data. However, ionic radius considerations suggest that although solution of strontium in these phases may be important, solution of barium may be negligible due to its much larger ionic size.

It is important to note that the effect of both these factors is to increase the strontium 100% condensation temperature without appreciably affecting the barium condensation temperature. Thus, both factors allow perovskite-gas equilibrium to be stopped at higher temperatures when more Ba is in the gas phase, leading to higher $BaTiO_3$ condensation temperatures.

SUMMARY AND CONCLUSIONS

The observation of pure $BaTiO_3$ particulates in the Allende meteorite (Tanaka and Okumura, 1977; Masuda and Tanaka, 1977) has stimulated the development of a simple and consistent model to explain the observations. Condensation calculations along a solar nebula adiabat demonstrate that neither pure $BaTiO_3$ nor pure $SrTiO_3$ condense prior to perovskite ($CaTiO_3$) condensation. Thus, models invoking

titanate solid solutions to explain the observation of pure $BaTiO_3$ particulates need to be considered.

Phase equilibrium studies of alkaline earth titanate systems indicate that the $SrTiO_3$-$CaTiO_3$ solid solution is nearly ideal and that the $BaTiO_3$-$CaTiO_3$ solid solution exhibits a miscibility gap and is nonideal. The phase diagram for the $BaTiO_3$-$CaTiO_3$ system and simple analytic functions representing thermodynamic properties have been used to calculate activity coefficients for $BaTiO_3$ in $BaTiO_3$-$CaTiO_3$ solid solutions. The calculated activity coefficients indicate that significant fractionation of Ba from Ca and Sr can occur during condensation. In particular, a significant fraction of the barium is still in the gas phase after all strontium is condensed in perovskite. The gaseous barium can then react with titanium remaining in the gas to form $BaTiO_3$. The $BaTiO_3$ particulates subsequently agglomerate due to the unique electrical properties of $BaTiO_3$ as suggested by Masuda and Tanaka (1977). Calculated $BaTiO_3$ condensation temperatures are compatible with the observed mode of occurrence of $BaTiO_3$ in Allende.

Finally, an important aspect of the present work is the quantitative treatment of trace element solid solution formation. This treatment provides a firm basis for analogous discussions of trace element fractionations in

meteorites or other solar system material by using activity coefficients determined from experimental phase diagrams.

PART 2

CHEMICAL EQUILIBRIA IN PLANETARY ATMOSPHERES

CHAPTER III: THERMOCHEMISTRY OF SELECTED TRACE ELEMENTS IN JUPITER'S ATMOSPHERE.

INTRODUCTION

The spectroscopic observations of PH_3, CO, and possibly GeH_4 in Jupiter's atmosphere (Ridgway, 1974; Ridgway et al., 1976; Beer, 1975; Larson et al., 1977; Larson et al., 1978; Beer and Taylor, 1978; and Fink et al., 1978) have opened up a new area of research dealing with the use of chemical species as tracers of atmospheric motions. The presence of PH_3 and possibly GeH_4 is attributed to rapid vertical transport of these high-temperature, high-pressure species to cool levels in the atmosphere, a process which is faster than the reactions which destroy these gases in the hot lower atmosphere. Prinn and Barshay (1977) have presented a quantitative treatment of the rapid transport model for CO which indicates that the vertical mixing rates previously estimated from heat flux considerations are rapid enough to quench the reduction of CO and make it observable. However, the observed differences in the CO rotational temperature (Beer and Taylor, 1978; Larson et al., 1978) indicate that a stratospheric CO source such as meteoritic

infall (Prather et al., 1978) may also be required. It will be difficult if not impossible to assess the relative magnitudes of different proposed CO sources until data on the vertical distribution profile of CO in the Jovian atmosphere is obtained from a Jupiter entry probe such as Galileo.

The considerations outlined above and the somewhat distressing fact that kinetic data appear to be lacking for the relevant PH_3 oxidation reaction, which has been postulated to destroy PH_3 in the Jovian atmosphere (Lewis, 1969b; Prinn and Lewis, 1975), have led to the initiation of this study. The thermochemistry of twelve selected moderately volatile elements (Ge, Se, Ga, As, Te, Pb, Sn, Cd, Sb, Tl, In, Bi) along a Jovian adiabat has been investigated in detail in order to suggest possible chemical tracers in addition to those already proposed by Barshay and Lewis (1978). Seven of these elements have not been previously studied and five were investigated by Barshay and Lewis (1978) but are studied in substantially more detail here. The basic reasoning behind this approach has been discussed in detail by Barshay and Lewis (1978), and will be only briefly recapitulated here.

The utility of equilibrium calculations rests on the assumption that rapid vertical transport of atmospheric

gases from the deep lower atmosphere quenches all gas phase reactions thereby freezing in the high-pressure, high-temperature equilibrium configuration. Using the present results it then becomes possible to interpret observed abundances of high-pressure, high-temperature species, e.g., GeH_4, in terms of rapid vertical transport from specific atmospheric levels and to suggest other possible tracers of atmospheric dynamics. In addition to suggesting possible tracers the present results are also used to place reasonably firm upper limits on the abundances of many gases, to describe the stability fields of condensates, and to list compounds which will not be detectable with significant concentration.

EQUILIBRIUM CALCULATIONS: METHODS AND ASSUMPTIONS

Chemical equilibrium calculations were done along an adiabatic temperature-pressure profile in the Jovian atmosphere. The temperature range covered was 1000°-300°K. The construction of the Jovian adiabat used in this study is identical to the construction of the solar nebula adiabat, which is described in Chapter I. The only exception is that the starting point for the adiabat (P_o, T_o) was chosen as (1 bar, 175°K), consistent with

ground-based and spacecraft observations (summarized by various authors in Gehrels, 1976). The relationships between temperature and pressure and between temperature and altitude along the adiabat are presented in Barshay and Lewis (1978). For reference, two other T-P points along the adiabat are 500°K-30 bars and 1500°K-1.4 kilobars. The elements studied, their assumed abundances in a solar composition gas (Cameron, 1973), and the figure number(s) in which they appear are listed in Table III-1. The computational method used is described in Chapter I.

The thermodynamic data used in the present calculations came from approximately 100 sources which are listed in Appendix III-2. In many cases the equilibrium constant for formation of an element or compound from the constituent elements in their designated reference states had to be calculated from the literature data. If at all possible this calculation was done by a third law method and double checked using data from a separate source. In some cases, a second law method which is less accurate was used and the results were still double checked with data from a separate source. Details of the second and third law treatments of equilibrium data are available in the JANAF tables or any standard thermodynamic text.

Table III-1

Assumed Elemental Abundances from Cameron (1973)*

Element	Normalized Abundance ($Si=10^6$)	Figure No.
Ge	115	III-1
Se	67.2	III-1,-3,-4,-6
Ga	48	III-2
As	6.6	III-2
Te	6.42	III-1,-3,-4,-5
Pb	4	III-3
Sn	3.6	III-4
Cd	1.48	III-3
I	1.09	
Sb	0.316	III-5
Tl	0.192	III-5
In	0.189	III-4
Bi	0.143	III-6

*Only elements not previously listed in Table I-1 are included.

RESULTS

The results of the calculations are discussed element by element in order of decreasing abundance. Compounds which do not appear in the figures due to extremely low abundances or activities less than 1 are listed in Appendix III-1.

Germanium

The calculated equilibrium abundances of germanium-bearing gases and the stability fields of Ge condensates are displayed in Figure III-1. These results, which differ from those of Barshay and Lewis (1978), illustrate several important points. First, at temperatures less than 1000°K the major gas phase species are the germanium chalcogenides (GeS, GeSe, and GeTe) and GeH_4. Germane is at best only the second most abundant Ge-bearing gas, and is the third most abundant gas over a wide temperature range. Digermane (Ge_2H_6) is seen to be negligible at all temperatures less than 1000°K along the adiabat.

Second, the condensates are Ge(s), GeTe(s), GeSe(s), GeS(s), and GeO_2(s). Solid GeO does not condense as previously indicated because the thermodynamic data source used by Barshay and Lewis (1978) for GeO(s) (Dean, 1973) is incorrect (the tabulated ΔG°_f, ΔH°_f and S° values at

298.15°K do not satisfy the relation $\Delta G° = \Delta H° - T\Delta S°$). This error coupled with the inclusion of the important chalcogenide compounds GeSe and GeTe into the data set accounts for the differences between the results.

The reported observation of GeH_4 with a mole fraction $\sim 6 \times 10^{-10}$ (Fink et al., 1978) is seen from Figure III-1 to imply rapid vertical transport of GeH_4 from the $T \geq 800°K$ level. At this level there is approximately ten times as much GeS as GeH_4 and about an equal amount of GeSe. However, since the condensation of GeS(g) and GeSe(g) is probably faster than the conversion of GeH_4 to either of these two gases, GeH_4 may be the most abundant Ge-bearing gas at temperatures lower than $T \sim 520°K$ if equilibrium is not exactly attained. Because of direct condensation of GeS and GeSe, they are not included on the list of potential tracers.

Selenium

The results of the calculations on selenium-bearing gases and condensates are presented in Figures III-1, -3, -4, and -6. Hydrogen selenide is the most abundant selenium-bearing gas at temperatures less than 1000°K, with GeSe being the second most abundant selenium gas. Condensation of GeSe(s) at $T \sim 520°K$ severely depletes the abundance of

FIGURE III-1: Equilibrium abundances of germanium-bearing gases and stability fields of germanium condensates along the Jupiter adiabat. The temperature scale is linear in 1/T. The mole fraction X_i of a species i is defined as its partial pressure p_i divided by the total pressure P. The heavy lines which indicate the stability fields of the five condensates have nothing to do with their abundances. The abundances of the different condensates may be estimated from the abundances and rates of disappearance of the gases which constitute them. Notice that solid GeTe and GeSe are always stable once they appear but that Ge(s) becomes unstable relative to GeS(s) which in turn is replaced by GeO_2(s).

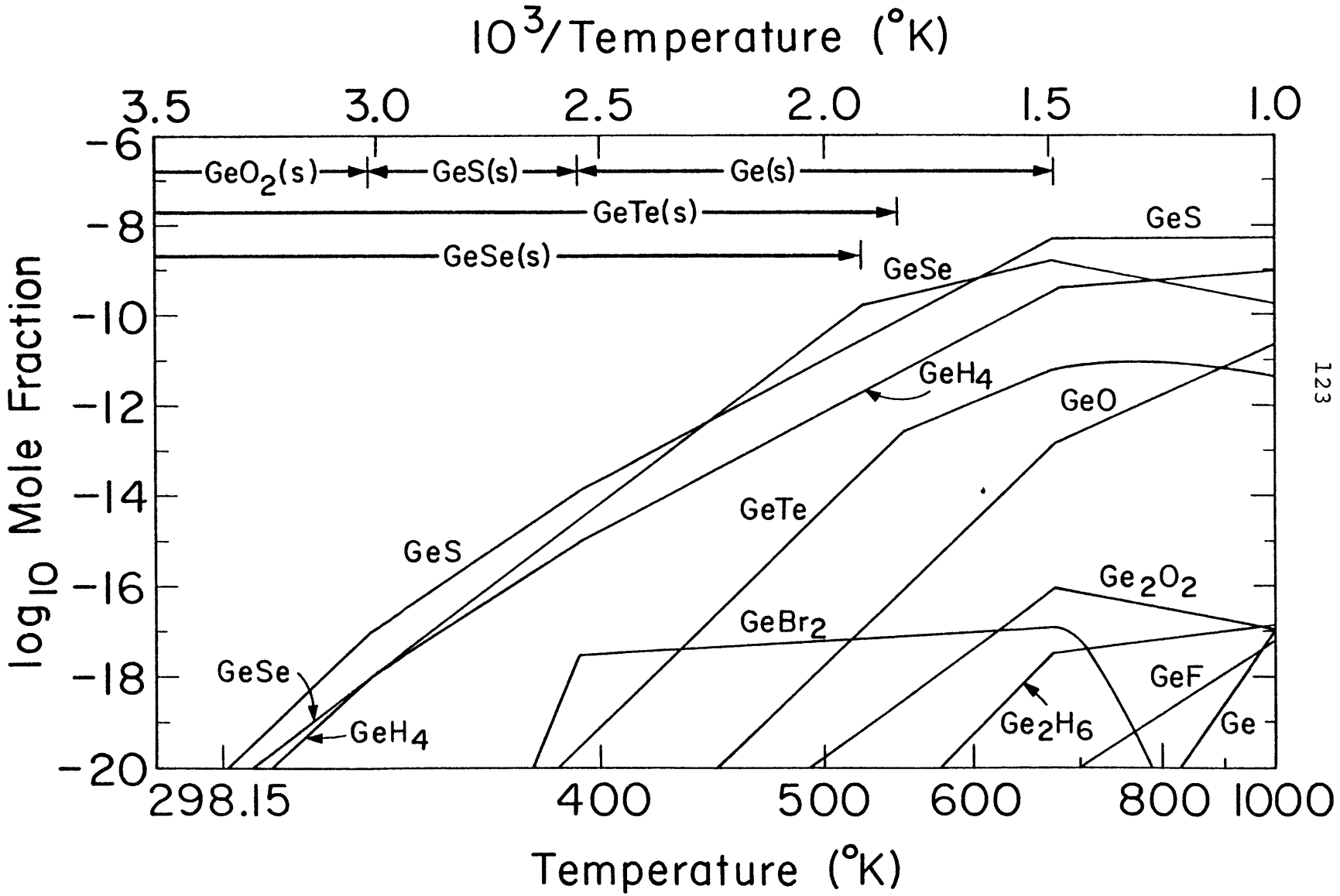
10^3/Temperature (°K)
3.5
3.0
2.5
2.0
1.5
1.0
-6
-8
-10
-12
-14
-16
-18
-20
$\log_{10}$ Mole Fraction
$GeO_2(s)$
GeS(s)
Ge(s)
GeTe(s)
GeSe(s)
GeS
GeSe
GeH_4
GeO
GeTe
GeS
Ge_2O_2
$GeBr_2$
GeSe
GeH_4
GeF
Ge_2H_6
Ge
298.15
400
500
600
800
1000
Temperature (°K)

$H_2Se(g)$.

The low temperature condensation of $H_2Se(g)$ as solid ammonium hydroselenide (NH_4HSe) has also been studied. If equilibrium is not attained at $T \sim 500°K$, H_2Se may be present at essentially solar abundance ($X_{H_2Se} \sim 3.7 \times 10^{-9}$) until NH_4HSe condensation occurs at $T \sim 219°K$. As the H_2Se abundance decreases the condensation of NH_4HSe is delayed until lower temperatures and higher altitudes.

The photolysis of H_2Se in the Jovian upper atmosphere has also been briefly investigated in connection with the possible depletion of H_2Se in the upper atmosphere. The results of calculations made using H_2Se absorption coefficients from Goodeve and Stein (1931), the radiative transfer model of Prinn (1970), and solar flux data from Schultz and Holland (1963) are presented in Figure III-7. Although the results are only approximate they indicate that rapid photolysis of H_2Se around the 200-250°K region will deplete the gas on the time scale of 2 days to 2 weeks. Thus, even if equilibrium is not attained in the lower atmosphere, H_2Se may still be unobservable due to depletion by NH_4HSe condensation and solar UV photolysis. Thus in several ways H_2Se behaves similarly to H_2S.

Gallium

The chemistry of gallium is illustrated in Figure III-2. Lewis (1969b) briefly mentioned that gallium's chemical behavior in the Jovian atmosphere at high temperatures was unknown, although oxides and gallium metal are involatile at 300°K. At high temperatures ($T \sim 1000°K$) Figure III-2 shows that gallium hydroxide is present at solar abundance: $X_{GaOH} \sim 2.7 \times 10^{-9}$. Condensation of solid GaS at $T \sim 970°K$ rapidly reduces the abundances of all Ga-bearing gases to less than 1% of the gallium solar abundance within 100° of its condensation temperature, and no Ga-bearing gas is expected to be observable.

Arsenic

Figure III-2 also displays the relatively simple gas phase chemistry of arsenic. AsF_3, which was not included in the calculations of Barshay and Lewis (1978), is seen to be the major As-bearing gas at $T \leq 360°K$ if equilibrium is attained.

The large stability of AsF_3 also inhibits arsenic precipitation, which may still occur if arsine is not converted to the trifluoride. Low temperature calculations indicate that $AsF_3(s)$ should saturate around the tropopause.

FIGURE III-2. Equilibrium abundances of arsenic- and gallium-bearing compounds along the Jovian adiabat. AsF_3 is the dominant arsenic-bearing gas at low temperatures. The stability of this gas inhibits the condensation of solid arsenic. The abundances of all gallium-containing gases are rapidly reduced by the appearance of solid GaS at ∿970°K. Less than 1% of all gallium is still in the gas phase 100° below this point.

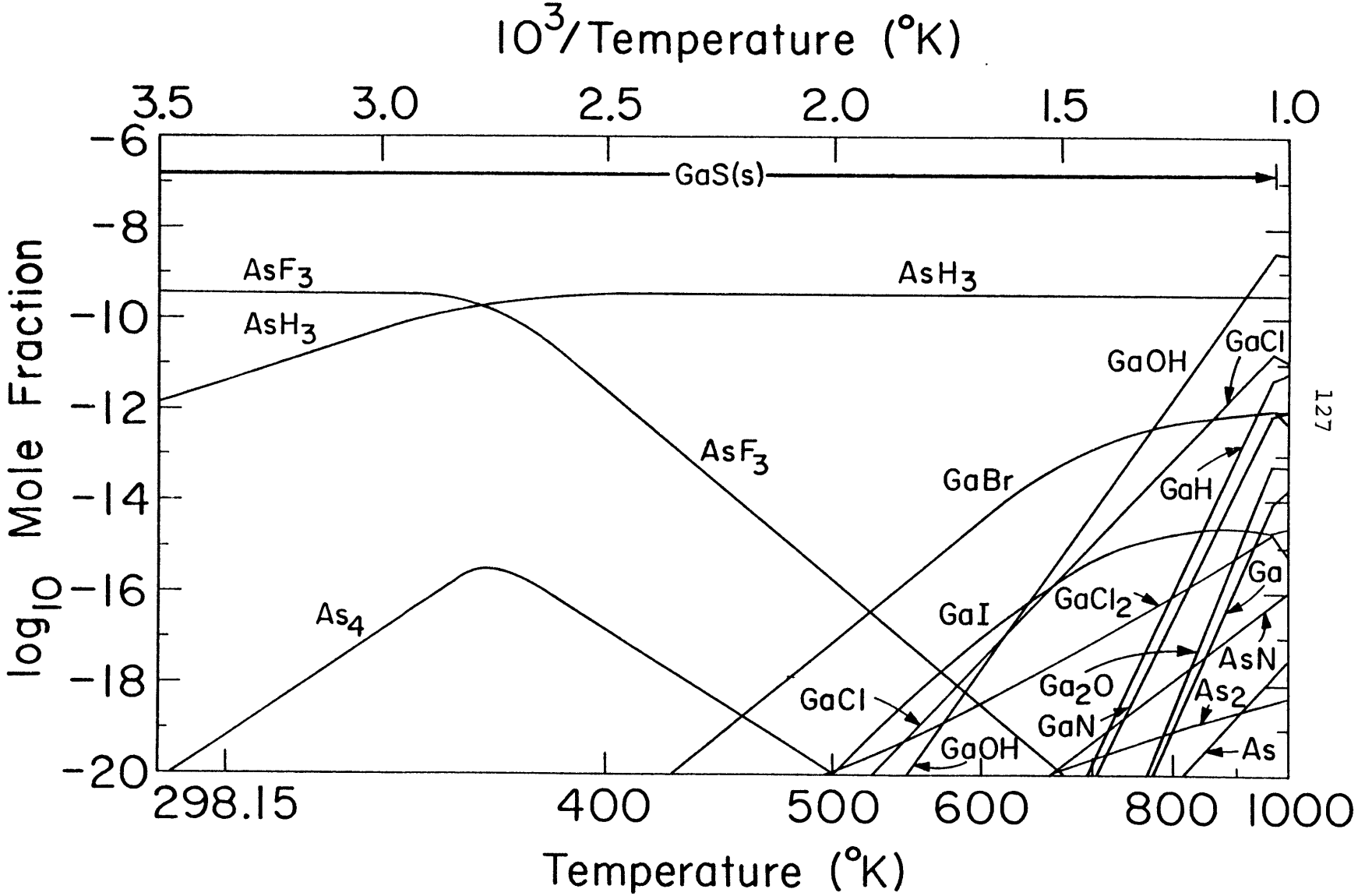
10³/Temperature (°K)
3.5
3.0
2.5
2.0
1.5
1.0
GaS(s)
AsF3
AsH3
AsH3
AsF3
As4
GaOH
GaCl
GaBr
GaH
GaI
GaCl2
Ga
AsN
Ga2O
As2
GaN
GaCl
GaOH
As
log10 Mole Fraction
-6
-8
-10
-12
-14
-16
-18
-20
298.15
400
500
600
800
1000
Temperature (°K)

However, the presence of this condensate in Jupiter's atmosphere must be considered a moot topic until it is known if the conversion of arsine to the trifluoride occurs readily.

Tellurium

The equilibrium chemistry of tellurium is displayed in Figures III-1, -3, -4, and -5. Although tellurium has been investigated by Barshay and Lewis (1978), their results are incorrect because of incorrect data on the thermodynamic functions of $H_2Te(g)$ from Rossini et al. (1952). The ΔH_f° (298.15) value from the compilation of Rossini and coworkers does not agree with a more recent determination (Gunn, 1964) which makes $H_2Te(g)$ more stable with respect to other Te-bearing gases. Thus, if the formation of group IV tellurides (GeTe, SnTe, PbTe) is excluded, H_2Te is present at solar abundance $X_{H_2Te} \sim 3.5 \times 10^{-10}$ down to $T \sim 440°K$ where solid Te condenses. If equilibrium is reached, the H_2Te abundance is reduced due to the successive condensation of PbTe(s), SnTe(s), CdTe(s), and GeTe(s). Calculations on the low temperature stability of solid ammonium hydrotelluride (NH_4HTe) indicates that even at $X_{H_2Te} \sim 3.5 \times 10^{-10}$ the solid NH_4HTe will not condense until the $T \sim 130°K$ level is reached. Depending on the degree to which equilibrium is achieved at higher temperatures

NH_4HTe may not be a stable condensate in the Jovian upper atmosphere.

Lead

The behavior of lead is illustrated in Figure III-3. At equilibrium monatomic Pb and PbTe are the major gases. Plumbane (PbH_4) is highly unstable and never achieves a mole fraction larger than 10^{-18} at temperatures of 1000°K and lower. An interesting feature of the equilibrium chemistry displayed is the stability of liquid Pb. Solid Pb is unstable relative to PbTe(s) and does not condense.

Tin

Figure III-4 depicts the chemistry of tin. The major gases are SnS and SnTe. Stannane (SnH_4) never reaches a mole fraction greater than 10^{-12} ($\sim$0.5% of the Sn solar abundance) at temperatures of 1000°K and below. Analogous to Pb, liquid Sn is stable over a narrow temperature range, but solid Sn is never stable.

Cadmium

The chemistry of cadmium is presented in Figure III-3. Monatomic Cd gas is the only Cd-bearing gas for which data are available. Its abundance is depleted by CdTe(s) condensation at $T \sim 605$°K and then by CdS(s) condensation at $T \sim 440$°K.

FIGURE III-3: Equilibrium abundances of lead- and cadmium-bearing compounds along the Jupiter adiabat. The chemistry of lead contains one of the few instances where a liquid condensate is stable. Lead telluride is more stable than solid lead which never condenses. Plumbane (PbH_4) is seen to be very unstable. The condensation of solid CdTe and later solid CdS dramatically reduces the Cd(g) abundance. Thermodynamic data could not be found for any other cadmium-containing gases. Refer to Barshay and Lewis (1978) to relate the temperature scale to pressure and depth scales.

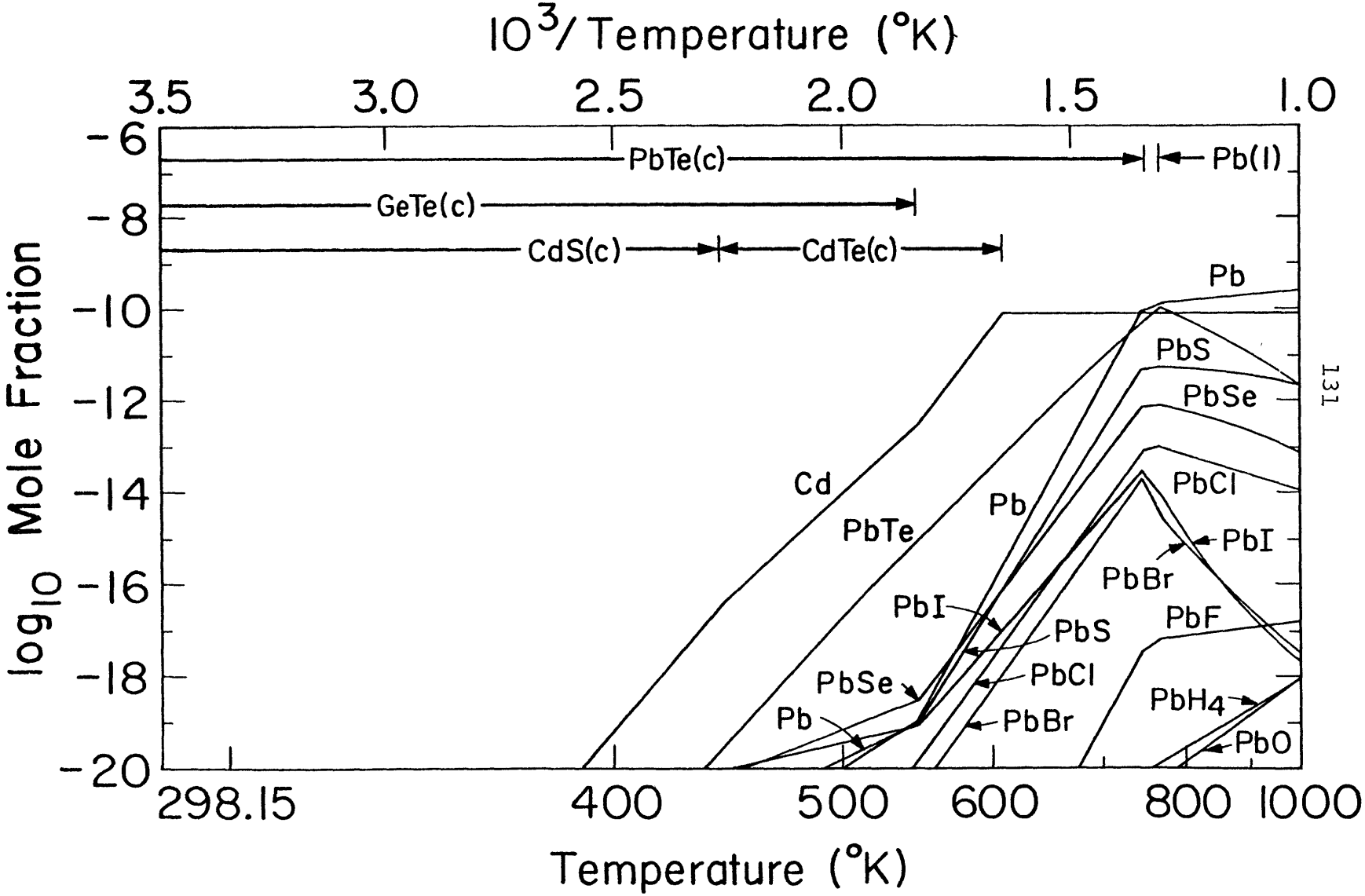
10^3/ Temperature (°K)
3.5
3.0
2.5
2.0
1.5
1.0
-6
-8
-10
-12
-14
-16
-18
-20
$\log_{10}$ Mole Fraction
PbTe(c)
Pb(l)
GeTe(c)
CdS(c)
CdTe(c)
Pb
PbS
PbSe
PbCl
PbI
PbBr
PbF
PbH4
PbO
Cd
PbTe
Pb
PbI
PbS
PbSe
PbCl
Pb
PbBr
298.15
400
500
600
800
1000
Temperature (°K)

FIGURE III-4: Equilibrium abundance of tin-, indium- and tellurium-bearing compounds along the Jupiter adiabat. The major tin-containing gases are SnS and SnTe. Liquid tin condenses at ∿770°K but becomes unstable relative to tin telluride at ∿ 633°K. Tin sulfide is stable at temperatures less than about 450°K. The dominant indium-bearing gases over a wide temperature range are InBr and InI. InCl is also important at high temperatures. The first stable indium condensate is indium sesquisulfide which appears at ∿406°K. The hydrogen telluride abundance is decreased sequentially by the formation of PbTe(s), SnTe(s), CdTe(s), and GeTe(s). Other tellurium-bearing gases are graphed in Figures III-1, -3, and -5.

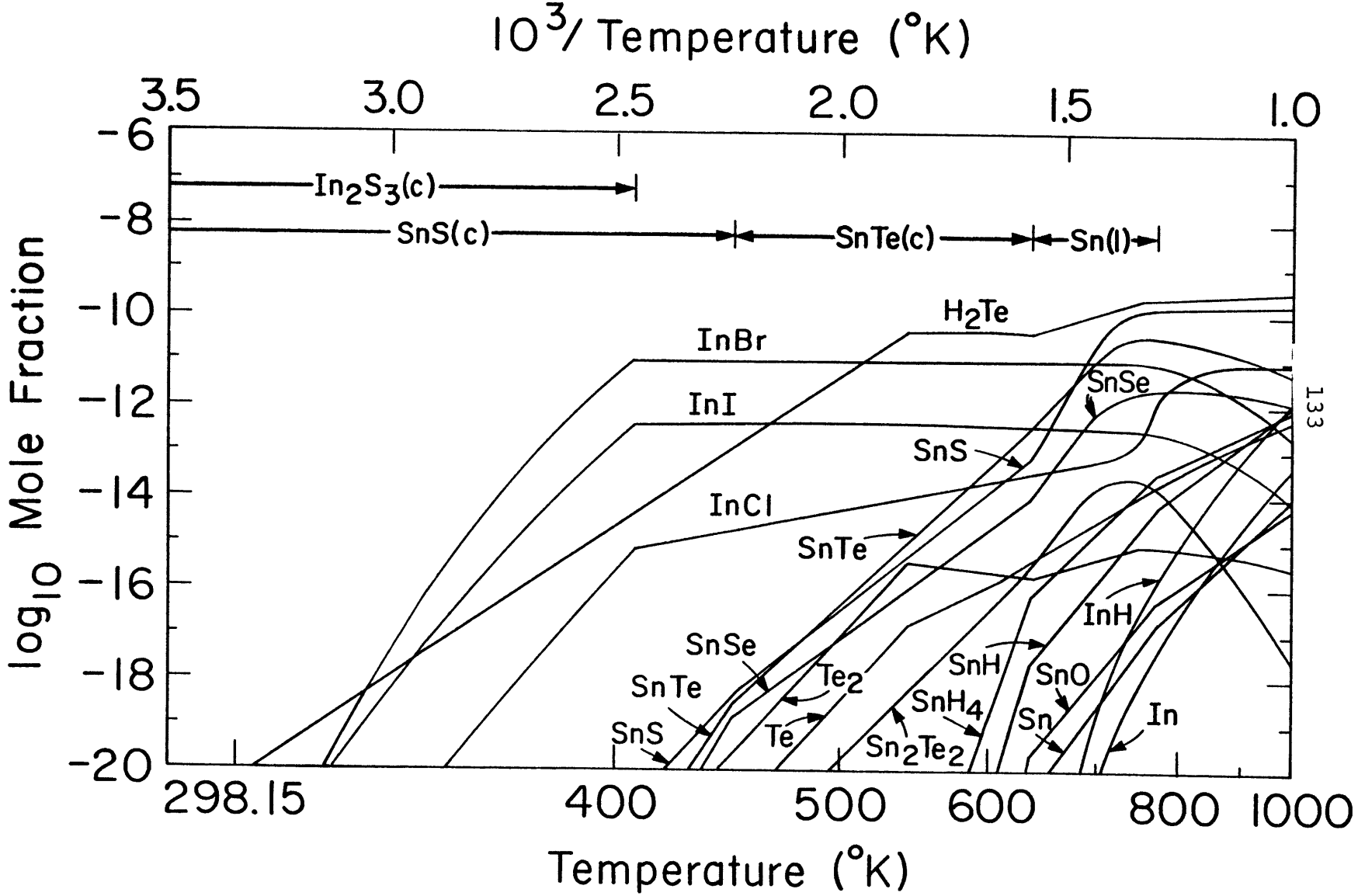
10³/ Temperature (°K)
3.5
3.0
2.5
2.0
1.5
1.0
-6
-8
-10
-12
-14
-16
-18
-20
log10 Mole Fraction
In2S3(c)
SnS(c)
SnTe(c)
Sn(l)
H2Te
InBr
InI
InCl
SnSe
SnS
SnTe
InH
SnH
SnO
SnH4
Sn
In
Te2
Te
Sn2Te2
298.15
400
500
600
800
1000
Temperature (°K)

Antimony

Figure III-5 presents the results of calculations on Sb-bearing gases and condensates. Stibine (SbH_3) and SbS which have similar abundances and Sb_4 are the major gases. Solid Sb condenses at T ∿ 600°K because Sb_2Te_3(s) is unstable owing to the prior depletion of H_2Te by PbTe(s), SnTe(s), and CdTe(s) condensation.

Thallium and Indium

The equilibrium chemistry of thallium and indium is displayed in Figures III-5 and III-4, respectively. In both cases at temperatures less than T ∿ 800°K the major gases are the monochloride, monobromide, and monoiodide. Indium condenses as the sesquisulfide In_2S_3(s) at T ∿ 406°K, whereas thallium condenses as the monoiodide TlI(s) at T ∿ 390°K.

Bismuth

Figure III-6 illustrates the behavior of bismuth along the adiabat. At temperatures greater than approximately 550°K monatomic and diatomic bismuth are the major gases, while BiI and BiBr are the dominant Bi-bearing gases below this temperature. Liquid Bi first condenses at T ∿ 680°K and solid Bi becomes unstable relative to Bi_2S_3(s)

FIGURE III-5: Equilibrium abundances of thallium- and antimony-bearing compounds along the Jupiter adiabat. Major thallium-containing gases are TlI, TlBr, and TlCl. Abundances of all three gases drop when TlI condenses at ∿390°K. At high temperatures stibine (SbH_3) and SbS are the major antimony-bearing gases. As the temperature drops Sb_4 gas rapidly becomes dominant. Antimony condenses at ∿600°K and is always more stable than Sb_2Te_3(s).

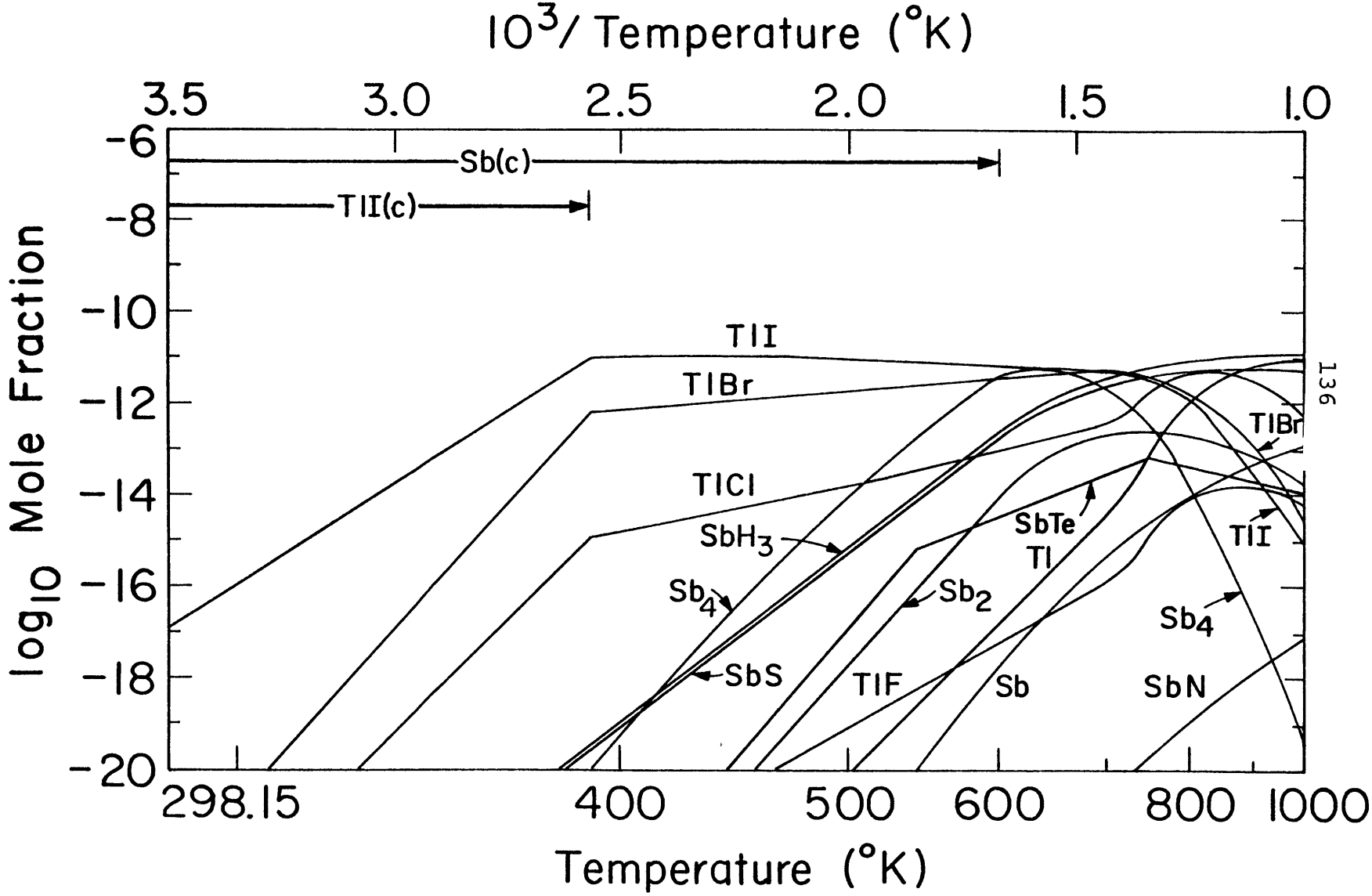
10³/ Temperature (°K)
3.5
3.0
2.5
2.0
1.5
1.0
-6
-8
-10
-12
-14
-16
-18
-20
log10 Mole Fraction
Sb(c)
TlI(c)
TlI
TlBr
TlCl
SbH3
Sb4
SbS
Sb2
Tl
SbTe
TlF
Sb
SbN
298.15
400
500
600
800
1000
Temperature (°K)

FIGURE III-6: Equilibrium abundances of bismuth-bearing compounds and of hydrogen selenide along the Jovian adiabat. Monatomic and diatomic bismuth are the major gases at high temperatures and BiI and BiBr are the most abundant bismuth-containing gases at lower temperatures. Bismuth condenses while it is still a liquid at ∿680°K. At ∿360°K Bi_2S_3 becomes stable relative to solid Bi. The abundance of H_2Se is relatively constant until solid GeSe condenses at ∿520°K. Other selenium-bearing compounds are graphed in Figures III-1, -3, and -4.

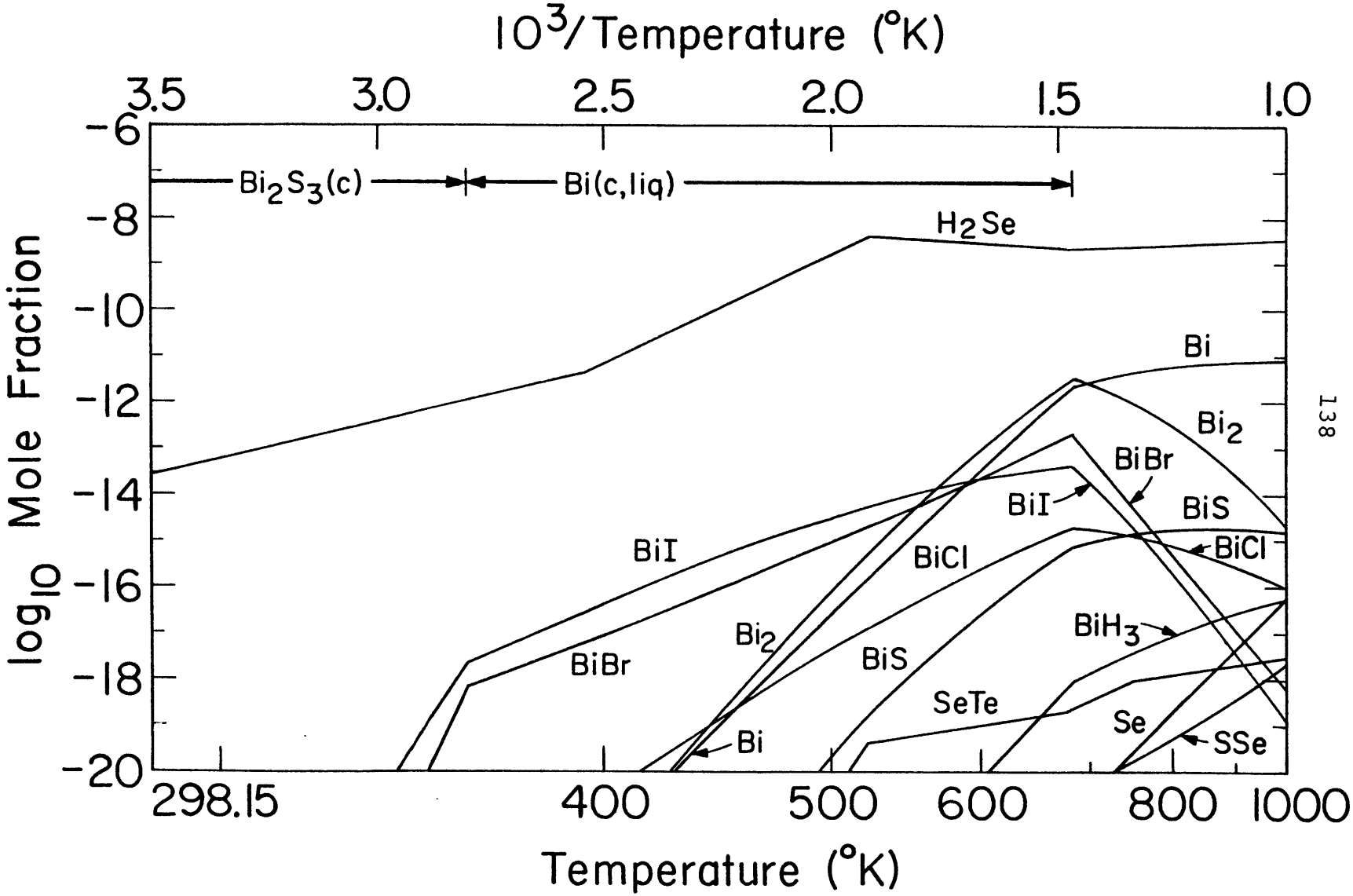
10³/Temperature (°K)
3.5
3.0
2.5
2.0
1.5
1.0
-6
-8
-10
-12
-14
-16
-18
-20
log10 Mole Fraction
Bi2S3(c)
Bi(c,liq)
H2Se
Bi
Bi2
BiBr
BiI
BiS
BiCl
BiH3
SeTe
Se
SSe
298.15
400
500
600
800
1000
Temperature (°K)

FIGURE III-7: The lifetime of hydrogen selenide against depletion by photolysis. Condensation of H_2Se as solid NH_4HSe and rapid depletion of the H_2Se gas phase abundance by photolysis both occur in the same region of the atmosphere around the 220°K level. The graph was calculated assuming a solar abundance of H_2Se below this level (higher temperatures), a H_2Se abundance fixed by the vapor pressure of NH_4HSe(s) above this level (lower temperatures), and complete clearing of high-altitude cloud cover (the Belts). Approximate dynamic mixing times are indicated for $K = 10^8$ cm^2 sec^{-1} (300°K level), 10^6 (220°), and 10^4(140°): mixing probably cannot maintain a near-solar H_2Se abundance against photolysis above the ∿250°K level. Thus NH_4HSe condensation probably is limited to regions of NH_3(s) cloud cover (the Zones).

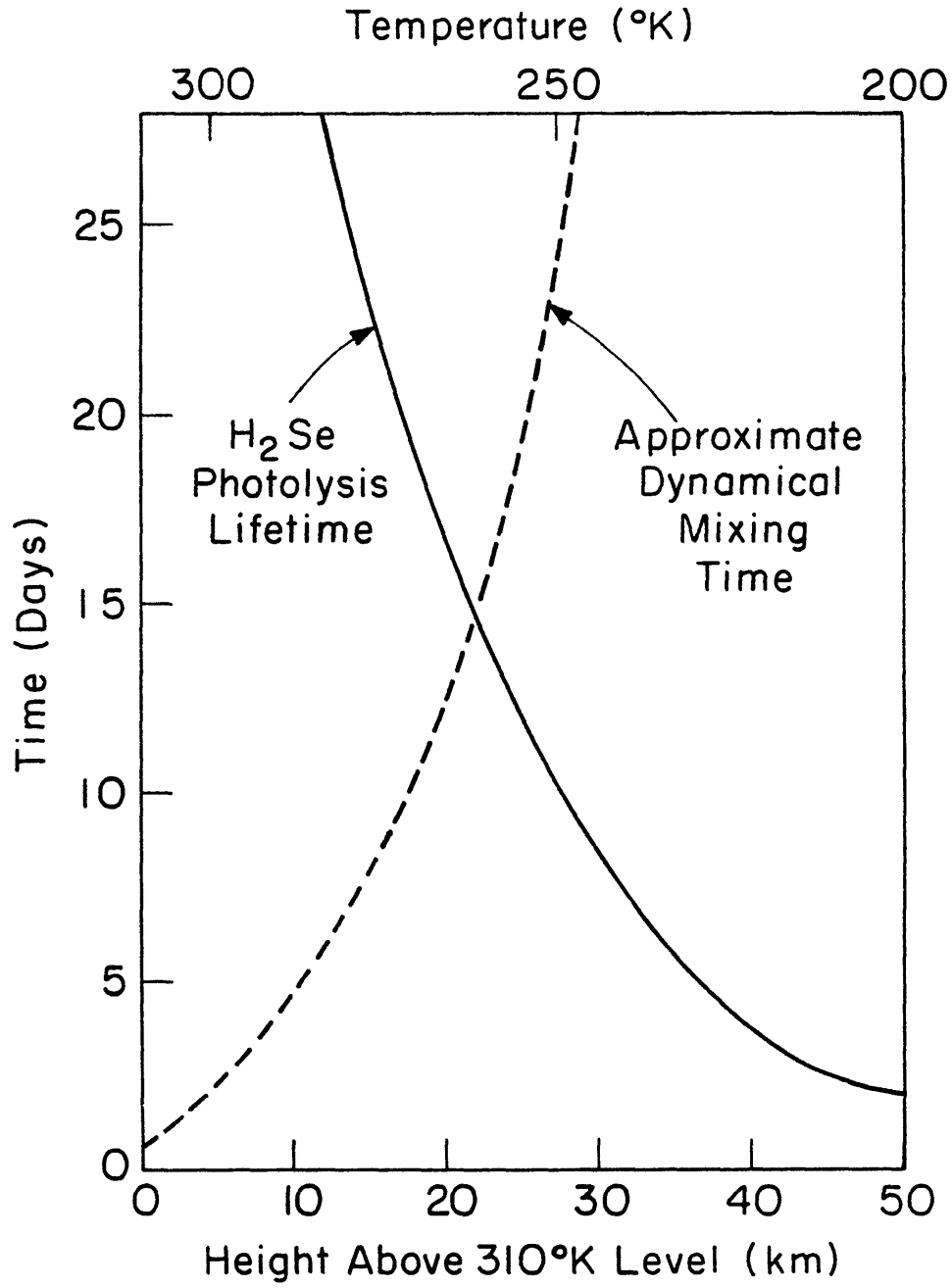
Temperature (°K)
300
250
200
25
20
15
10
5
0
Time (Days)
H_2Se Photolysis Lifetime
Approximate Dynamical Mixing Time
0
10
20
30
40
50
Height Above 310°K Level (km)

at T $\sim$ 360°K. Bismuthine (BiH_3) is seen to be very unstable and it never reaches a mole fraction larger than 10^{-16} at 1000°K and below.

SUMMARY AND CONCLUSIONS

Potential chemical tracers of atmospheric dynamics revealed by this study (excluding those already mentioned by Barshay and Lewis, 1978) are AsF_3, InBr, TlI, and SbS. Although H_2Se (proposed as a tracer by Barshay and Lewis, 1978) and H_2Te are both present at solar abundances at T $\sim$ 1000°K, their depletion by the condensation of group IV selenides and tellurides may render them unobservable. Furthermore, additional considerations such as the condensation of NH_4HSe around the 220°K level and rapid photolysis of H_2Se in the 200-250°K region may also decrease the H_2Se abundance and make its observation above the NH_3 cloud layer even more unlikely. Of course these same considerations also mean that H_2Se is a potential tracer of dynamics both in the deep atmosphere where selenide condensation occurs and also in the upper atmosphere where solar UV photolysis is important. Similar reasoning applies to H_2Te which is both highly photolabile (Goodeve and Stein,1931) and susceptible to telluride condensation

in the lower atmosphere.

The reported observation of GeH_4 in Jupiter's atmosphere (Fink et al., 1978) can be explained by the present calculations if rapid mixing from the T ∿ 800°K region of the Jovian atmosphere occurs. This explanation is in accord with the postulated rapid vertical transport of PH_3 from the T ∿ 800-1000°K region and of CO from the T ∿ 1100°K level of Jupiter's atmosphere (Barshay and Lewis, 1978; Prinn and Barshay, 1977). A more precise explanation of the presence of GeH_4 must await confirmation of the observations and an investigation of the kinetics of relevant reactions.

Of the potential tracers identified in the present study, three have mole fractions close to 10^{-11}. Quenching of SbS from the T ∿ 700°K level could provide one such tracer, while the abundances predicted for InBr and TlI near the 400°K level are $\sim 10^{-11}$ without the need for high temperature quenching. The abundance of AsF_3 if it forms readily from AsH_3 can reach a mole fraction of 3×10^{-10}. It is felt that the prospects for discovery of other tracers of deep mixing beyond those theoretically identified so far are not bright: the ∿700 compounds of the 34 elements which have now been studied carefully include all the abundant and volatile elements.

ACKNOWLEDGEMENTS

Many people have helped me and have contributed to my intellectual development during my tenure at MIT, and to thank all of them in such a short space is impossible. However, several individuals, groups of people, and organizations merit special thanks.

My advisor Professor John Lewis has greatly influenced my thinking and has provided encouragement and support throughout the time I have worked with him. My association with his former and present students, who are too numerous to name, has also been beneficial.

Other faculty members in the Earth and Planetary Science and Meteorology departments who have aided my education (either through courses or personal contact) include Roger Burns, Frederick Frey, Patrick Hurley, and Ronald Prinn.

Professor Clark Stephenson of the Chemistry department also merits special thanks for his advice in many areas of thermodynamics.

I also want to thank Professor Gordon Pettengill, The Meteoritical Society, and the Earth and Planetary Sciences Department for help in obtaining financial support

to attend the Heidelberg meeting of The Meteoritical Society.

Finally, I thank my wife Marie for her constant support and encouragement which have been invaluable.

APPENDIX I

ADDITIONAL COMPOUNDS WHICH WERE STUDIED

This appendix lists compounds which were investigated but not included in the figures for Chapter I. Unstable condensates (pure solids and liquids with less than unit activity and solid solutions that are of negligible importance in an elemental mass balance sum) and minor gases (mole fractions always less than 10^{-15}) are listed. The different phases are indicated by (c) for crystalline pure solid, (l) for liquids (ss) for solid solution, and (g) for gases. The lack of one of the above labels indicates a gas. Compounds are listed under the least-abundant constituent element.

Na

$(NaOH)_2$, $(NaCN)_2$, NaH(c), NaOH(c,l), Na_2O(c,l), Na_2S(c,l), $Na_2Si_2O_5$(c,l), NaCN(c,l), Na_2CO_3(c,l), NaO_2(c), Na_2O_2(c), Na_2SO_4(c,l), $NaNO_3$(c,l), $NaAlO_2$(c).

P

P_4, P_4O_{10}(c,g), P_4S_3(c,l,g), $Mg_3(PO_4)_2$(c), P(white, c), P(red, c).

Cl

NaCl(c,l), Na_3AlCl_6(c), $NaAlCl_4$(c), $POCl_3$, PCl_3, $PSCl_3$,

PCl_5, Cl_2, $Ca_5(PO_4)_3Cl$(c,ss), CCl, CNCl, $FeCl_2$(c,l), $MgCl_2$(c,l), NH_4Cl(c).

K

K_2, $(KOH)_2$, $(KCN)_2$, KH(c), KCl(c,l), KOH(c,l), K_2O(c), K_2S(c,l), K_3AlCl_6(c), $KAlO_2$(c), $KAlCl_4$(c), $KClO_4$(c), KCN(c,l), K_2CO_3(c,l), KO_2(c), K_2O_2(c), K_2SO_4(c,l), $KAl(SO_4)_2$(c), KNO_3(c,l).

F

F_2, $NaAlF_4$, $(NaF)_2$, NaF(c,l), Na_3AlF_6(c,l), Na_2SiF_6(c), PFS, PF_2, POF_3, PF_3, PSF_3, PF_5, $(KF)_2$, KF(c,l), K_3AlF_6(c), $KMg_3AlSi_3O_{10}F_2$(c), MgF_2(c,l,g), CaF_2(c,l,g), FeF_2(c,l,ss), NH_4F(c).

Br

Br_2(l,g), $(NaBr)_2$, $(KBr)_2$, NaBr(c,l), KBr(c,l), NH_4Br(c), $FeBr_2$(c,l,g), $CaBr_2$(c,l,g), $MgBr_2$(c,l,g).

APPENDIX II

THERMODYNAMIC DATA SOURCES FOR CHAPTER II

The thermodynamic data sources for selected phases are listed. Thermodynamic data for many compounds included in the study came from standard compilations. The data for JANAF compounds were taken from the most recent table (Chase et al., 1974, 1975, 1978; Stull and Prophet, 1971). Data for USGS minerals were taken from the first printing of Robie et al. (1978). Data for minerals which are in both sets of compilations were taken from the table judged to be more reliable. The labels (s), (l), and (g) indicate solid, liquid, and gas, respectively. The lack of a label indicates a gas.

The log K values for formation of an element or compound from the constituent element(s) in their designated reference states are taken from the following sources. JANAF tables and supplements: Ti(s,l,g), TiO, TiO_2(s,g), Ti_3O_5(s), Ti_4O_7(s), TiF, TiF_2, Zr(s,g), ZrO, ZrO_2(s,g), ZrF, Ca(s,l,g), Ca_2, CaO, CaOH, $Ca(OH)_2$, Sr(s,l,g), SrO(s,g), SrOH, $Sr(OH)_2$, SrF, SrF_2, SrCl, $SrCl_2$, Ba(s,l,g), BaO(s,g), BaOH, $Ba(OH)_2$, BaF, BaF_2, BaCl, and $BaCl_2$. Robie et al. (1978): zircon, perovskite, gehlenite, akermanite, and diopside.

The log K values are calculated by combining enthalpy, entropy, and free energy data from one or more sources. Mills (1974): CaS, SrS, and BaS. Kelley (1960) and Parker *et al.* (1971): $SrTiO_3(s)$, $Sr_2TiO_4(s)$, $BaTiO_3(s)$, and $Ba_2TiO_4(s)$. Levitskii *et al.* (1976) and Parker *et al.* (1971): $SrZrO_3(s)$. Odoj and Hilpert (1976) and Parker *et al.* (1971): $BaZrO_3(s)$. Parker *et al.* (1971): $CaZrO_3(s)$.

APPENDIX III-1

ADDITIONAL COMPOUNDS WHICH ARE NOT GRAPHED

This appendix lists compounds which were investigated but not included in the figures for Chapter III. Refer to Appendix I of Fegley and Lewis (1979).

APPENDIX III-2

THERMODYNAMIC DATA SOURCES FOR CHAPTER III

Refer to Appendix II of Fegley and Lewis (1978).

REFERENCES

Allen, R.O. and Clark, P.J. (1977). Fluorine in meteorites. Geochim. Cosmochim. Acta, 41, 581-585.

Barshay, S.S. and Lewis, J.S. (1976). Chemistry of primitive solar material. Ann. Rev. Astron. Astrophys., 14, 81-94

Barshay, S.S. and Lewis, J.S. (1978). Chemical structure of the deep atmosphere of Jupiter. Icarus, 33, 593-611.

Barshay, S.S. and Lewis, J.S. (1979). Accretion and the equilibrium condensation model. In preparation.

Beer, R. (1975). Detection of carbon monoxide in Jupiter. Astrophys. J., 200, L167-L169.

Beer, R. and Taylor, F.W. (1978). The abundance of carbon monoxide in Jupiter. Astrophys. J., 221, 1100-1109.

Boynton, W.V. (1975). Fractionation in the solar nebula: condensation of yttrium and the rare earth elements. Geochim. Cosmochim. Acta, 39, 569-584.

Boynton, W.V. (1978). Fractionation in the solar nebula. II. Condensation of Th, U, Pu and Cm. Earth Planet. Sci. Lett., 40, 63-70.

Cameron, A.G.W. (1968). A new table of abundances of the elements in the solar system. In Origin and Distribution of the Elements (L.H. Ahrens, Ed.), pp.125-143. Pergamon, Oxford.

Cameron, A.G.W. (1973). Abundances of the elements in the solar system. Space Sci. Rev., 15, 121-146

Cameron, A.G.W. (1978). Physics of the primitive solar nebula and of giant gaseous protoplanets. In Protostars and Planets (T. Gehrels, Ed.), pp.453-487. Univ. of Arizona Press, Tucson.

Castellan, G.W. (1971). Physical Chemistry, second ed., pp.357-362. Addison-Wesley, Reading, MA.

Chase, M.W., Curnutt, J.L., Hu, A.T., Prophet, H., Syverud, A.N. and Walker, L.C. (1974). JANAF Thermochemical Tables, 1974 Supplement. J. Phys. Chem. Ref. Data, 3, 311-480.

Chase, M.W., Curnutt, J.L., McDonald, R.A. and Syverud, A.N. (1978). JANAF Thermochemical Tables, 1978 Supplement. J. Phys. Chem. Ref. Data, 7, 793-940.

Chase, M.W., Curnutt, J.L., Prophet, H., McDonald, R.A. and Syverud, A.N. (1975). JANAF Thermochemical Tables, 1975 Supplement. J. Phys. Chem. Ref. Data, 4, 1-175.

Clark, B.C. and Baird, A.K. (1979). Chemical analysis of Martian surface materials: status report. Lunar and Planetary Science, X, 215-217.

Clark, B.C., Baird, A.K., Rose, H.J., Jr., Toulmin, P., III, Keil, K., Castro, A.J., Kelliher, W.C., Rowe, C.D. and Evans, P.H. (1976). Inorganic analyses of Martian surface samples at the Viking landing sites. Science, 194, 1283-1288.

CODATA Task Group. (1977). CODATA recommended key values for thermodynamics, 1977. J. Chem. Thermo., 10, 903-906.

Connes, P., Connes, J., Benedict, W.S. and Kaplan, L.D. (1967). Traces of HCl and HF in the atmosphere of Venus. Astrophys. J., 147, 1230-1234

Curtis, D.B. and Schmitt, R.A. (1979). The petrogenesis of L-6 chondrites: insights from the chemistry of minerals. Geochim. Cosmochim. Acta, 43, 1091-1103.

Davis, A.M. and Grossman, L. (1979). Condensation and fractionation of rare earths in the solar nebula. Geochim. Cosmochim. Acta, 43, 1611-1632.

Dean, J.A. (1973). Lange's Handbook of Chemistry, 11th ed. McGraw-Hill, New York.

De Laeter, J.R. and Hosie, D.J. (1978). The abundance of barium in stony meteorites. Earth Planet. Sci. Lett., 38, 416-420.

DeVries, R.C. and Roy, R. (1955). Phase equilibria in the system $BaTiO_3$-$CaTiO_3$. J. Am. Ceram. Soc., 38, 142-146.

Dreibus, G., Spettel, B., and Wänke, H. (1979). Halogens in meteorites and their primordial abundances. In Origin and Distribution of the Elements, Proceedings of the Second Symposium, Paris, May 1977. (L.H. Ahrens, Ed.), pp.33-38. Pergamon Press, Oxford.

Duff, E.J. (1972a). Orthophosphates-Xl. Bromapatite: Stability of solid solutions of bromoapatite with other calcium apatites under aqueous conditions. J. Inorg. Nucl. Chem., 34, 101-108.

Duff, E.J. (1972b). Orthophosphates-IX. Chloroapatite: Phase relationships under aqueous conditions along the $Ca_5F(PO_4)_3$-$Ca_5Cl(PO_4)_3$ and $Ca_5OH(PO_4)_3$-$CA_5Cl(PO_4)_3$ joins of the system CaO-$CaCl_2$-CaF_2-P_2O_5-H_2O. J. Inorg.Nucl. Chem., 34, 859-871.

Durst, G., Grotenhuis, M. and Barkow, A.G. (1950). Solid solubility study of barium, strontium and calcium titanates. J. Am. Ceram. Soc., 33, 133-139.

El Goresy, A., Nagel, K. and Ramdohr, P. (1978). Fremdlinge and their noble relatives. Proc. Lunar Planet. Sci. Conf. 9th, 1279-1303.

Farrington, O.C. (1915). Meteorites. pp.157-160. Published by the author.

Fegley, B., Jr. (1978). Paper presented at the 10th Annual meeting of the Division of Planetary Sciences of the AAS. Pasadena, CA., October 1978.

Fegley, B., Jr. (1979a). Chondrite mineralogy and equilibrium chemistry of the alkalis, halogens and phosphorus in the primitive solar nebula. Nininger Meteorite Award Essay, 1978-79.

Fegley, B., Jr. (1979b). Chondrite mineralogy and equilibrium chemistry of the alkalis, halogens, and phosphorus. Meteoritics, 14, 395-397.

Fegley, B., Jr. (1979c). Paper presented at the 11th Annual meeting of the Division of Planetary Sciences of the AAS, Clayton, MO., October 1979.

Fegley, B., Jr. (1980a). Condensation of barium, strontium, and zirconium in the primitive solar nebula. Lunar and Planetary Science, XI, 279-281.

Fegley, B., Jr. (1980b). Barium titanate condensation and alkaline earth fractionation in the primitive solar nebula. In preparation.

Fegley, B., Jr. and Lewis, J.S. (1979). Thermodynamics of selected trace elements in the Jovian atmosphere. Icarus, 38, 166-179.

Fegley, B., Jr. and Lewis, J.S. (1980). Volatile element chemistry in the solar nebula: Na, K, F, Cl, Bl and P. Icarus, 41,

Fink, U., Larson, H.P. and Treffers, R.R. (1978). Germane in the atmosphere of Jupiter, Icarus, 34, 344-354.

Fuchs, L.H. (1969a). The phosphate mineralogy of meteorites. In Meteorite Research. (P.M. Millman, Ed.), pp.683-695. D. Reidel, Dordrecht-Holland.

Fuchs, L.H. (1969b). X-ray crystallographic evidence for the meteoritic occurrence of nepheline. Meteoritics, 4, 176-177.

Gehrels, T. (Ed.) (1976). Jupiter. University of Arizona Press, Tucson.

Goldberg, R.H., Burnett, D.S., Furst, M.J. and Tombrello, T.A. (1974). Fluorine concentrations in carbonáceous chondrites. Meteoritics, 9, 347-348.

Goodeve, C.F. and Stein, N.O. (1931) The absorption spectra and the optical dissociation of the hydrides of the oxygen group. Trans. Faraday Soc., 27, 393-404.

Gottschal, A.J. (1958). Heats of formation of hydroxy-, fluor- and chlorapatites. J.S. African Chem. Inst., 11, 45-52.

Grossman, L. (1972). Condensation in the primitive solar nebula. Geochim. Cosmochim. Acta, 36, 597-619.

Grossman, L., Ganapathy, R., Methot, R.L. and Davis, A.M. (1979). Trace elements in the Allende meteorite-IV. Amoeboid olivine aggregates. Geochim. Cosmochim. Acta., 43, 817-829.

Grossman, L. and Larimer, J.W. (1974). Early chemical history of the solar system. Rev. Geophys. Space Phys., 12, 71-101.

Grossman, L. and Olsen, E. (1974). Origin of the high-temperature fraction of C2 chondrites, Geochim. Cosmochim. Acta, 38, 173-187.

Grossman, L. and Steele, I.M. (1976). Amoeboid olivine aggregates in the Allende meteorite. Geochim. Cosmochim. Acta, 40, 149-155.

Gunn, S.R. (1964). The heats of formation of H_2Se and H_2Te. Correlations of simple covalent hydrides. J. Phys. Chem., 69, 949-952.

Handbook of Chemistry and Physics. (1961). 43rd ed., p.2325. Chemical Rubber Pub. Co., Cleveland, Ohio.

Helgeson, H.C., Delany, J.M., Nesbitt, H.W. and Bird, D.K. (1978). Summary and Critique of the Thermodynamic Properties of Rock-Forming Minerals. Am. J. Sci., 278A, 1-229.

Jacques, J.K. (1963). The heats of formation of fluorapatite and hydroxyapatite. J. Chem. Soc., 3820-3822.

Keil, K. (1968). Mineralogical and chemical relationships among enstatite chondrites. J. Geophys. Res., 73, 6945-6976.

Keil, K. et al. (1976). Progress by the consorts of Angra dos Reis. Lunar Science, VII, 443-445.

Kelley, K.K. (1960). Contributions to the Data on Theoretical Metallurgy, XIII, High-Temperature Heat-Content, Heat-Capacity, and Entropy Data for the Elements and Inorganic Compounds. U.S. Bureau of Mines Bulletin, 584, Washington, D.C.

Komarek, K.L. (1963). Direct reduction of iron ores containing phosphorus. Metall. Soc. AIME Trans., 227, 136-145.

Kubaschewski, O., Evans, L.L. and Alcock, C.B. (1967). Metallurgical Thermochemistry, 4th ed., pp. 215-220. Pergamon Press, Oxford.

Kurat, G. (1967). Einige chondren aus dem meteoriten von Mezö-Madaras. Geochim. Cosmochim. Acta, 31, 1843-1858.

Larimer, J.W. and Bartholomay, M. (1979). The role of carbon and oxygen in cosmic gases: some applications to the chemistry and mineralogy of enstatite chondrites. Geochim. Cosmochim. Acta, 43, 1455-1466.

Larson, H.P., Fink, U., and Treffers, R.R. (1978). Evidence for CO in Jupiter's atmosphere from airborne spectroscopic observations at 5 microns. Astrophys. J., 219, 1084-1092.

Larson, H.P., Treffers, R.R. and Fink, U. (1977). Phosphine in Jupiter's atmosphere: the evidence from high-altitude observations at 5 micrometers. Astrophys. J., 211, 972-979.

Lattimer, J.M. and Grossman, L. (1978). Chemical condensation sequences in supernova ejecta. Moon and Planets, 19, 169-184.

Letoffe, J.M., Joly, R.D. Thourey, J., Perachon, G. and Bousquet, J. (1974). Determination of enthalpy of formation of potassium polysulfides. J. Chim. Phys. Physiochim. Biol., 71(3), 427-430.

Letoffe, J.M., Thourey, J., Perachon, G. and Bousquet, J. (1976). Determination des enthalpies standards de formation des polysulfures de sodium et de lithium. Bull. Soc. Chim. Fr., 1976, 424-426.

Levitskii, V.A., Tsagareishvili, D.Sh., and Gvelesiani, G.G. (1976). Enthalpy and specific heat of strontium and barium zirconates at high temperatures. High Temp., 14, 69-72.

Lewis, J.S. (1969a). The clouds of Jupiter and the NH_3-H_2O and NH_3-H_2S systems. Icarus, 10, 365-378.

Lewis, J.S. (1969b). Observability of spectroscopically active compounds in the atmosphere of Jupiter. Icarus, 10, 393-409.

Lewis, J.S. (1970). Venus: Atmospheric and lithospheric composition. Earth Planet. Sci. Lett., 10, 73-80.

Lewis, J.S. (1971). Consequences of the presence of sulfur in the core of the Earth. Earth Planet. Sci. Lett., 11, 130-134.

Lewis, J.S. (1972). Metal/silicate fractionation in the solar system. Earth Planet. Sci. Lett., 15, 286-290.

Lewis, J.S. (1974). The temperature gradient in the solar nebula. Science, 186, 440-443.

Lewis, J.S., Barshay, S.S. and Noyes, B. (1979). Primordial retention of carbon by the terrestrial planets. Icarus, 37, 190-206.

Lewis, J.S. and Kreimendahl, F.A. (1980). Oxidation state of the atmosphere and crust of Venus from Pioneer Venus results. Icarus, in press.

Lewis, J.S. and Prinn, R.G. (1980). Kinetic inhibition of CO and N_2 reduction in the solar nebula. Astrophys. J. 236,

McQuarrie, M. (1955). Structural behavior in the system (Ba, Ca, Sr)TiO_3 and its relation to certain dielectric characteristics. J. Am. Ceram. Soc., 38, 444-449.

McQuarrie M. and Behnke, F.W. (1954). Structural and dielectric studies in the system (Ba,Ca)(Ti,Zr)O_3. J. Am. Ceram. Soc., 37, 539-543.

McSween, H.Y., Jr. (1979). Are carbonaceous chondrites primitive or processed? A review. Rev. Geophys. Space Phys., 17, 1059-1078.

Marvin U.B. and Klein, C., Jr. (1964). Meteoritic Zircon. Science, 146, 919-920.

Mason, B. (Ed.) (1971). Handbook of Elemental Abundances in Meteorites. Gordon and Breach, New York.

Mason, B. (1979). Cosmochemistry Part 1. Meteorites. In Data of Geochemistry, 6th ed. (M. Fleischer, Ed.), pp.1-132. U.S. Geol. Surv. Prof. Paper 440-B-1, U.S. Govt. Print. Off., Washington, D.C.

Mason, B. and Graham, A.L. (1970). Minor and trace elements in meteoritic minerals. Smithsonian Contr. Earth Sci., 3, 1-17.

Masuda, A. and Tanaka, T. (1977). How did barium titanate particulates stick together in the nebula? Nature, 267, 231-233.

Mills, K.C. (1974). Thermodynamic Data for Inorganic Sulphides, Selenides and Tellurides. Butterworths, London.

Mueller, R.F. (1963). Chemistry and petrology of Venus: Preliminary deductions. Science, 141, 1046-1047.

Mueller, R.F. (1964). A chemical model for the lower atmosphere of Venus. Icarus, 3, 285-298.

Mueller, R.F. (1965). Stability of sulfur compounds on Venus. Icarus, 4, 506-512.

Noonan, A.F., Nelen, J.A., and Fredriksson, K. (1978). Ca-Al-Na rich inclusions and aggregates in H-group and carbonaceous chondrites. Meteoritics, 13, 583-587.

Odoj, R. and Hilpert, K. (1976). Evaporation and standard enthalpy of formation of $BaZrO_3(s)$. Z. Phys. Chem. N.F., 102, 191-201.

Oetting, F.L. and McDonald, R.A. (1963). The thermodynamic properties of magnesium orthophosphate and magnesium pyrophosphate, J. Phys. Chem., 67, 2737-2743.

Orville, P.M. (1972). Plagioclase cation exchange equilibria with aqueous chloride solution at 700°C and 2000 bars in the presence of quartz. Am. J. Sci., 272, 234-272.

Pagel, B.E.J. (1979). Solar abundances. A new table (October 1976) In Origin and Distribution of the Elements, Proceedings of the Second Symposium, Paris, May 1977. (L.H. Ahrens, Ed.), pp.79-80. Pergamon Press, Oxford.

Palme H. and Wlotzka, F. (1976). A metal particle from a Ca, Al rich inclusion from the meteorite Allende, and the condensation of refractory siderophile elements. Earth Planet. Sci. Lett., 33, 45-60.

Parker, V.B., Wagman, D.D. and Evans, W.H. (1971). Selected Values of Chemical Thermodynamic Properties. Tables for the Alkaline Earth Elements (Elements 92 through 97 in the Standard Order of Arrangement). NBS Technical Note 270-6. Washington, D.C.

Prather, M.J., Logan, J.A. and McElroy, M.B. (1978). Carbon monoxide in Jupiter's upper atmosphere: An extra-planetary source. Astrophys. J., 223, 1072-1081.

Prinn, R.G. (1970). UV radiative transfer and photolysis in Jupiter's atmosphere. Icarus, 13, 424-436.

Prinn, R.G. and Barshay, S.S. (1977). Carbon monoxide on Jupiter and implications for atmospheric convection. Science, 198, 1031-1034.

Prinn, R.G. and Lewis, J.S. (1975). Phosphine on Jupiter and implications for the Great Red Spot. Science, 190, 274-276.

Reed, Jr., G.W. (1971). Chlorine. In Handbook of Elemental Abundances in Meteorites, (B. Mason, Ed.), pp.143-148. Gordon and Breach, New York.

Richardson, F.D. and Jeffes, J.H.E. (1949). The thermodynamic background of iron and steel making processes. I.- The blast furnace. J. Iron and Steel Inst., 163, 397-420.

Ridgway, S.T. (1974). The infrared spectrum of Jupiter, 750-1200 cm^{-1}. Bull. Am. Astron. Soc., 6, 376.

Ridgeway, S.T., Larson, H.P. and Fink U. (1976). The infrared spectrum of Jupiter. In Jupiter. (T. Gehrels, Ed.), pp.348-417. University of Arizona Press, Tucson.

Robie, R.A., Hemingway, B.S. and Fisher, J.R. (1978). Thermodynamic Properties of Minerals and Related Substances at 298.15K and 1 Bar (10^5 Pascals) Pressure and at Higher Temperatures. USGS Bulletin 1452, Washington D.C. (1st printing.)

Robie, R.A. and Waldbaum, D.R. (1968). Thermodynamic Properties of Minerals and Related Substances at 298.15°K (25.0°C) and one Atmosphere (1.013 bars) Pressure and at Higher Temperatures. USGS Bulletin, 1259, Washington, D.C.

Rossini, F.D., Wagman, D.D., Evans, W.H., Levine, S. and Jaffe, I. (1952). Selected Values of Chemical Thermodynamic Properites. U.S. Natl. Bur. Stand. Circular No. 500, Washington, D.C.

Saxena, S.K. (1973). Thermodynamics of Rock-Forming Crystalline Solutions. Springer-Verlag, New York.

Schultz, E.D. and Holland, A.C. (1963). The solar flux incident at the top of the atmospheres of Earth and neighboring planets for the spectral region 50Å to 3000Å. NASA CR-11.

Sears, D.W. (1978). Condensation and the composition of iron meteorites. Earth Planet. Sci. Lett., 41, 128-138.

Sears, D.W. (1980). Formation of E chondrites and aubrites-A thermodynamic model. Icarus, in press.

Seck, H.A. (1971). Koexistierende alkali feldspate und plagioklase im system $NaAlSi_3O_8$-$KAlSi_3O_8$-$CaAl_2Si_2O_8$-H_2O bei temperaturen von 650°C bis 900°C. N Jb Mineral. Abh., 115, 315-345.

Shima, M. (1979). The abundances of titanium, zirconium and hafnium in stony meteorites. Geochim. Cosmochim. Acta, 43, 353-362.

Smith, J.V. (1977). Possible controls on the bulk composition of the earth: Implications for the origin of the earth and moon. In Proc. Eighth Lunar Sci. Conf., Geochim. Cosmochim. Acta Suppl. 8, pp. 333-369. Pergamon Press, New York.

Somerville, M. and Ahrens, T.J. (1980). Shock compression of $KFeS_2$ and the question of potassium in the core. Submitted to J. Geophys. Res.

Spencer, P. and Kubaschewski, O. (1978). A thermodynamic assessment of the iron-phosphorus system. Arch. Eisenhuttenwes. 49, 225-228.

Stephenson, C.C. (1975). Lecture notes for chemical thermodynamics 5.71: Thermodynamic properties of solid solutions of alkali-metal halides. Fall 1975).

Stull, D.R. and Prophet, H. (1967). The calculation of thermodynamic properties of materials over wide temperature ranges. In The Characterization of High Temperature Vapors (J.L. Margrave, Ed.), pp.359-424. John Wiley, New York.

Stull, D.R. and Prophet, H. (1971). JANAF Thermochemical Tables, 2nd ed. NSRDS-NBS 37. Washington D.C.

Suess, H.E. (1980). New solar elemental abundances. Private communication.

Suess, H.E. and Urey, H.C. (1956). Abundances of the elements. Rev. Mod. Phys., 28, 53-74.

Surkov, Y.A., Kirnozov, F.F., Glazov, V.N. and Fedoseyev, G.A. (1976). Investigations of Venusian Gamma-Radiation by Venera 9 and Venera 10. In Cospar Space Research, vol. XVII. (M.J. Rycroft, Ed.), pp.659-662, Pergamon Press, New York.

Tanaka, T. and Okumura, K. (1977). Ultrafine barium titanate particles in the Allende meteorite. Geochem. J., 11, 137-145.

Trivedi, B.M.P. and Larimer, J.W. (1980). Some new mineral stability relations in cosmic systems. Lunar and Planetary Science, XI, 1165-1166.

Turekian, K.K. and Clark, S.P. (1969). Inhomogeneous accumulation of the earth from the primitive solar nebula. Earth Planet Sci. Lett., 6, 346-348.

Urey, H.C. (1952). The Planets, Yale University Press, New Haven.

Van Schmus, W.R. and Ribbe, P.H. (1968). The composition and structural state of feldspar from chondritic meteorites. Geochim. Cosmochim. Acta., 32, 1327-1342.

Van Schmus, W.R. and Ribbe, P.H. (1969). Composition of phosphate minerals in ordinary chondrites. Geochim. Cosmochim. Acta 33, 637-640.

Vinogradov, A.P., Surkov, Y.A. and Kirnozov, F.F. (1973). The content of uranium, thorium, and potassium in the rocks of Venus as measured by Venera 8, Icarus, 20, 253-259.

Wagman, D.C., Evans, W.H., Parker, V.B., Halow, I., Bailey, S.M. and Schumm, P.H. (1968). Selected Values of Chemical Thermodynamic Properties. Tables for the First Thirty Four Elements in the Standard Order of Arrangement. NBS Technical Note 270-3. Washington, D.C.

Wagman, D.C., Evans, W.H., Parker, V.B. Halow, I., Bailey, S.M. and Schumm, R.H. (1969). Selected Values of Chemical Thermodynamic Properties Tables for Elements 35 through 53 in the Standard Order of Arrangement. NBS Technical Note 270-4, Washington, D.C.

Wagman, D.D., Evans, W.H., Parker, V.B. and Schumm, R.H. (1976). Chemical thermodynamic properties of compounds of sodium, potassium and rubidium: an interim tabulation of selected values. NBS Interim Report. 76-1034.

Wai, C.M. and Wasson, J.T. (1977). Nebular condensation of moderately volatile elements and their abundances in ordinary chondrites. Earth Planet Sci. Lett. 36, 1-13.

Mark, D.A. and Lovering, J.F. (1977). Marker events in the early evolution of the solar system: Evidence from rims on Ca-Al rich inclusions in carbonaceous chondrites. In Proc. Eighth Lunar Sci. Conf., Geochim. Cosmochim. Acta. Suppl. 8, pp. 95-112. Pergamon Press.

Weibke, F. and Schrag, G. (1941). Die Bildungswarmen der Niederen Phosphide einiger Schwermetalle. Z. Elektrochem., 47, 222-238.

Weidenschilling, S.J. and Lewis, J.S. (1973). Atmospheric and cloud structures of the Jovian Planets. Icarus, 20, 465-476.

Wellman, T.R. (1969). The vapor pressure of NaCl over decomposing sodalite. Geochim. Cosmochim. Acta., 33, 1302-1304.